SCIENTIFIC REPORTS
nature research

OPEN

# Method and its Composition for encapsulation, stabilization, and delivery of siRNA in Anionic polymeric nanoplex: An *In vitro-In vivo* Assessment

Nidhi Raval, Hardi Jogi, Piyush Gondaliya, Kiran Kalia & Rakesh K. Tekade*

**Small interfering RNA (siRNA) are synthetic RNA duplex designed to specifically knockdown the abnormal gene to treat a disease at cellular and molecular levels. In spite of their high potency, specificity, and therapeutic potential, the full-fledged utility of siRNA is predominantly limited to *in vitro* set-up. Till date, Onpattro is the only USFDA approved siRNA therapeutics available in the clinic. The lack of a reliable *in vivo* siRNA delivery carrier remains a foremost obstacle towards the clinical translation of siRNA therapeutics. To address the obstacles associated with siRNA delivery, we tested a dendrimer-templated polymeric approach involving a USFDA approved carrier (albumin) for *in vitro* as well as *in vivo* delivery of siRNA. The developed approach is simple in application, enhances the serum stability, avoids *in vivo* RNase-degradation and mediates cytosolic delivery of siRNA following the endosomal escape process. The successful *in vitro* and *in vivo* delivery of siRNA, as well as targeted gene knockdown potential, was demonstrated by HDAC4 inhibition in *vitro* diabetic nephropathy (DN) podocyte model as well as in *vivo* DN C57BL/6 mice model. The developed approach has been tested using HDAC4 siRNA as a model therapeutics, while the application can also be extended to other gene therapeutics including micro RNA (miRNA), plasmids oligonucleotides, etc.**

Ribonucleic acid interference (RNAi) refers to a post-transcriptional gene silencing tool to neutralize or silence the pathological protein via activating RNA-induced silencing complex (RISC), endogenously. Gene allows clinicians to treat a disease by administering RNAi therapeutics (such as small interfering RNA (siRNA) or micro RNA (miRNA) into a patient's instead of using drugs or surgical interventions[1]. However, the degradation of administered siRNA by circulatory RNase, their short half-life ($t_{1/2}$) as well as rapid renal clearance are some of the prime challenges that complicate the clinical translation of siRNA therapeutics[2,3]. Further, the endo-lysosomal trapping of delivered siRNA is yet another key issue that results in the enzymatic-degradation of delivered siRNA leading to null-effect. Ideally, the siRNA delivery vector must find their way to escape from the endosomes/lysosomes compartment after entering inside the target cell to efficiently release the loaded siRNA in the cytosolic compartment[4]. Failure to overcome this barrier would significantly weaken or even totally eliminate the therapeutic effect of siRNA.

Initially, the viral vectors have been employed to deliver siRNA into the cell. However, the stimulation of the immune system through the activation of viral pathogens was found to be the foremost hurdle[5–7]. Tremendous efforts were made to develop a non-viral and clinically translatable approach for the intracellular transfection of siRNA[8]. In this context, Lipofectamine is the most widely employed siRNA transfection materials, but its application is primarily limited to *in vitro* set-up[9]. Some modified versions of lipofectamine have been developed, however, none of the existing modalities represents an ideal carrier to facilitate clinical translation of siRNA therapeutics. Invivofectamine and *in vivo*-jet-PEI are some of the potential siRNA carriers, but the applications of these agents are primarily restricted for the delivery of siRNA to the liver[10].

National Institute of Pharmaceutical Education and Research (NIPER) – Ahmedabad, Palaj, (An Institute of National Importance), Opposite Air Force Station, Gandhinagar, 382355, Gujarat, India. *email: rakeshtekade@gmail.com

Some of the novel approaches for delivery of siRNA/miRNA including smarticles for miR-34a delivery *in vivo*[11], ligand-mediated N-acetyl glucosamine-siRNA (GalNAc) delivery to liver[12], folate gated miRNA for breast and lung cancer[13], other lipidic nanoparticles[14] as a siRNA delivery tactics are currently under preclinical and clinical trials. Recently, the USFDA has approved the lipidic nanoparticle for the delivery of siRNA (Patisiran: Onpattro; by Alnylam Pharmaceuticals) to treat polyneuropathy in patients with hereditary transthyretin-mediated (hATTR) amyloidosis[15,16]. It has been largely advocated that polymeric vectors could offer numerous advantages over the viral vector, for instance, eliminating the off-target effect, prolonged extracellular or serum stability, non-immunogenicity, and easy formulation steps to name the few[17]. Quality-by-design (QbD) driven synthesis of cationic polymeric nano vector (CPNVs), incorporation of the fitting level of crosslinking agents, pH redox-responsive units, osmo-responsive agents, etc. are some of the typical strategies to improve siRNA encapsulation, stabilization and delivery capabilities of polymeric vectors[8]. In an attempt to promote the escape of polymeric vectors from endosomes/lysosomes, moieties that elevate intra-osmotic pressure in endosomes/lysosomes were extensively employed to eventually burst these compartments. However, the premature separation of siRNA from the polymeric vectors in the body fluids, and subsequent degradation by endogenous serum nucleases still stand as the unaddressed challenges[18].

Several cell-penetrating peptides (CPPs) were developed to increase the extent of cytosolic delivery of siRNAs and other genetic materials[19]. However, despite three decades of research, the fundamental basis for CPP activity remains elusive and non-conclusive. The biomedical application and clinical translation of most of the siRNA delivery devices have been impeded to a great extent due to its poor containment property as well as associated toxicities[20]. To facilitate the intracellular disassembly and facilitate cytosolic release of loaded siRNA, the stimuli-sensitive linkages with the capability to get readily cleaved in response to intracellular acidity or redox conditions were also coupled with PNVs[21]. However, the delivery capability of these hybrid vectors is largely compromised by complex physiological and biological barriers, which restrict their applications in a clinical setting[22].

Albumin, a natural polymer offers an optimal platform for the development of the drug as well as siRNA delivery vehicles pertain to the countless advantages including abundantly available protein, easy modification, easy purification, non-immunogenic, biodegradable, inertness, encapsulation of hydrophilic payload in the hydrophobic corona and low cost[23]. An albumin-based platform for the delivery of anticancer drug Paclitaxel has already made its way to the market in the form of a USFDA approved product (Abraxane; Celgene Corporation, USA)[24]. Literature suggests that albumin-based nanoparticle selectively binds podocytes of renal bowman's capsule via FcRn receptor to regulate proteinuria[25]. This makes albumin an advantageous biopolymer for the development of siRNA delivery vector. However, the inherent architectural configuration of albumin is not adequate to guarantee a complete escape of the nanovector from the endo-lysosomal compartment as well as protect the loaded siRNA therapeutics from the harsh endo-lysosomal environment. Further, the anionic carboxylic side chain of albumin imparts limitation towards the encapsulation of anionic siRNA molecules (due to the existence of anionic phosphate side chain in siRNA architect)[26,27].

Histone deacetylases (HDACs) have been implicated in podocyte dysfunction to mediate the onset and development of diabetic nephropathy (DN)[28,29]. The development of HDAC4-specific gene inhibitors may provide an efficacious therapeutic tool for DN. Hence, in this study, we aim to deliver HDAC4 siRNA using the innovative siRNA delivery tool developed by us as a proof of concept. We evaluate and report it's *in vitro* and *in vivo* HDAC4 gene silencing capability using podocytes as well as in DN mouse model. The core goal of this study was to develop and test the siRNA delivery vehicle that can offer *in vivo* stabilization, overcome endosomal degradation, and can mediate intracellular siRNA delivery (Fig. 1A). For proof of concept; we employed HDAC4 siRNA in the treatment of DN, however, the reported technology can be extended to other gene therapeutics viz miRNA, plasmid, etc. to name the few.

## Results

**Screening of Dendrimer/siRNA (*d*:siR) complex.** The binding efficiency of siRNA with the polycationic dendrimer template was investigated by determining the band binding efficiency and band intensity of the siRNA (Fig. 1B,C). The results infer that at a *surface to charge ratio (n/p)* of 1 and 0.5, the binding of siRNA with dendrimer template was $94.78 \pm 1.07\%$ and $90.50 \pm 0.93\%$, respectively. The binding of siRNA with dendrimer template was well complemented by the absence of migration of free siRNA in the gel electrode compared to other *n/p* ratios. On the other hand, upon reducing the *n/p* ratio to 0.25 or 0.125, the binding efficiency significantly reduced to $30.25 \pm 2.85\%$ ($p < 0.001$) and $18.33 \pm 19.26\%$ ($p < 0.001$), respectively. The ineffective siRNA binding at *n/p* ratio below 0.5 can be seen by the emergence of band intensities corresponding to free/uncomplexed siRNA. This suggests that a specific *d*:siR composition and *n/p* ratio (*d*:siR: *n/p* ratio 0.5) is required to form an effective *d*:siR complex Fig. 1B,C.

**Net Surface zeta potential of *d*:siR complex.** The surface zeta potential of *d*:siR complex formed at various *n/p* ratio was determined (Fig. 1D). The free dendrimer bears a net positive surface zeta potential of $+24.04 \pm 3.52$ mV, which upon complexation with siRNA reduced to $+20.06 \pm 2.00$ mV, $+16.76 \pm 1.37$ mV, $+13.24 \pm 2.91$ mV, and $+11.57 \pm 1.45$ mV, respectively of *d*:siR formed using *n/p* ratio of 1, 0.5, 0.25, and 0.125, respectively.

**Quality-by-Design (QbD) driven synthesis and characterization of siRNA Nanoplex.** The purity of albumin was assessed via SDS-PAGE (Fig. S9), BCA assay ($\geq$96%; Fig. S10), and MALDI-TOF/MS (Fig. S11) for the evaluation of any other component from the fraction V. The synthesis process design and process parameters were optimized using the Box-Banken QbD approach to produce siRNA loaded Nanoplex (siANp) and dendrimer templated siRNA nanoplex (DTsiANp) (Target particle size: $\leq$70 nm). The blank nanoplex counterparts including ANp and DTANp were also produced following the same protocol for comparison (*refer supporting*

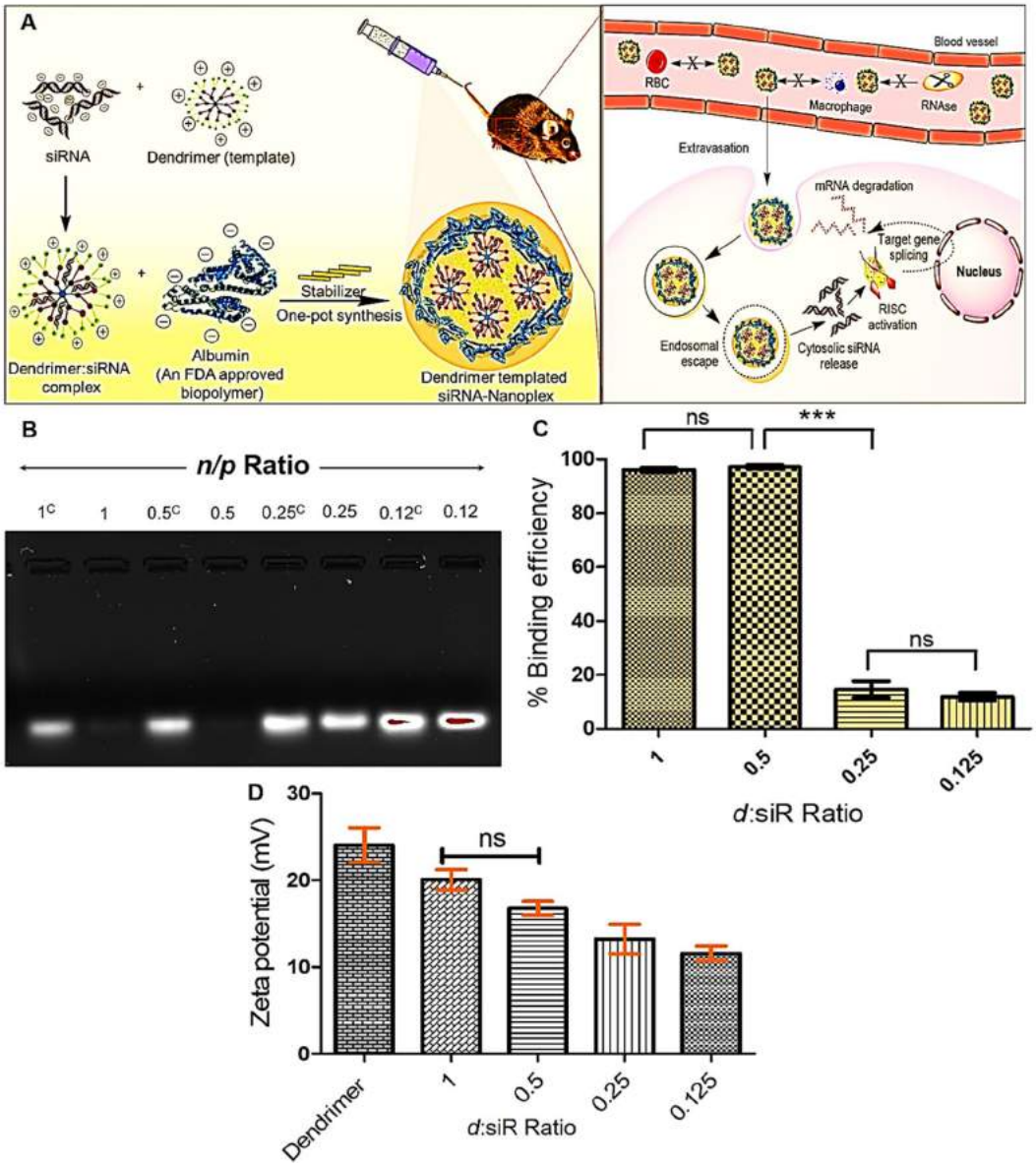


**Figure 1.** (**A**) Scheme showing encapsulation, stabilization, and delivery of siRNA in Anionic polymeric nanoplex. The developed siRNA-nanoplex imparts serum stability, avoids *in vivo* RNase degradation and mediates its cytosolic delivery following the endosomal escape. The endosomal escape leads to a selective siRNA release of loaded siRNA in the cytosolic region, and this phenomenon was facilitated by strategic incorporation of the dendrimer in the architectural configuration of siRNA-nanoplex. (**B**) Gel electrophoresis for the selection of *d*:siR complexation condition, Here, Lane 1 ($1^C$): positive control having siRNA in equivalent amount as in *d*:siR complex prepared at 1 *n/p* ratio; Lane 2: *d*:siR complex prepared at 1 *n/p* ratio; Lane 3 ($0.5^C$): positive control having siRNA in equivalent amount as in *d*:siR complex prepared at 0.5 *n/p* ratio; Lane:4: *d*:siR complex prepared at 0.5 *n/p* ratio; Lane 5 ($0.25^C$): positive control having siRNA in equivalent amount as in *d*:siR complex prepared at 0.25 *n/p* ratio; Lane 6: *d*:siR complex prepared at 0.25 *n/p* ratio; Lane 7 ($0.12^C$): positive control having siRNA in equivalent amount as in *d*:siR complex prepared at 0.12 *n/p* ratio; Lane 8: *d*:siR complex prepared at 0.12 *n/p* ratio (**C**) Binding efficiency of *d*:siR complex, (**D**) surface zeta potential of *d*:siR formed using *n/p* ratio of 1, 0.5, 0.25, and 0.125. Results are represented as mean ± S.D. *(n = 3)*.

*information*). The dynamic light scattering (DLS), scanning electron microscopy (SEM), transmission electron microscopy (TEM), and atomic force microscopy (AFM) was performed to characterize the properties of siRNA nanoplex for hydrodynamic particle size, polydispersity index (PDI), surface zeta potential (ζ, mv), and surface topography morphology. DLS suggested siANp and DTsiANp be of nanometric size with a hydrodynamic particle size of 66.93 ± 2.90 nm (ζ, −26.8 ± 0.89 mV; PDI: 0.210 ± 0.01I) and 64.51 ± 0.83 nm (ζ, −16.1 ± 1.06 mV; PDI: 0.187 ± 0.06), respectively (Fig. 2A). The representative TEM, SEM and AFM images of DTsiANp showed the nanoplexes to be nanometric, rounded-oval with smooth surface topography (Figs 2B–D; S16). The AFM analysis suggested nanoplex to be aggregates of spherical particles of ~30 nm in diameter. It may be noted that

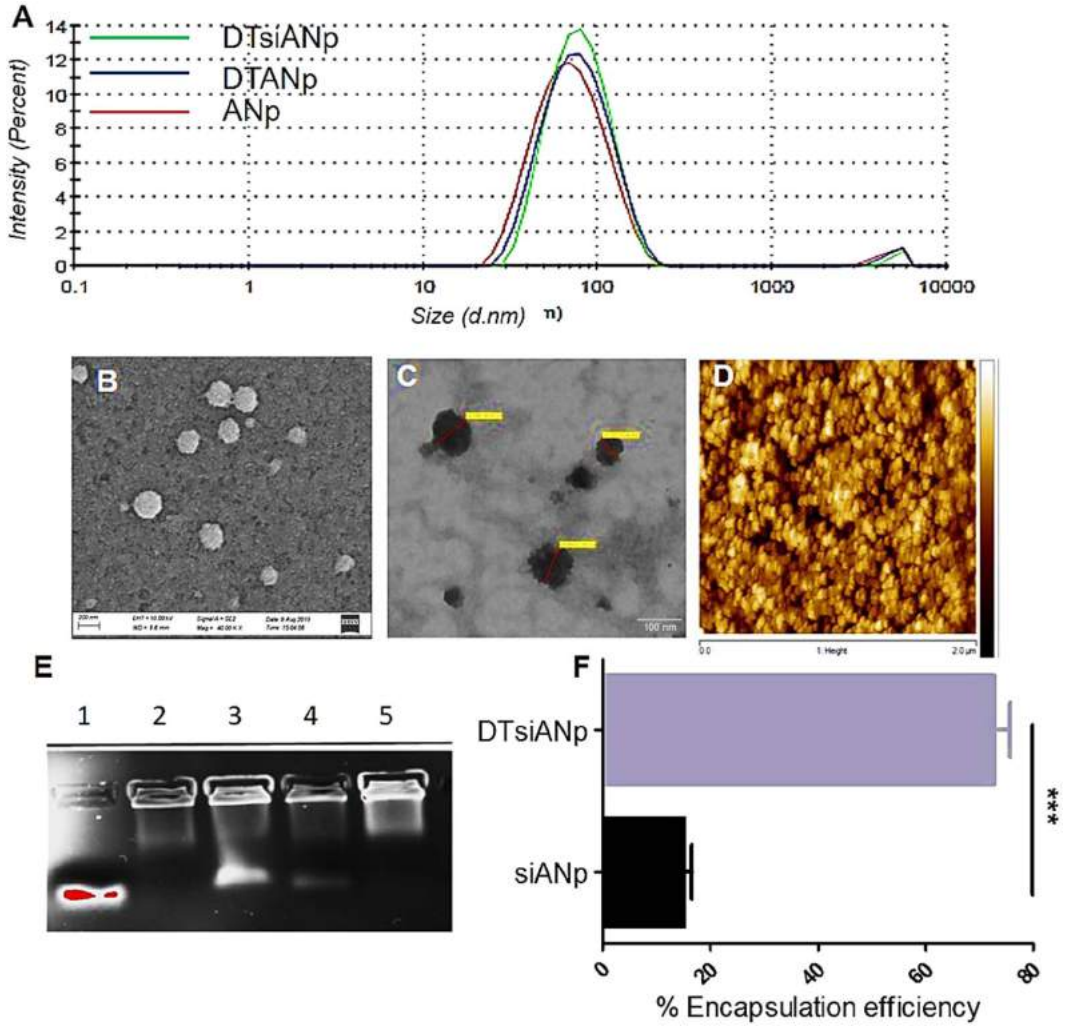


**Figure 2.** (**A**) Hydrodynamic particle size distribution of ANp, DTANp, and DTsiANp using DLS, (**B**) SEM image of DTsiANp (**C**) TEM of DTsiANp, (**D**) AFM of DTsiANp (**E**) Gel electrophoresis, Lane 1: naked siRNA, Lane 2: siANp after centrifugation, Lane 3: siANP after centrifugation (supernatant), Lane 4: DTsiANp after centrifugation (supernatant), Lane: 5 DTsiANp after centrifugation, (**F**) encapsulation efficiency of siRNA in siANp and DTsiANp determined using Ribogreen assay (***$p < 0.0001$). Results are represented as mean ± SD *(n = 3)*.

the nanoplex size observed by AFM for ANp, DTANp, siANp, and DTsiANp found to be smaller than the ones recorded via DLS technique. This is probably due to the shrinkage of the nanoparticles during the drying process employed during the sample preparation for AFM imaging analysis (Fig. S17). These outcomes are in agreement with reported literature on the size of albumin nanoparticles[30].

After characterization of nanoplex, the assays were also done to confirm the presence of albumin and dendrimer inside the nanoplex. It was found that albumin remained intact after nanoplex preparation and forms the major component of the nanoplex system (~95%; Fig S10 and S12). The presence of dendrimeric template in the nanoplex was confirmed via TNBSA assay. It observed that number of the primary amino group got significantly enhanced in DTsiANp (22.54 ± 1.67%; $p < 0.05$) and DTANp (23.11 ± 1.08%; $p < 0.05$) after the incorporation of the dendrimeric template as compared to the siANp and ANp (Fig. S13). The incorporation of dendrimeric template in nanoplex was further confirmed by zeta potential analysis (Fig. S14).

**The siRNA encapsulation efficiency of Nanoplex.** The encapsulation efficiency of siRNA nanoplex was determined using gel retardation assay and re-verified by Ribogreen assay. The quantitation of gel showed the presence of approximately 18.51 ± 4.07% naked siRNA following gel electrophoresis of DTsiANp, as against to almost 89.21 ± 7.05% naked siRNA as observed (Fig. 2E) in case of siANp ($p < 0.05$). This encapsulation of siRNA in nanoplex was also assessed by Ribogreen assay, and the outcomes were analogous to the results obtained by gel retardation assay. The siRNA encapsulation efficiency in DTsiANp and siANp was found to be 72.62 ± 3.01% and 14.90 ± 1.53%, respectively (Fig. 2F). The result infers that the siRNA encapsulation efficiency in albumin nanoplex gets significantly enhanced while adopting the dendrimer templated approach. Herein, the siRNA

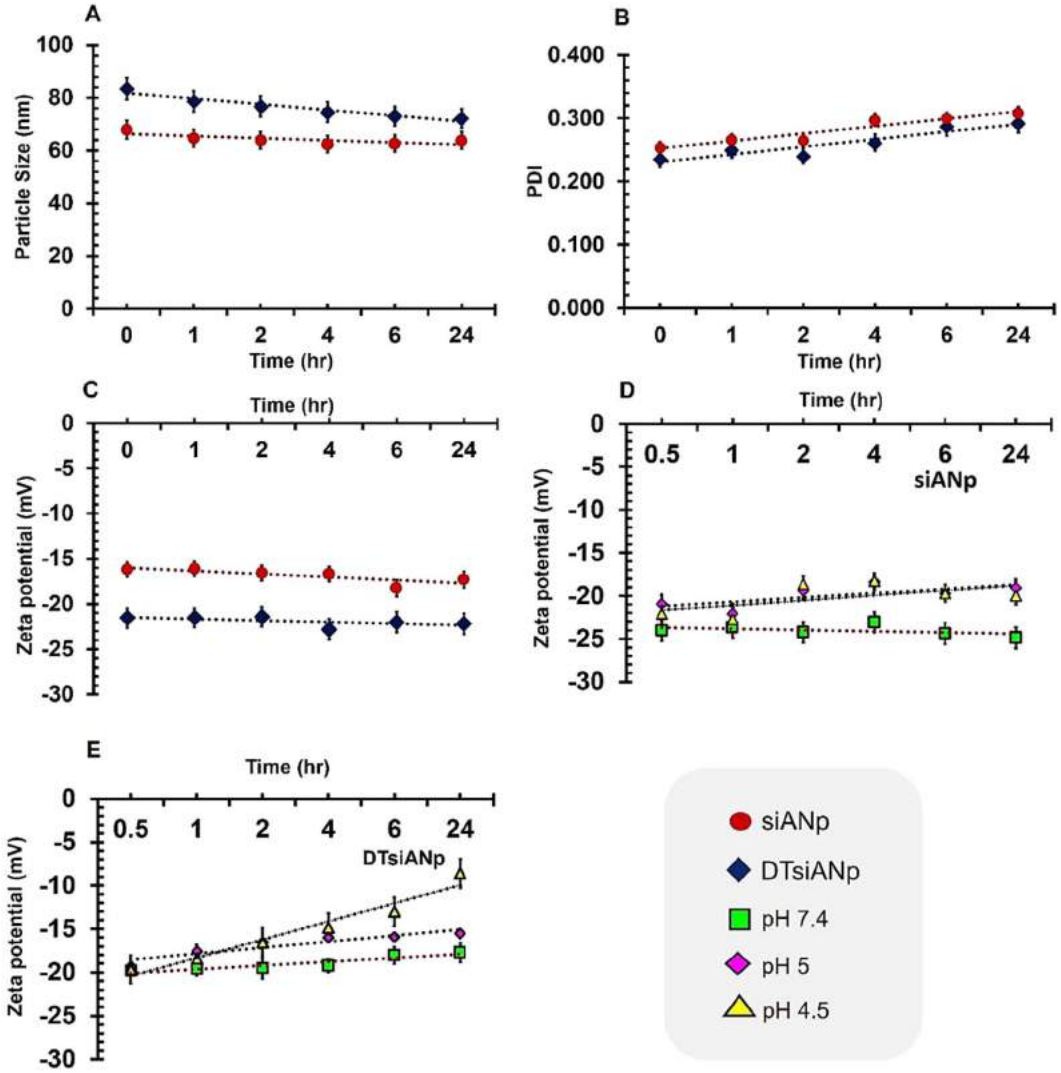


**Figure 3.** Illustration of serum stability of siANp and DTsiANp in terms of (**A**) hydrodynamic particle size (**B**) PDI (**C**) surface zeta potential. pH responsiveness of nanoplexs in terms of surface zeta potential (**D**) siANp, (b) DTsiANp at pH 7.4, 5.5 and 4.5. Results are represented as mean ± S.D. *(n = 3)*.

encapsulation efficiency enhanced by 3.87 ± 1.04 fold ($p < 0.0001$) as compared siANp. Further, the actual encapsulation of siRNA in nanoplex was confirmed using RNase protection assay. This assay was also performed to verify that the siRNA exists inside the nanoplex and is not the mere precipitate of siRNA and the biopolymer. The outcome of this investigation confirmed that the siRNA exists inside the nanoplex as encapsulated form rather than simple precipitation of siRNA (Fig. S15).

**Serum stability of siRNA Nanoplex.** The outcome of this investigation suggested that in presence of serum, there was an insignificant change in the particle size, PDI and zeta potential of siANp and DTsiANp even after 24 hr (Fig. 3A–C; $p > 0.05$). It may be noted that naked siRNA exposed to the serum is highly prone to undergo degradation by serum RNase enzyme (Fig. 4A–F). Hence, the capability of siANp and DTsiANp to protect siRNA against serum RNase enzyme was investigated by gel electrophoresis assay. Here, at zero time point (serum untreated), the siRNA bands were remained intact and considered as starting control for succeeding time points. It was found that in the presence of serum, naked siRNA (Fig. 4D) degrades completely in less than 1 hr incubation time. While in the case of siANp, the siRNA was degraded and was not able to remain stable in the presence of serum due to surface-bound siRNA on siANp (Fig. 4E). On the other hand, DTsiANp (Fig. 4F), showed retention of siRNA band in the presence of serum till 24 hr. The percentage siRNA stability in the presence of serum was further confirmed through percentage siRNA band intensity with reference to siRNA band intensity of serum untreated group (Fig. S8). It was found that the siRNA remains stable in DTsiANp, which can be ascribed to the presence of dendrimeric template in this formulation. Because of the dendrimeric template, siRNA does not easily come in contact with the serum and hence remain stable until a prolonged period of time (>24 hr).

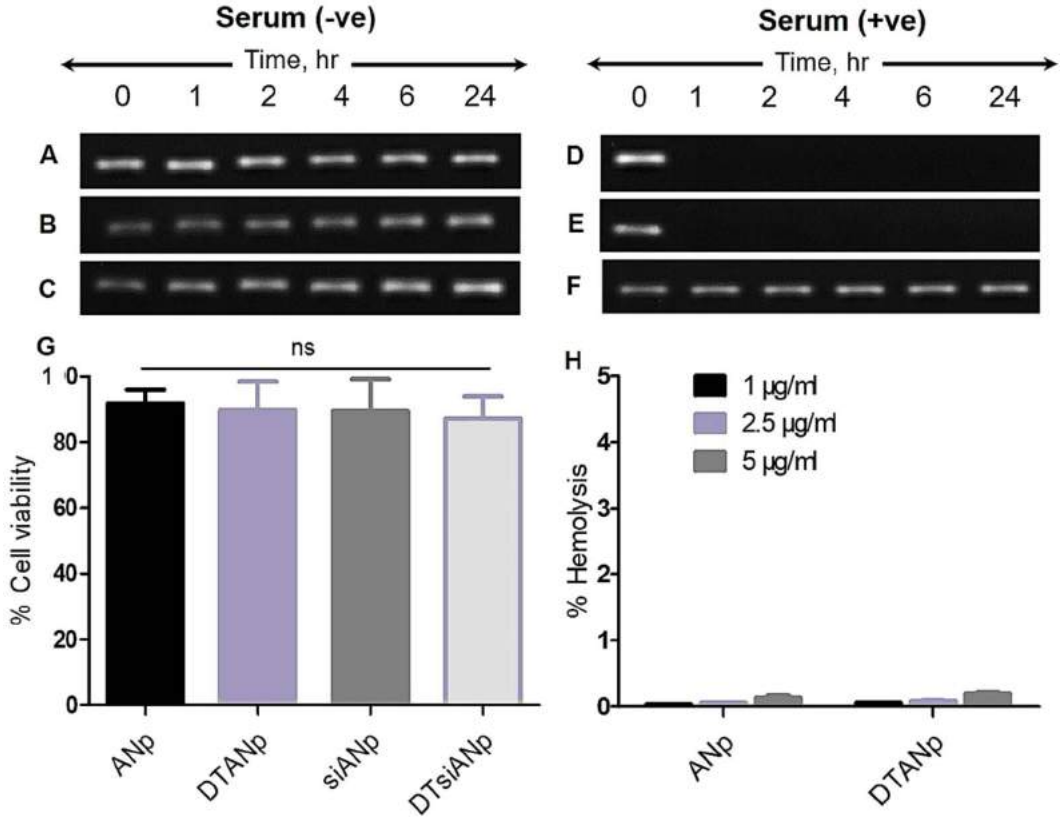


**Figure 4.** Stability profile of siRNA in absence of serum as evaluated by gel electrophoresis (**A**) naked siRNA, (**B**) siANp, (**C**) DTsiANp. Stability profile of siRNA in presence of serum as evaluated by gel electrophoresis (**D**) naked siRNA, (**E**) siANp, (**F**) DTsiANp. (**G**) MTT assay for percentage cell viability of ANp, DSAN, siANp, and DTsiANp in HG (30 mM) exposed podocytes cells (**H**) Hemo-compatibility assay for ANp and DTANp. Results are represented as mean ± S.D. ($n = 3$).

**Endo/Lysosomal Escape tendency of developed siRNA Nanoplex.** The pH sensitivity of nanoplexes and their ability to undergo physicochemical and morphological amendments inside the endo-lysosomal compartment was assessed under pH 5.5, pH 4.5 and pH 7.4. Here, pH-dependent protonation behavior of siANp (conventional plain albumin-based nanoplex) compared to DTsiANp (nanoplex that contain dendrimer) was evaluated. A significant change in the hydrodynamic particle size, PDI and sur\face charge was noted ($p < 0.05$) when the pH of the incubation milieu was changed from physiological pH to endosomal (acidic) environment. An insignificant change in the particle size and zeta potential of siANp (particle size: 0.084-fold change; ζ: 2.65 ± 1.98% change) and DTsiANp (particle size: 0.062-fold change; ζ: 1.2 ± 1.32% change ($p > 0.05$)) was observed following their incubation in physiological pH 7.4 inferring their stability under physiological condition (Figs S4; 3D,E).

The incubation of siANp under pH 7.4, 5.5 and 4.5 did not elicit any change in its effective particle size. However, after incubation of DTsiANp under acidic environment (pH 5.5; early endosomal pH) and under pH 4.5 (late endosomal pH), a significant enhancement in their particle size was observed. Here, the particle size of DTsiANp increased by 41.98 ± 2.47% (under pH 5.5; $p < 0.001$) and 74.14 ± 0.41% (under pH 4.5; $p < 0.001$) (Fig. S4).

In addition, surface zeta potential also affected significantly upon a change in pH (Fig. 3D,E; $p < 0.05$). In case of, plain albumin, the surface zeta potential was not significantly increased in endosomal pH 5.5 (17.92 ± 2.06%; $p > 0.05$) and in pH 4.5 (15.55 ± 1.92%; $p > 0.05$) over pH 7.4 (15.11 ± 0.93%; $p > 0.05$). Whereas, in case of the plain dendrimer, the zeta potential was enhanced significantly by 24.05 ± 1.01% (pH 5.5; $p < 0.05$) and 41.41 ± 1.67% (pH 4.5; $p < 0.05$) as compared to pH 7.4 (11.77 ± 1.72%) (Fig. S18). DTsiANp surface charge was enhanced to 19.36 ± 1.15% (pH 5.5; $p < 0.05$) and 56.31 ± 1.84% (pH 4.5; $p < 0.01$) compared to pH 7.4 (−14.9 ± 1.26 mV). Suggestively, the results infer the pH-responsive morphological changes in the architect of DTsiANp owing to the protonation of free primary amines of dendrimeric template in acidic pH environment.

The Endo/lysosomal escape effect of nanoplex was also evaluated by means of lyso-tracker red dye. Results (Fig. S19) suggested that DTsiANp treated cells were showed significant yellow fluorescence due to co-localization of green (FAM-siRNA) and red fluorescence (endosome selective lyso-tracker red) after 8 hr. Initially, at 6 hr there was very less red fluorescence was observed in comparison to 8 hr and suggesting endosomal uptake of DTsiANp. At 12 hr, reduction in the red fluorescence and parallel enhanced green fluorescence was appeared in the cytosolic region, which infers the endosomal escape ability of DTsiANp. Whereas, siANp was not exhibiting any fluorescence even at 12 hr.

**Biocompatibility of Nanoplex.** MTT assay was employed to evaluate the biocompatibility of developed nanoplexes viz: ANp, DTANp, siANp, and DTsiANp in normal as well as in high glucose (30 mM) HG-treated podocytes DN model. The results inferred that all prepared nanoplexes were biocompatible with approximately 100% cellular viability of podocytes (Fig. 4G).

**Hemocompatibility assay.** As illustrated in Fig. 4H, all the prepared nanoplexes were found to be highly hemocompatible. The ANp and DTANp showed less than 0.2% hemolysis ($p > 0.05$) when tested under all possible clinically applicable concentrations (1 μg/ml, 2.5 μg/ml and 5 μg/ml) inferring endogenous albumin-based ANp and DTANp to be safe and biocompatible with the blood compartment.

**Cellular uptake of siRNA nanoplex in HG-treated podocytes DN model.** The cellular uptake of naked siRNA, siANp, and DTsiANp was performed in HG-treated podocytes DN model[31] and investigated by confocal laser scanning microscopy (CLSM). Here, HG treated podocytes cells showing morphological chages such as cellular membrane blebbing, reduction in cellular volume and rounding of the cell[32]. The results (Fig. 5A) suggested that DTsiANp gets internalized inside the cell in 12 hr as observed by the higher FAM-siRNA associated green fluorescence inside the cell as compared to naked siRNA and siANp. The cellular uptake of DTsiANp was found to be 4.45-fold and 1.63-fold higher mean fluorescence in podocytes cells as compared to naked siRNA and siANp (Fig. 5B).

***In vitro* gene silencing efficiency of siRNA nanoplex in HG-treated podocytes DN model.** In HG condition, HDAC4 gene primarily contributes to podocytes injury in DN[33] and hence, HDAC4 gene was selected as a target for testing the siRNA delivery system as proposed in this investigation. qRT-PCR was performed to evaluate the expression level of HDAC4 gene at a transcriptional to recognize the molecular mechanism of its therapeutic effect. The HDAC4 gene was found to be significantly overexpressed in HG treated podocytes, which is in agreement with existing reports[33]. The HG treated podocytes were then treated with naked siRNA, DTsiANp/HDAC4, and DTsiANp/scramble for 24 hr. Naked siRNA treated podocytes showed an insignificant suppression of HDAC4 expression ($3.5 \pm 0.93\%$, $p > 0.05$). Whereas, DTsiANp/HDAC4 treated cells showed $28.39 \pm 1.37\%$ ($p < 0.05$) repression of HDAC4 mRNA expression compared to DTsiANp/Scramble. A $32.11 \pm 1.87\%$ ($p < 0.05$) and $34.51 \pm 1.87\%$ ($p < 0.01$), respective downregulation of HDAC4 mRNA was noted following the treatment of DTsiANp/HDAC4 as compared to naked siRNA and HG treated podocytes (Fig. 5C). This suggests efficient silencing of dysregulated HDAC4 in HG treated podocytes cells by DTsiANp. Further, the effect of gene silencing on HDAC4 protein was also evaluated by western blot analysis.

**Evaluation of HDAC4 protein expression in siRNA nanoplex treated HG-podocytes DN model.** HDAC4 is one of the centrally acting biomolecules involved in the functioning of podocytes. In HG condition, overexpression of HDAC4 induces the inflammation, apoptosis, and autophagy in podocytes[33]. In line with the reported literature, we also observed an enhanced HDAC4 protein expression in HG treated podocytes[33]. The treatment of naked siRNA to HG treated podocytes cells did not exhibit significant downregulation ($4.02 \pm 0.90\%$; $p > 0.05$) in the relative HDAC4 protein level. In agreement with the qRT-PCR outcomes, relative HDAC4 protein expression was found to be significantly suppressed following the treatment of DTsiANp/HDAC4 by $44.24 \pm 2.10\%$ ($p < 0.01$) and $45.56 \pm 3.61\%$ ($p < 0.001$) as compared to the naked siRNA and DTsiANp/scramble, respectively (Fig. 5D). Further, DTsiANp/HDAC4 successfully repressed the relative HDAC4 protein level ($46.27 \pm 3.96\%$; $p < 0.001$) in HG treated podocytes model.

**Effect of siRNA nanoplex treatment on metabolic parameters in C57BL/6 DN mice model.** As shown in Fig. 6A–C, the glucose level, urine volume, and urinary albumin excretion ratio (UAER; representative of severity of proteinuria) was found to be markedly increased in DN induced mice group ($p < 0.05$) as compared to control (healthy mice) group. The four-week treatment of DTsiANp/HDAC4 in DN mice group did not reduced the urine volume and glucose concentration significantly as compared to the DN mice group treated with the naked siRNA and DTsiANp/Scramble (Fig. 6B). Further, it was observed that the naked siRNA was not significant in urine volume and glucose concentration as compared to vs. DTsiANp/Scramble ($p > 0.05$). The UAER was found to be extremely low in the healthy control group ($0.113 \pm 0.02$), which severely got amplified in DN diseased mice ($1.80 \pm 0.56$; in 4 weeks; $p < 0.001$). In case of DTsiANp/scramble and naked siRNA treated group, UAER was found to be $1.72 \pm 0.29$ ($p > 0.05$) and $1.65 \pm 0.20$ ($p > 0.05$), respectively which was found similar as shown in DN mice group. However, upon treating the DN induced mice with DTsiANp/HDAC4, significant repression was observed in the UAER at 4 weeks as compared to DN disease group ($1.07 \pm 0.30$; $p < 0.01$ vs DN mice, $p < 005$ vs. DTsiANp/Scramble, $p < 0.05$ vs. naked siRNA; Fig. 6C).

***In vivo* Evaluation of HDAC4 protein expression in siRNA nanoplex treated C57BL/6 DN mice model.** The HDAC4 protein expression was evaluated by western blot analysis following isolation of protein from the cortical region of kidneys from healthy control, streptozotocin-induced DN mice group and nanoplex treated groups (DTsiANp/HDAC4, DTsiANp/scramble, naked siRNA (Fig. 6D,E). A significantly enhanced HDAC4 protein ($1.0 \pm 0.089$-fold) was observed in DN mice control group as compared to the healthy control group. The treatment of DN induced mice with naked HDAC4 siRNA leads to a slight downregulation of HDAC4 protein expression by $3.90 \pm 0.95\%$ ($p > 0.05$). The treatment of DTsiANp/Scramble to DN induced mice elicited no protective effect and showed a significant rise in relative HDAC4 protein level by $1.5 \pm 0.12$-fold as compared to healthy control. The treatment of DTsiANp/HDAC4 in the DN mice led to a significant reduction in the relative expression of HDAC4 protein by $31.87 \pm 1.13\%$ ($p < 0.05$) compared to naked siRNA and $45.87 \pm 2.01\%$ ($p < 0.001$) compared to DTsiANp/scramble (Fig. 6E).

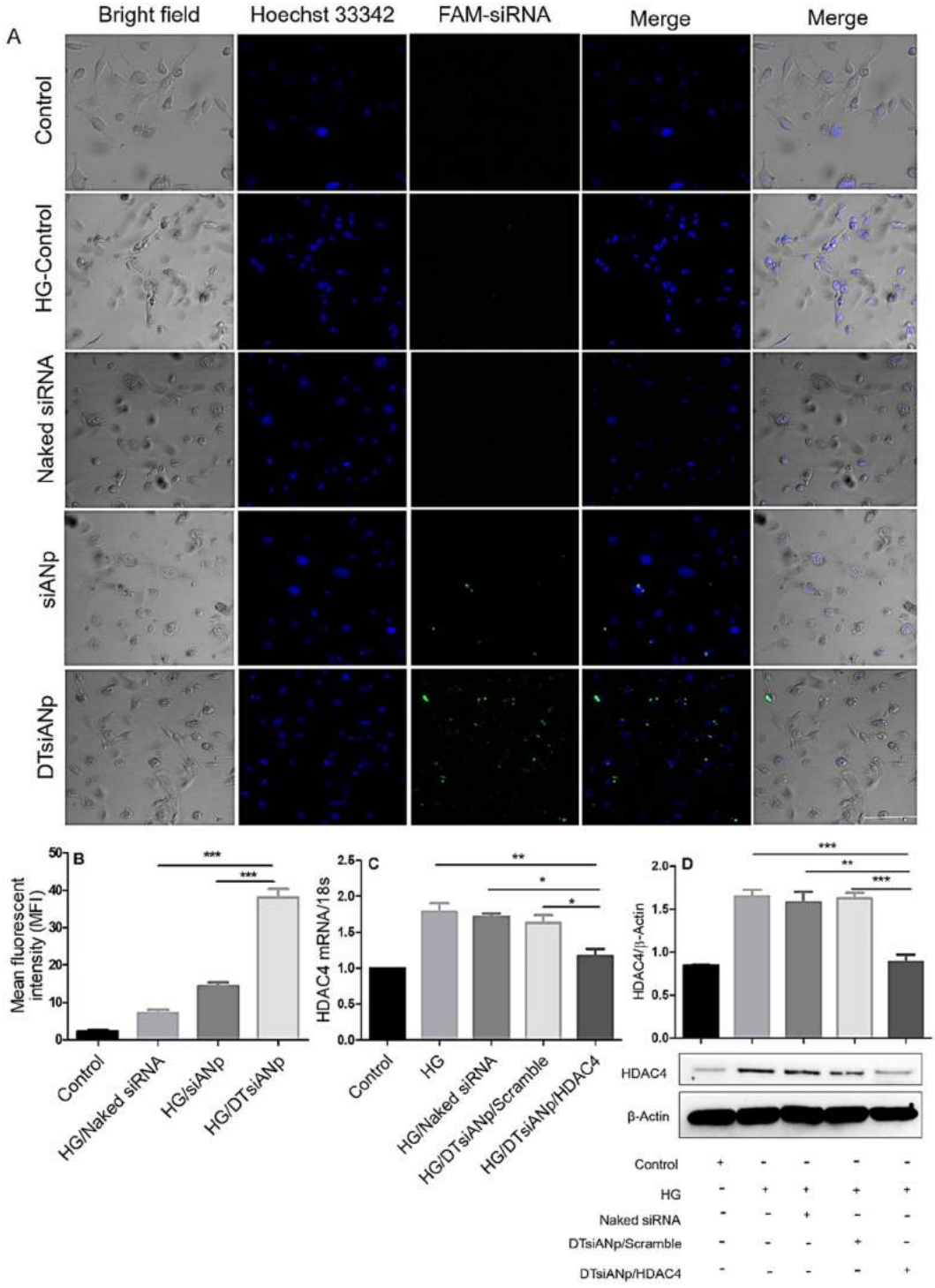


**Figure 5.** (**A**) Confocal microscopic image of FAM-siRNA cellular uptake in HG (30 mM) treated podocyte DN model following treatment of naked siRNA, siANp and DTsiANp. (**B**) Mean fluorescence intensity of FAM-siRNA (**C**) HDAC4 silencing efficiency by qRT-PCR in HG-treated podocytes, $*p < 0.05$ vs. DTsiANp/Scramble, $*p < 0.05$ vs. Naked siRNA, $**p < 0.01$ vs. HG treated *p*odocytes (**D**) western blot analysis for HDAC4 protein expression in HG-treated podocytes. HG-treated cells were taken as a positive control. Western blot analysis was done using ImageJ (NIH, Bethesda, MD). Results are represented as mean ± SD, *(n = 3)*. *indicates $p < 0.05$. Scale bar: 50 µm; Blue fluorescence: Hoechst 33342 (Bisbenzimide), green fluorescence: FAM-siRNA (6-carboxyfluorescein).

**Renal histopathological analysis in siRNA nanoplex treated C57BL/6 DN mice model.** The renal histological changes in the kidney tissue sections of C57BL/6 DN mice stained with hematoxylin-eosin is shown in Fig. 6F. The figure revealed the presence of damaged glomerulus of kidneys of DN mice. Further, the kidney sections

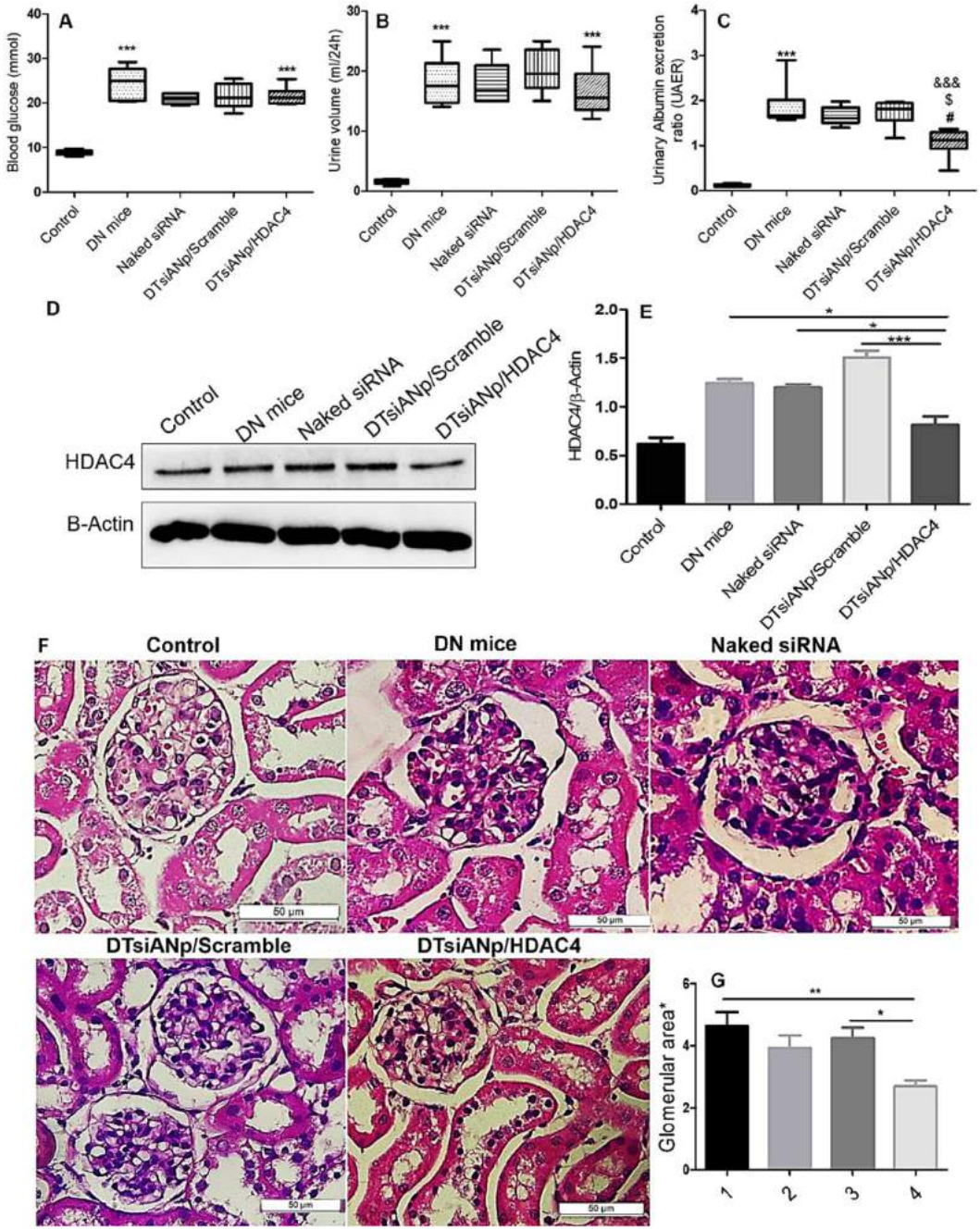


**Figure 6.** (**A**) Mice glucose level, (**B**) urine volume (**C**) Urinary albumin excretion ratio (UAER) in control, DN mice, and treated groups (naked siRNA, DTsiANp/Scramble and DTsiANp/HDAC4), $^{\#}p < 0.05$ vs. naked siRNA, $^{\$}p < 0.05$ vs. DTsiANp/Scramble, $^{\&\&\&}p < 0.001$ vs. DN mice, $^{***}p < 0.0001$; control vs. DN mice (**D**) HDAC4 protein expression in healthy control and DN diseased kidneys as detected by western blot analysis, (**E**) protein levels in kidneys of mice post-treatment. Relative quantification was normalized by β-actin expression $^{*}p < 0.05$ versus DN mice, $^{***}p < 0.001$ vs. DN mice treated with DTsiANp/scramble, $^{*}p < 0.05$ versus DN treated with naked siRNA (**G**) Histological studies of the kidney after 4-week treatment (**F**) glomerular area (*ratio healthy control group) 1; DN mice, 2; Naked siRNA, 3; DTsiANp/Scramble, 4; DTsiANp/HDAC4. $^{**}p < 0.01$ vs. DN mice. Results are represented as mean ± SEM of 5–8 mice/group.

also suggested the existence of significant masses of accumulated mesangial matrix or hyper proliferated mesangial cell and glomerular sclerosis as compared to the control healthy mice group (Fig. 6F–G). It was confirmed through an increased glomerular area ratio by about 4.63 ± 1.35 ($p < 0.001$) of DN over healthy control. Naked siRNA (3.93 ± 1.24 ratio; $p > 0.05$) and DTsiANp/scramble (4.23 ± 1.10; $p > 0.05$) treated mice showed an insignificant change in the glomerular area ratio compared to DN mice group. After 4-week treatment with DTsiANp/HDAC4 glomerular ratio was found 2.69 ± 0.61 ($p < 0.001$ vs. DN mice and $p < 0.05$ vs. DTsiANp/scramble). These

morphological changes in terms of the mean ratio of glomerular area were reduced significantly after treatment of DTsiANp/HDAC4 by 36.49 ± 2.18% ($p < 0.05$) (Fig. 6G) over DTsiANp/scramble treated DN mice.

## Discussion

With years of appreciable research data support, therapeutic potency, as well as a winning Noble Prize of Medicine (Award year 2006; Sir Craig Mello @ Sir Andrew Fire), has greatly enhanced the expectation with RNAi therapeutics[1]. However, due to the lack of an apt siRNA delivery system, the science has greatly stagnated or progressing sluggishly in context to their movement from lab-to-clinic translation[5]. Numerous efforts have been made to come up with an apt siRNA delivery vector with superior delivery attributes, commercial viability, safety as well as high clinical translation capability[17]. There was some extent of success with viral vectors and lipidic transfecting reagents, however, either the safety concerns or the lack of *in vivo* fittingness discourages their clinical utilization. In this meadow, cationic polymeric systems were extensively utilized, however, the toxicity issues associated with them substantially impedes the further development[34,35].

Herein, we report a novel, simple and clinically translatable approach for the encapsulation, stabilization, as well as safe delivery of siRNA using a biocompatible and FDA-approved albumin carrier. It may be noted that the conventional albumin-based siRNA delivery vector was found insufficient, incapable of encapsulating as well as effective homing of siRNA payload in the cytosolic compartment. This can be ascribed to the mismatch in their physiochemical attributes, wherein both being negatively charged[27]. At the same time, conventional albumin siRNA vector lacks the capability to avoid premature siRNA release in blood as well as mediate endo/lysosomal escape in the cellular compartment leading to its substantially reduced efficacy[22]. This scientific report presents a simple protocol based on the unpretentious and scientifically acclaimed phenomenon that can transform albumin to a resourceful biopolymer for siRNA delivery.

The siRNA effectively forms the complex with dendrimer template owing to the existence of opposite electrostatic charges on them[8]. Depending upon the associated *n/p* value, the *d*:siR complex of varying net charge was formed ranging from +24.04 ± 3.52 to +11.57 ± 1.45 mV. Our overall goal was thus to develop a *d*:siR complex of net positive charge and then develop a simple process to load siRNA inside an anionic albumin biopolymer. Hence, at first instance, our target was to develop *d*:siR complex that stably complex siRNA and avoid its degradation. For this, we strategically prepared *d*:siR at varying *d*:siR *n/p* ration and found that at *d*:siR *n/p* value of >0.5 complexation between siRNA and dendrimer was most firm and complete. During gel electrophoresis, the positively charged dye, ethidium bromide can bind with negatively charged siRNA, if available freely and accessible to give proportionate band in Gel Doc instrument (Bio-Rad, USA).

It was found that the *d*:siR forms a stable and viable complex at *n/p* value of 1 and 0.5 as evinced by the inability of ethidium bromide to approach as well as bind siRNA (Fig. 1B,C). From this experiment, we selected *d*:siR *n/p* ration of 0.5 considering the insignificant difference in the property and quality of resulted *d*:siR complex.

The resultant *d*:siR complex was encapsulated inside albumin biopolymer to form siRNA nanoplex (DTsiANp; 64.51 ± 0.83 nm; ζ, −16.1 ± 1.06 mV; PDI: 0.187 ± 0.06). A QbD approach was adapted to attain DTsiANp of average hydrodynamic particle size ≤70 nm. It may be noted that the glomerular fenestrations bear the effective pore size of 70 to 100 nm. A wide array of available literature suggests nanoplex of target size ≤70 nm does not get filtered from the renal pathway but gets passively localized inside the kidney glomerular fenestrations[36–38]. The formed DTsiANp showed an appreciable siRNA encapsulation efficiency of ~75% as confirmed through gel retardation and Ribogreen assay as compared to the nanoplex formed without dendrimer template approach (~15%; classical approach using plain albumin; Fig. 2F).

A prime challenge in *vivo* administration of siRNA lies in their degradation by circulatory RNase enzymes[39]. Hence, the prime requirement of an ideal nanoplex is to ameliorate the encapsulated siRNA as well as prevent its *in vivo* RNase degradation. To deduce this ability, a serum stability study profile of developing nanoplex was studied. It may be noted that the serum interaction of nanoplex comes with an adjusted alternation in the morphology, particle size as well as a surface charge of the nanocomplex. After incubating the developed nanoplexes with the serum, an insignificant change in the morphology, effective particle size, PDI as well as surface zeta potential was noticed (Fig. 3A–C). This infers the inertness of the nanoplex towards the serum, which can be ascribed to the omnipresence of albumin skeleton in the nanoplex. Albumin is a natural biopolymer with its wide availability in the body as well as is known for its inertness[38].

The naked siRNA exposed to the serum was highly prone to undergo degradation by serum RNase enzyme due to the direct accessibility of siRNA with serum (Fig. 4D). Hence, the capability of developed nanoplexes to protect the encapsulated siRNA against serum RNase enzyme was investigated following its gel electrophoresis. Notably, it was found that the siANp lacks the ability to protect siRNA from serum RNase enzyme due to availability of siRNA in loosely bound form. This can be ascribed to the loose and open architect of siANp that makes it directly accessible to the serum RNase enzyme and siRNA was easily degraded within 1 hr under serum condition (Fig. 4E). This also supports our original notion regarding the insufficiency of conventional albumin nanoplex in siRNA delivery, and our concept to bring innovation to albumin architect to make them siRNA delivery capable. The dendrimer templated encapsulation of siRNA in DTsiANp protects the encapsulated siRNA from serum RNase enzyme degradation. Due to the dendrimeric template, the formed DTsiANp gains an electrostatically stable architect as evinced by the stability study. The tight electrostatically stable architect of DTsiANp protects the encapsulated siRNA from coming in direct contact with the serum RNase enzyme and hence protect it from serum degradation (Fig. 4F). Therefore, it can be stated that DTsiANp is capable enough to hold and protect the encapsulated siRNA from serum endonucleases enzyme for more than 24 hr.

Another foremost challenge with siRNA lies in their degradation in the endo-lysosomal compartment. Hence, one of the overarching goals of this research to develop a nanoplex with the capability to escape from the acidic endo-lysosomal compartment. The pH-dependent stability of developed nanoplex was performed at pH 7.4 (to assess physiological stability), pH 5.5 (effect of early endosomal pH), and pH 4.5 (effect of late endosomal pH).

An insignificant change in the particle size of developed DTsiANp was observed following their incubation in physiological pH 7.4 inferring their capability to remain stable under physiological stability. Upon incubation of DTsiANp at pH 5.5 and pH 4.5, a significant and progressive enhancement in their particle size was observed. The increase in particle size of DTsiANp is ascribed to the presence of dendrimer in the architect of nanoplex that elicits pH-responsive '*proton-sponge-effect*'. Our prior research infers the ability of dendrimer to undergo a pH-responsive change in the architecture of dendrimer[40].

The pH-responsive change in the particle size of DTsiANp was corroborated by an analogous change in the surface zeta potential ($p < 0.05$). In the case of DTsiANp, the surface charge was significantly enhanced to more than 50% at pH 4.5 as compared to their original surface charge at pH 7.4 (Fig. 3D,E). The results conclude the pH-responsive behaviour of DTsiANp owing to the existence of free primary amines in dendrimeric template present in the nanoplex. The amine groups of dendrimers undergo protonation under acidic pH leading to enhancement in net surface positive charge. The protonation of the nanoplex assembly under the acidic environment of endosome generates the repulsive microenvironment in the architect of nanoplex. This repulsive microenvironment existing within the nanoplex leads to an increment in its hydrodynamic crevices volume with a marked increase in ionic concentration osmotically. The cumulative enhancement in size of DTsiANp leads to the swelling of the endosomal compartment ultimately leading to the rupture of the endosomal membrane to mediate endosomal escape of DTsiANp. This event liberates the DTsiANp from the endosomal compartment before its degradation by lysozyme (phenomenon referred as endosomal escape). This outcome is in good agreement with our pH-responsive particle size analysis as discussed previously.

This effect was further confirmed by evaluating the pH-responsive change in the surface zeta potential of plain albumin and dendrimer (Fig. S18). There was no significant effect of pH on the characteristic of siANp due to the absence of dendrimeric template in their architect. Further, it may be noted that the changes in the hydrodynamic particle size and zeta potential of DTsiANp as compared to siANp was not due to the siRNA but was predominantly due to the dendrimeric template. This is because the pH has no notable impact on siRNA and vice versa. The observed effect can be ascribed to the protonation behaviour of dendrimeric template present in the nanoplex[41]. Further, DTsiANp showed the localization in the endo/lysosomal compartment in 8 hr as confirmed by yellow fluorescence of co-localized FAM-siRNA and lyo-tracker dye (Fig. S19). After 8 hr, the diffused red fluorescence suggests the escape of DTsiANp from endo/lysosomal compartment which is evidenced via green fluorescence of FAM-siRNA in the cytoplasmic compartment of the cell. The result ascribed that the existence of dendrimeric template in the DTsiANp provided the endosomal escape capability due to proton sponge effect at the endo/lysozymal pH. The prepared nanoplex were found biocompatible when tested on podocytes and as well as on RBCs inferring them to be safe for *in vivo* administration (Fig. 4G–H; $p > 0.05$). The siRNA bears negative charge and hence poses its interaction as well as permeation across the negatively charged plasma membrane[5,8]. The cationized albumin nanoplex bear the capability to undergo endocytosis[41]. In agreement with this property, the cellular uptake of DTsiANp nanoplex shows 4.45-fold higher cellular uptake as compared to naked siRNA (Fig. 5A). Albumin binds to hormone, transferrin, fatty acid and other hydrophobic molecules in serum[42]. The commercial albumin employed for the preparation of nanoplex comes with ~96% purity, may containing fatty contaminants. It is envisaged that the lipidic fractions fatty acid contaminants present in albumin might be responsible for the passive cellular uptake of siANp (mean fluorescence intensity: $14.38 \pm 2.89$) via lipidic cell membrane fusion mechanism. Further, it is advocated that the effect of lipidic fractions fatty acid contaminants on membrane fusion of albumin and albumin-based architectures needs to be explored to reach a statistically meaningful conclusion.

Pathologically, in diabetic (HG) condition, the podocytes show hemodynamic and metabolite changes that result in glomerular lesions and proteinuria[31]. HDAC4 is majorly a central molecule that governs the function regulation in podocytes and is also vital to maintain the integrity of podocytes[33]. It was well reported that in HG condition, the overexpression of HDAC4 induces the inflammation, apoptosis, and autophagy in podocytes. Under HG state, HDAC4 gene primarily contributed to podocytes injury in DN[33]. HG exposed podocytes treated with DTsiANp/HDAC4 showed significantly downregulated HDAC4 mRNA expression ($27.47 \pm 0.27\%$; $p < 0.05$) (Fig. 5C). This effect can be ascribed to the efficient delivery of HDAC4 siRNA to the podocytes by DTsiANp as compared to DTsiANp/scramble and naked HDAC4 siRNA control. The effect of gene silencing on HDAC4 protein was further confirmed by western blot analysis.

In agreement with the qRT-PCR outcomes, the expression of HDAC4 protein was found to be significantly suppressed following the treatment of DTsiANp/HDAC4 nanoplex by more than $44.024 \pm 2.10\%$ ($p < 0.01$), and $45.56 \pm 3.61\%$ ($p < 0.001$) as compared to the naked siRNA and DTsiANp/Scramble treated group *in vitro* (Fig. 5D; $p < 0.05$). The treatment of DTsiANp/HDAC4 in C57BL/6 DN mice model significantly lowered the levels of proteinuria (UAER:$1.07 \pm 0.32$) as compared to DTsiANp/scramble and naked siRNA. It is well reported that the knockdown the overexpressed HDAC4 could able to regulate HG-induced transcriptional activity or deacetylation of STAT1 in podocytes leads to suppress inflammation and apoptosis[29]. The effective reduction in UAER with DTsiANp/ HDAC4 infers the superior therapeutic potential of the developed nanoplex (Fig. 6C).

After the treatment of DTsiANp/ HDAC4, the proportion of damaged glomerulus significantly reduced in the kidneys of C57BL/6 DN mice as observed during the renal histopathological analysis Fig. 6F. Upon treatment of DTsiANp/HDAC4, the glomerular area ratio was reduced by almost 0.32-fold as compared to DTsiANp/scramble treated group. As shown in Fig. 6G, the mean glomerular area was reduced after 4-week treatment of HDAC4 siRNA nanoplex indicating the reduction in glomerular injury and ameliorate the podocytes in DN.

In conclusion, the study provides a novel and simple approach to encapsulate, stabilize and deliver loaded siRNA payload with high efficiency. The concept was established and tested using HDAC4 siRNA, however, the same approach can be extended to diverse gene therapeutics including micro RNA (miRNA), oligonucleotide, DNA, etc. A detailed investigation pertains to safety, scalability, and versatility is currently under exploration in our lab. It is expected that the knowledge reported in the work will significantly assist in research aiming at the

clinical translation of siRNA therapeutics, which is one of the unmet dire need of a clinician and pharmaceutical industry working towards transforming siRNA as a therapeutic modality. Other innovative versions of this strategy including kidney directed nanoplex is also under exploration and it is expected that in near future more research will come in this line to assist development of a more fitting and clinically translatable generally regarded as safe (GRAS) tag bearing nanoplex for the safe delivery of siRNA and other RNAi gene therapeutics.

## Material and Methods

**Materials.** Bovine Serum Albumin-Fraction V was purchased from HiMedia Laboratories GmbH, Germany). Sodium phosphate, sodium chloride, and sodium acetate were purchased from Sigma Aldrich (St. Louis, USA). Scramble (Silencer) 5′-FAM labelled siRNA (sense: 5′-UUCUCCGAACGUGUCACGUdTdT-3′; antisense: 5′-ACGUGACACGUUCGGAGAAdTdT-3′), HDAC4 siRNA (sense: 5′-GGUGCUUAUGGAAAGGGAUTT-3′; antisense: 5′-AUCCCUUUCCAUAAGCACCTT-3′), bicinchoninic acid (BCA) protein assay kit and MTT reagent (3-(4,5-Dimethylthiazol-2-yl)-2,5-Diphenyltetrazolium Bromide) was acquired from Thermo Fisher Scientific (Massachusetts, USA). DEPC treated RNase free water was used for further experimentation with siRNA and procured from Invitrogen (Thermo scientific, Massachusetts, USA). All other reagents and solvents were of analytical grade unless otherwise specified. Agarose and sodium chloride were obtained from Sigma Aldrich (Mumbai, India). RPMI 1640 media, fetal bovine serum (FBS), trypsin-EDTA, penicillin-streptomycin and 1x ITS (Insulin-Transferrin-Selenium) were obtained from Invitrogen and Gibco (Invitrogen, California, USA, Gibco, Life Technologies, Grand Island, USA). Opti-MEM media, Hoechst 33342 were obtained from Gibco, (Life Technologies, Grand Island, USA).

**Cell culture: cell propagation and differentiation.** An immortalized human podocyte cell line was gifted by Dr. Jeffrey Kopp, National in the statute of Health (NIH), Maryland, USA, and the cells were cultured as described earlier[43,44]. In brief, podocytes cells were cultured in RPMI 1640 media comprising 10%v/v FBS, 1x ITS (Insulin-Transferrin-Selenium) and 100 IU/ml penicillin and 100 µg/ml streptomycin sulfate as antibiotics. And cells were grown at 33 ± 0.5 °C under 5% $CO_2$ condition in Type 1 collagen-coated culture tissue culture flask (25 $cm^3$ BD Falcon, Bedford, USA). After 70–80% confluence, cells were shifted to 37 ± 0.5 °C with 5% $CO_2$ for 10–14 days for differentiation. High glucose 20–40 mM (30 mM) condition stimulates the expression of HDAC4 in kidney podocytes[33]. Therefore, *in-vitro* DN model i.e. high glucose model was generated on differentiated podocytes cells (6 well plates; $20 \times 10^4$ cells/well) using 30 mM glucose containing RPMI 1640 with 1%v/v FBS treated for 48 hr[45,46]. Developed *in vitro* DN model of podocytes were used for different assays as mentioned in respective sections.

**Screening of *d*:siR complex.** Dendrimer/siRNA (*d*:siR) complex was prepared by self-assembly method through charged based electrostatic interaction using gentle vortexing[47]. Here, the *d*:siR complexes with different molar ratio were 1:1, 1:2, 1:4 and 1:8 ratio (~1, 0.5, 0.25, and 0.125 *n/p* ratio; (*n*: cationic primary amine groups on polymer, *p*: anionic phosphate groups present on siRNA)). For that, siRNA (200 pmol, 10 µM; 0.266–0.4 µg/µL) was diluted in DEPC treated nuclease-free water and mixed with dendrimer at increasing molecular ratio. For ratios, siRNA and dendrimers were mixed and incubated at room temperature using frequent gentle vertexing (after every 15 min for the 30 s), aid in complex formation. The *d*:siR complex confirmation was done by gel retardation assay and for the surface charge using Malvern zeta sizer ZS-90 (Malvern Instruments, Worcestershire, UK) comprised with He-Ne laser (wavelength: 633 nm).

**Gel retardation assay for determination of *d*:siR ratio.** The gel retardation assay was performed to determine *d*:siR ratio and evaluate the progression of dendrimer-siRNA complex formation. The prepared ratios were mixed with 5 µL of 6X loading dye and volume of the samples were adjusted by nuclease-free water. Accurately, 15 µL total sample (260 ng/well siRNA) volume was load into 2% w/v agarose gel comprising ethidium bromide (2 µg/ml) for siRNA visualization. Gel electrophoresis was done in 1X TBE buffer at 80 V and run for 60 min. The retardation of siRNA inside the dendrimer was imaged using UV transilluminator (Bio-rad, USA)[48].

**Quality-by-Design (QbD) driven optimization of nanoplex preparation methodology.** Albumin nanoplex were prepared using a modified protocol of our laboratory to attain nanoplex of target size (≤70 nm), which as per existing reports bear the capability to reach and localize in the podocytes foot process in DN complications[49]. In brief, plain albumin nanoplex (ANp) were prepared via one-step desolvation technique[29,31]. The utilized albumin purity was initially assessed for presence of any other component from the fraction V albumin using matrix-assisted laser desorption/ionization mass spectrophotometry (MALDI-TOF/MS) and sodium dodecyl sulfate-polyacrylamide gel electrophoresis (SDS-PAGE) (*refer supplementary material*). To prepare ANp, a double quantity of ethanol was added dropwise (1 mL/min) in prepared albumin solution (4%w/v; 1 mL) and left under the stirring condition for 2 hr at 1000 rpm (IKA Magnetic Stirrer (RT 5) Germany). Then, the free amino group of albumin nanoplex was cross-linked with genipin (1%w/v) solution and solution was kept for stirring for a further 2 hr at 700 rpm. The nanoplex preparation was accomplished after purification by centrifugation method at 14,000 g for 25 min. The obtained pellet was resuspended in DEPC treated nuclease-free water up to its original volume. To obtain desired particle size (≤70 nm) of ANp, Quality by design approach was applied as discussed in the supplementary section (*refer supplementary material*).

According to the requirement of the experiment, siRNA (200 pmol; approximately 2.5–3.5 µg/µL in DEPC treated nuclease-free water) loaded inside ANp for siANp. Selected *d*:siR (~0.5 *n/p*) ratio was incubated with (4%w/v; 1 mL) albumin for electrostatic interaction for 2 h at 1000 rpm at (37 ± 0.5 °C) and the solution was desolvated using ethanol to obtain DTsiANp/HDAC4. Here, stoichiometric ratio for nanoplex preparation was 1000:0.066:1::Albumin:siRNA:dendrimer. The physicochemical evaluation was done for particle size, surface zeta potential and polydispersity index (PDI) using Zetasizer Nano ZS 90 (Malvern Instruments, UK). Thereafter,

nanoplex were lyophilized for stability concern using 3%w/v trehalose[50]. Further DEPC treated nuclease-free PBS (1×) was added to the nanoplex for making the final dose and was utilized for administration.

## Characterization of siRNA Nanoplex

**Dynamic light scattering (DLS), SEM, TEM, and AFM.** The prepared and optimized nanoplexs were determined for particle size, polydispersity index (PDI), and zeta potential with the help of Zetasizer (Nano-ZS90, Malvern Instruments, Worcestershire, UK). In brief, suspension of nanoplex was diluted using ultra-pure water and the sample was measured at a fixed angle (173° backscattering). By means of the electrophoretic analyzer, the zeta potential of the nanoplex was measured using Zetasizer (Nano-ZS90, Malvern Instruments, Worcestershire, UK). All the samples were measured at 25 ± 2 °C and the measurements were done in triplicate for evaluation of the efficacy of the results.

Particle size and morphology of prepared nanoplex were determined after lyophilization by means of scanning electron microscopy (SEM) using a JSM-7001FA microscope (JEOL, Tokyo, Japan). Aqueous suspension of nanoplex was kept on a silicon wafer which adheres to a metal stub. Thereafter, mater wafer was dried under vacuum and enclosed with a 20-nm layer of gold. The stubs were observed at an emission of 5.0 kV with 9.5–10.5 mm of working distance[51]. Further, the morphology of DTsiANp was performed through a transmission electron microscope (TEM; Philips, Tecnai 20, Holland; acceleration voltage: 200 kV; magnification: 40,000×). The size of the DTsiANp was measured using AnalySIS software (Soft Imaging Systems, Reutlingen, Germany). A drop of diluted nanoplex was kept on a carbon-coated copper grid. The sample was stained with 1%v/v aqueous solution of phosphotungstic acid and set aside to absorb. After drying, the sample was focused and images were taken[52]. Further, the atomic force microscopy (Probe: SCANASYST-AIR (Modulus range: <20 MPa; k~ 0.4 N/m nominal, tip radius <10 nm typical), AFM; Bruker Multimode 8, Bruker, USA) was also performed for DTsiANp[53]. After characterization of nanoplex, the presence of intact albumin in prepared ANp, DTANp, siANp, and DTsiANp was evaluated by means of SDS-PAGE and BCA reagent assay kit. The dendrimeric template was further confirmed in the nanoplex by TNBSA assay, and the changes in surface charge via zeta potential are represented in supplementary file.

**Determination of siRNA encapsulation efficiency of siRNA nanoplex by Gel retardation assay.** siRNA binding and encapsulation efficiency of *d*:siR ratio with siANp and DTsiANp were determined using agarose gel electrophoresis. Briefly, naked siRNA was taken as a control and the unbound siRNA from siANp and DTsiANp was separated by means of VivaSpin (MW cut-off: 50 kDa; GE Healthcare, Thermo Scientific, USA) at 16,000 g for 10 minutes at 4 °C. The supernatant was collected and the pellet was redispersed in DEPC treated nuclease-free water (Ambion, USA). Then, nanoplex suspension and supernatant (10 µL) were mixed with the 5 µL (6X) loading dye and made a final volume of 15 µL using DEPC treated nuclease-free water (Ambion, USA). The prepared composition was loaded on to 2%w/v agarose gel and run through Tris-borate (TBE) (40 mM Tris-HCl, 1%v/v acetic acid, 1 mM EDTA) buffer at 80 V. The electrophoretic mobility was analysed by ethidium bromide stained gel using an ultraviolet (UV) illuminator (GelDoc, Bio-Rad, USA)[2]. Further, the actual encapsulation of siRNA inside the nanoplex was confirmed using siRNA protection assay. The experimental protocol as stated in the supplementary material.

**Determination of siRNA entrapment efficiency of siRNA nanoplex by Ribogreen assay.** Further, confirmation of encapsulation of siRNA was determined by the amount of extracted siRNA from the lyophilized DTsiANp and siANp as protocol reported by Cun *et al*. with slight modification[54]. For the assay, accurately weighed (1.5 mg) lyophilized nanoplexes was solubilized in 150 µL of chloroform with 500 µL of TE buffer. To extract the siRNA from organic to aqueous phase, the mixture was mixed and rotated continuously at 25 ± 2 °C for about 90 min. Then the mixture was centrifuged at 16,000 g for 25 min at 4 °C to separate an aqueous and organic phase. And the residues of chloroform was removed via incubating the supernatant at 37 ± 2 °C for 5 min. Than the supernatants were diluted with the TE buffer and concentration of the siRNA was measured by means of Ribogreen reagent (Thermo Scientific, USA) based on manufacturer's instruction via multimode plate reader (excitation wavelength: 485 nm and emission wavelength: 520 nm; Varioskan LUX Multimode, Thermo Fisher Scientific, Massachusetts, USA). Analysis of all samples was performed in triplicate. The encapsulation of siRNA was calculated using actual weight of siRNA (ng) in nanoplex upon the whole weight of nanoplex (mg). As well as, the encapsulation of siRNA in nanoplex was also calculated via the given equation as following:

$$siRNA\ encapsulation = \frac{loading\ of\ siRNA}{theoratical\ loading\ of\ siRNA} \quad (1)$$

**Serum stability of siRNA nanoplex.** siRNA was found unstable in serum due to the serum nucleases, therefore, after entrapment of *d*:siR ratio, the stability of siRNA in presence of serum was checked for both siANp and DTsiANp with reference to naked siRNA as stated protocol by Tarantula *et al*. with slight modification[55]. For the assay, naked siRNA (260 ng/well siRNA; 10 µM), 1.5 mg (equivalent to 260 ng/well siRNA) siANp and DTsiANp were taken for the investigation. Nanoplexs and naked siRNA were incubated with an equal volume (50 µL) of RPMI 1640 comprised 10%v/v fetal bovine serum (FBS) at 37 ± 0.5 °C. At defined time interval i.e. 0, 1, 2, 4, 6 and 24 hr, aliquots were centrifuged at 21,000 g for 15 min at 4 °C. The supernatant was removed and pallet stored at −20 °C till gel electrophoresis was executed. After 24 hr of sample collection, the stability of siRNA was assessed by gel electrophoresis. For that, aliquots (10 µL) were mixed with the 5 µL (6X) loading dye and prepared composition was loaded on to 2%w/v agarose gel and run through 1 X TBE (Tris-borate) (40 mM Tris-HCl, 1%

v/v acetic acid, 1 mM EDTA) buffer at 80 V. The electrophoretic mobility was analyzed due to the ethidium bromide using an ultraviolet (UV) illuminator (GelDoc, Bio-Rad, USA).

Furthermore, the effect of serum on particle size, PDI and surface zeta potential was also evaluated for that siAN and DTsiANp were incubated with an equal volume of RPMI 1640 comprised 10%v/v serum concentration at 37 ± 0.5 °C. At predetermined time point 0, 1, 2, 4, 6 and 24 hr, particle size, PDI and surface zeta potential was measured using Zetasizer Nano ZS90 (Malvern Instruments, UK). All the experiments were performed in triplicate at 37 ± 0.5 °C[51].

**Endo/Lysosomal Escape tendency of developed siRNA Nanoplex.** The amino group presented on the terminal end of the dendrimer was sensitive to endosomal pH (acidic)[41]. Therefore, to understand the effect of environmental pH (physiological and endosomal pH) on the siANp and DTsiANp were treated with phosphate buffer saline (pH 7.4), sodium acetate buffer (pH 5; endosomal pH) and acetate buffer (pH 4.5; late endosomal pH) for assessment of stability. The protocol was followed the same as reported by our group earlier with slight amendments[41]. Optimized ANp and DTANp were incubated with the varied buffer for 0, 1, 2, 4, 6 and 24 hr. The particle size, PDI and zeta potential of the nanoplexs was checked at predetermined time points using Zetasizer Nano ZS90 (Malvern Instruments, UK) to evaluate the stability of the nanoplexs. The effect of microenvironmental pH on plain albumin and dendrimer was also evaluated in terms of zeta potential at different time interval via Zetasizer Nano ZS90. All the experiments were performed in triplicate at 25 ± 2 °C. Further, endo/lysosomal escape activity of nanoplex was evaluated with help of lyso-tracker red dye on HG treated podocytes and protocol was as discussed in the supplementary section (*refer supplementary material*).

**Cell viability assay to elucidate biocompatibility of developed siRNA nanoplex.** Initially human kidney podocytes were for cell propagation in 25 $cm^3$ T-flask in RPMI 1640 complete medium (contained 10%v/v FBS, 0.5%v/v Insulin-Transferrin-Selenium (ITS) and 1%w/v penicillin-streptomycin antibiotic mixture) at 33 ± 0.5 °C with 5% $CO_2$ till 60–80% confluence. After that, cells were shifted to 37 ± 0.5 °C with 5% $CO_2$ for differentiation for 10–14 days. Fresh medium was provided to cells for three times a week[56,57]. These differentiated cells were utilized for each experiment. After differentiation, human podocytes cells were seeded in 96 well plates ($1 \times 10^4$ cells/well) and permit to grow overnight in complete RPMI 1640 medium at 37 ± 0.5 °C with 5% $CO_2$. Then, cells were treated with HG (30 mM) to induce *in vitro* DN model for 48 hr. After that, the equivalent amount of ANp, DTANp, siANp, and DTsiANp took for treatment (0.625 mg; 1 pmol siRNA/well and incubated for 24 hr. Afterward, MTT (3-(4,5-Dimethylthiazol-2-yl)-2,5-Diphenyltetrazolium Bromide) reagent was added to the cells (20 µL; 5 mg/ml) and incubated for further 4 hr at 37 ± 0.5 °C with 5% $CO_2$[58]. MTT solution was replaced with 100 µL DMSO to dissolve the formazan crystals. Untreated cells were taken as control with 100% cell viability. The absorbance was measured at 575 nm using UV microplate reader (Multiscan GO, Thermo Fisher Scientific, Massachusetts, USA) at 37 ± 0.5 °C. The viability of cells was calculated as follows[59].

$$Cell\ viability(\%) = \frac{Abs\ (sample)}{Abs\ (control)} \times 100\% \tag{2}$$

**Cellular uptake of siRNA nanoplex in HG podocyte DN model.** To evaluate the internalization, cellular uptake assay was performed on HG treated podocytes as protocol reported by Huang *et al.* with slight modification[60]. Differentiated podocytes cells were seeded into 6-well plate ($2 \times 10^5$ cells/well) with a glass coverslip. Cells were treated with high glucose (30 mM; HG)[31] for 48 hr in presence of serum compromised RPMI 1640 media (1%v/v FBS)[61] to generate *in vitro* DN model. Media was replaced with Opti-MEM comprised FAM-siRNA loaded DTsiANp (30 pmol of siRNA/well; 10 µM). After 12 hr cellular distribution of siRNA was observed using confocal microscopy (Excitation max: 494 nm; Emission max: 520 nm, Leica Microsystems, Wetzlar, Germany)[60].

**Gene silencing efficiency: Quantitative RT-PCR.** Real-time PCR was executed to evaluate the HDAC4 silencing efficiency of HDAC4 loaded nanoplex. Differentiated podocytes cells were grown in 6 well plates ($2 \times 10^5$ cells/ well) in RPMI 1640 complete medium till 60% confluence achieved. Then, media was removed and incubated with HG (30 mM) comprised serum compromised RPMI 1640 media (1%v/v FBS) for 48 hr[61]. Afterward, media was replenished with Opti-MEM containing DTsiANp/ HDAC4 (~30pmol siRNA/well) and incubated for 24 hr. Here, DTsiANp/Scramble selected as a negative control. After treatment, total RNA was extracted using RNeasy mini kit (Qiagen, Hilden, Germany) as stated by manufacturer's protocol and quantified using Nanodrop-2000 spectrophotometer (Thermo Fisher Scientific, Massachusetts, USA). The cDNA was prepared by iscript cDNA synthesis kit (Bio-Rad, California, USA). Then, HDAC4 gene expression was quantified with a 1:10 dilution of cDNA using the iScript SYBR green supermix (Bio-Rad, California, USA) through StepOne Real-time PCR, (Applied Biosystems, California, USA). PCR KiCqStart primers were utilized to amplify 18 s (forward: 5′-GTAACCCGTTGAACCCCATT-3′ and reverse: 5′-CCATCCAATCGGTAGTAGCG-3′) and HDAC4 gene (forward: 5′-AGTGTCGACCTCCTATAACCA-3′ and reverse: 5′-GCTTTAGCCTGGACCGTAAT-3′). The HDAC4 expression level was analyzed via Ct values (cycle threshold). The experiment was performed in triplicate[62].

**HDAC4 expression by western blot analysis: *In vitro* and *in vivo*.** To evaluate the expression of HDAC4 in podocytes cells and mouse model western blot was performed. After differentiation podocytes, cells were seeded in 6 well plates ($2 \times 10^5$ cells/well) in RPMI 1640 complete medium and treated with HG (30 mM) in serum compromised media (RPMI 1640 media with 1%v/v FBS) for 48 hr[31]. DTsiANp/ HDAC4 (30 pmol/ well siRNA; 6.5 mg nanoplex) and DTsiANp/ Scramble was treated for 48 hr. The protein was extracted and lysate resuspended in RIPA lysis buffer comprising 1 µL of protease inhibitor cocktail. Protein concentration from podocytes cell and tissue was estimated using BCA reagent. Protein (25 µg) was separated via SDS-PAGE (acrylamide

gel 10%) and transferred over PVDF membrane using RTA Trans Turbo kit (Bio-Rad, USA). Then, specific protein detection was done using incubation with primary antibody against (HDAC4 1:1000, Abcam, Cambridge, UK) and (β-actin 1:5000, Santacruz, USA) at 4 °C overnight. After completion of incubation with primary antibody, membrane washed with 0.1% TBST following that incubation with HRP-conjugated secondary antibody ((Goat anti-mouse IgG-HRP 1:20000, Santacruz and Goat anti-rabbit IgG-HRP 1:20000, Abcam) at room temperature for 2 hr. Detection of bands were using chemiluminescence substrate (Bio-Rad, USA)). Furthermore, Band intensity was quantified by means of ImageJ software (NIH, Bethesda, MD).

For *in vivo* western blot analysis healthy mice kidney, STZ induced DN control mice and nanoplex treated kidney was homogenate using tissue lyser (Tissue Lyser LT, Qiagen, Germany) and centrifuged (12,000 g for 5 min) for remaining of tissue removal. The collected supernatant was utilized for protein extraction and protein content measurement using BCA reagent and western blots analysis was performed as mentioned procedure above.

**Haemocompatibility assay.** To evaluate the biocompatibility of nanoplex haemocompatibility assay was performed[41,51]. Briefly, rat blood was taken in heparinized vials (5000 I.U./mL, Himedia, Mumbai, India) centrifuged at 1000 g for 10 min for RBCs pallet. The pellet was washed with the 0.9%w/v normal saline (5X). A 2%v/v RBC solution was prepared for experimentation. RBC solution was incubated with ANp, DTANp (1, 2.5 and 5 µg/ml concentrations of dendrimer), saline (0% hemolysis; negative control), and Triton X-100 (0.1%v/v) (100% hemolysis; positive control) for 2 hr at 37 ± 0.5 °C to allow interaction. After 2 hr, the suspension was centrifuged at 1000 g for 10 min and the supernatant obtained in each group was analyzed for the hemoglobin content via absorbance at 540 nm using UV microplate reader (Varioskan LUX Multimode, Thermo Fisher Scientific, Massachusetts, USA). The percentage of hemolysis was determined by using the following equation:

$$\%Hemolysis = 100 \times \frac{(Abs.\ Sample - Abs.\ Negative\ Control)}{(Abs.\ Positive\ Control - Abs.\ Negative\ Ccontrol)} \quad (3)$$

where Abs. Sample detonated for Absorbance of the sample, Absorbance of the negative control (0.9%w/v saline), Absorbance of positive control (Triton-X).

**Experimental Animal model and treatment.** All animal studies were performed in accordance with guidelines and protocols with National Institute of pharmaceutical education and research (NIPER) Guidelines for Care and Use of Laboratory Animals. All procedures and protocols followed in this study were approved by Institutional Animal Ethics Committee (IAEC) at NIPER-Ahmedabad, Gujarat, India vide approval letter number: NIPER-A/IAEC/2017/034. C57BL/6 male mice (average body weight: 18–23 g) (Supplier: Zydus Research Centre, Ahmedabad) were injected with 50 mg/kg of streptozotocin (STZ) (0.1 M citrate buffer (pH 4.5) intraperitoneally on 5 consecutive days to circumvent acute toxicity of STZ. Control animal was received citrate buffer only. Confirmation of diabetes was done through tail vein blood glucose levels (fasting glucose > 12 mmol; Accu Chek-Active glucometer, Roche, USA). Mice were divided randomly into an experimental group (per group six mice). All mice were sacrificed at 4 weeks post-injection of naked HDAC4 siRNA, DTsiANp/scramble, DTsiANp/HDAC4 to diabetes mice. The developed siRNA nanoplex was given to mouse via tail vein at 1 mg/kg dose for twice a week. After treatment, from the freshly harvested kidney glomerular portion was isolated from half kidney and homogenate the using tissue lyser (TissueLyser LT, Qiagen, Germany) then centrifuged (12,000 g for 5 min) to remove tissue remains. The supernatant was collected for protein extraction for Western blots analysis[63]. Other half portion was fixed in formalin for histological evaluation of glomeruli. Later completion of treatment, urinary albumin concentrations were measured with the Albumin mouse ELISA kit (ab108792, Abcam, Cambridge, UK) and represented as urine albumin excretion ratio (UAER)[64].

**Renal histopathological analysis.** Isolated kidney tissue was taken for histological evaluation, fixed in 4% paraformaldehyde and embedded in paraffin. 5-µm thick sections were processed for hematoxylin and eosin staining according to manufacturer's protocol. Morphological evaluation and semi-quantitative analysis of section were done for the glomerular area for glomerular injury using ImageJ software. The glomerular area was determined via ImageJ software using 15 random cortex region image per mouse under a low magnification field of vision (400×)[65].

**Statistical analysis.** Results are represented as mean ± S.D or mean ± SEM. Statistical differences among the groups were assessed by means of one-way analysis of variance (ANOVA) for *in vitro* and *in vivo* data analysis. Following that Bonferroni's post-test was applied to all pair of columns with control as well. $p < 0.05$ was considered significant. Statistical analysis was done through Graph Pad Prism (GraphPad software, SPSS, Chicago, IL, USA).

## Data availability

The author's consent to make materials, data and associated protocols promptly available to readers without undue qualifications in material transfer agreements.

Received: 12 June 2019; Accepted: 12 October 2019;
Published online: 05 November 2019

## References

1. Setten, R. L., Rossi, J. J. & Han, S.-P. The current state and future directions of RNAi-based therapeutics. *Nature Reviews Drug Discovery*, **1** (2019).
2. Youngren, S. R., Tekade, R. K., Gustilo, B., Hoffmann, P. R. & Chougule, M. B. STAT6 siRNA matrix-loaded gelatin nanocarriers: formulation, characterization, and *ex vivo* proof of concept using adenocarcinoma cells. *BioMed research international* **2013** (2013).

3. Kumar Tekade, R., GS Maheshwari, R., Sharma, A., Tekade, P. & Singh Chauhan, M. A. siRNA therapy, challenges and underlying perspectives of dendrimer as delivery vector. *Current pharmaceutical design* **21**, 4614–4636 (2015).
4. Zhu, J. *et al*. Dual-responsive polyplexes with enhanced disassembly and endosomal escape for efficient delivery of siRNA. *Biomaterials* **162**, 47–59 (2018).
5. Aagaard, L. & Rossi, J. J. RNAi therapeutics: principles, prospects and challenges. *Advanced drug delivery reviews* **59**, 75–86 (2007).
6. Almutiri, S., Berry, M., Logan, A. & Ahmed, Z. Non-viral-mediated suppression of AMIGO3 promotes disinhibited NT3-mediated regeneration of spinal cord dorsal column axons. *Scientific reports* **8** (2018).
7. Majowicz, A. *et al*. Successful repeated hepatic gene delivery in mice and non-human primates achieved by sequential administration of AAV5ch and AAV1. *Molecular Therapy* **25**, 1831–1842 (2017).
8. Yin, H. *et al*. Non-viral vectors for gene-based therapy. *Nature Reviews Genetics* **15**, 541 (2014).
9. Nakamura, T. *et al*. Small-sized, stable lipid nanoparticle for the efficient delivery of siRNA to human immune cell lines. *Scientific reports* **6**, 37849 (2016).
10. Kasuya, T. *et al*. Ribonuclease H1-dependent hepatotoxicity caused by locked nucleic acid-modified gapmer antisense oligonucleotides. *Scientific reports* **6**, 30377 (2016).
11. Kasinski, A. L. *et al*. A combinatorial microRNA therapeutics approach to suppressing non-small cell lung cancer. *Oncogene* **34**, 3547 (2015).
12. Nair, J. K. *et al*. Multivalent N-acetylgalactosamine-conjugated siRNA localizes in hepatocytes and elicits robust RNAi-mediated gene silencing. *Journal of the American Chemical Society* **136**, 16958–16961 (2014).
13. Orellana, E. A. *et al*. FolamiRs: Ligand-targeted, vehicle-free delivery of microRNAs for the treatment of cancer. *Science translational medicine* **9**, eaam9327 (2017).
14. Whitehead, K. A. *et al*. Degradable lipid nanoparticles with predictable *in vivo* siRNA delivery activity. *Nature communications* **5**, 4277 (2014).
15. Morrison, C. Alnylam prepares to land first RNAi drug approval. *Nature Reviews Drug Discovery* **17**, 156–157 (2018).
16. Adams, D. *et al*. Patisiran, an RNAi therapeutic, for hereditary transthyretin amyloidosis. *New England Journal of Medicine* **379**, 11–21 (2018).
17. Kauffman, K. J., Webber, M. J. & Anderson, D. G. Materials for non-viral intracellular delivery of messenger RNA therapeutics. *Journal of Controlled Release* **240**, 227–234 (2016).
18. Villar-Alvarez, E. *et al*. siRNA Silencing by Chemically Modified Biopolymeric Nanovectors. *ACS Omega* **4**, 3904–3921 (2019).
19. Zhao, Y. *et al*. Fine Tuning of Core–Shell Structure of Hyaluronic Acid/Cell-Penetrating Peptides/siRNA Nanoparticles for Enhanced Gene Delivery to Macrophages in Antiatherosclerotic Therapy. *Biomacromolecules* **19**, 2944–2956 (2018).
20. Copolovici, D. M., Langel, K., Eriste, E. & Langel, U. Cell-penetrating peptides: design, synthesis, and applications. *ACS nano* **8**, 1972–1994 (2014).
21. Fakih, H. H., Fakhoury, J. J., Bousmail, D. & Sleiman, H. F. Minimalist Design of a Stimuli-Responsive Spherical Nucleic Acid for Conditional Delivery of Oligonucleotide Therapeutics. *ACS applied materials & interfaces* (2019).
22. Wu, C., Li, J., Wang, W. & Hammond, P. T. Rationally designed polycationic carriers for potent polymeric siRNA-mediated gene silencing. *ACS nano* **12**, 6504–6514 (2018).
23. Elzoghby, A. O., Samy, W. M. & Elgindy, N. A. Albumin-based nanoparticles as potential controlled release drug delivery systems. *Journal of controlled release* **157**, 168–182 (2012).
24. Houghton, P. J. *et al*. Initial testing (stage 1) of the tubulin binding agent nanoparticle albumin-bound (nab) paclitaxel (Abraxane®) by the Pediatric Preclinical Testing Program (PPTP). *Pediatric blood & cancer* **62**, 1214–1221 (2015).
25. Wu, L. *et al*. Albumin-based nanoparticles as methylprednisolone carriers for targeted delivery towards the neonatal Fc receptor in glomerular podocytes. *International journal of molecular medicine* **39**, 851–860 (2017).
26. Kratz, F. Albumin as a drug carrier: design of prodrugs, drug conjugates and nanoparticles. *J Control Release* **132**, 171–183, https://doi.org/10.1016/j.jconrel.2008.05.010 (2008).
27. Wen, H., Yin, Y., Huang, C., Pan, W. & Liang, D. Encapsulation of RNA by negatively charged human serum albumin via physical interactions. *Science China. Chemistry* **60**, 130–135 (2017).
28. Hadden, M. & Advani, A. Histone deacetylase inhibitors and diabetic kidney disease. *International journal of molecular sciences* **19**, 2630 (2018).
29. Wei, Q. & Dong, Z. HDAC4 blocks autophagy to trigger podocyte injury: non-epigenetic action in diabetic nephropathy. *Kidney international* **86**, 666–668 (2014).
30. Singh, H. D., Wang, G., Uludağ, H. & Unsworth, L. D. Poly-L-lysine-coated albumin nanoparticles: stability, mechanism for increasing *in vitro* enzymatic resilience, and siRNA release characteristics. *Acta biomaterialia* **6**, 4277–4284 (2010).
31. Zhou, Z. *et al*. MicroRNA-27a promotes podocyte injury via PPARγ-mediated β-catenin activation in diabetic nephropathy. *Cell death & disease* **8**, e2658 (2017).
32. Huang, G. *et al*. Notoginsenoside R1 attenuates glucose-induced podocyte injury via the inhibition of apoptosis and the activation of autophagy through the PI3K/Akt/mTOR signaling pathway. *International journal of molecular medicine* **39**, 559–568 (2017).
33. Wang, X. *et al*. Histone deacetylase 4 selectively contributes to podocyte injury in diabetic nephropathy. *Kidney international* **86**, 712–725 (2014).
34. Am Hong, C., Son, H. Y. & Nam, Y. S. Layer-by-layer siRNA/poly (L-lysine) Multilayers on Polydopamine-coated Surface for Efficient Cell Adhesion and Gene Silencing. *Scientific reports* **8**, 7738 (2018).
35. Monnery, B. D. *et al*. Cytotoxicity of polycations: relationship of molecular weight and the hydrolytic theory of the mechanism of toxicity. *International journal of pharmaceutics* **521**, 249–258 (2017).
36. Du, B., Yu, M. & Zheng, J. Transport and interactions of nanoparticles in the kidneys. *Nature Reviews Materials*, **1** (2018).
37. Chen, D. *et al*. Kidney-targeted drug delivery via rhein-loaded polyethyleneglycol-co-polycaprolactone-co-polyethylenimine nanoparticles for diabetic nephropathy therapy. *International journal of nanomedicine* **13**, 3507 (2018).
38. Tan, Y. L. & Ho, H. K. Navigating albumin-based nanoparticles through various drug delivery routes. *Drug discovery today* **23**, 1108–1114 (2018).
39. Wu, Z. *et al*. Tumor Microenvironment-Response Calcium Phosphate Hybrid Nanoparticles Enhanced siRNAs Targeting Tumors *In Vivo*. *Journal of biomedical nanotechnology* **14**, 1816–1825 (2018).
40. Tekade, R. K. & Chougule, M. B. Formulation development and evaluation of hybrid nanocarrier for cancer therapy: Taguchi orthogonal array based design. *BioMed research international* **2013** (2013).
41. Tekade, R. K., Tekade, M., Kumar, M. & Chauhan, A. S. Dendrimer-stabilized smart-nanoparticle (DSSN) platform for targeted delivery of hydrophobic antitumor therapeutics. *Pharmaceutical research* **32**, 910–928 (2015).
42. Coverdale, J. P., Khazaipoul, S., Arya, S., Stewart, A. J. & Blindauer, C. A. Crosstalk between zinc and free fatty acids in plasma. *Biochimica et Biophysica Acta (BBA)-Molecular and Cell Biology of Lipids* (2018).
43. Kopp, J. B. & Heymann, J. c-Src is in the effector pathway linking uPAR and podocyte injury. *The Journal of clinical investigation* **129** (2019).
44. Saleem, M. A. *et al*. A conditionally immortalized human podocyte cell line demonstrating nephrin and podocin expression. *Journal of the American Society of Nephrology* **13**, 630–638 (2002).
45. Liu, B.-C. *et al*. High glucose induces podocyte apoptosis by stimulating TRPC6 via elevation of reactive oxygen species. *Biochimica et Biophysica Acta (BBA)-Molecular Cell Research* **1833**, 1434–1442 (2013).

46. Imasawa, T. *et al*. High glucose repatterns human podocyte energy metabolism during differentiation and diabetic nephropathy. *The FASEB Journal* **31**, 294–307 (2016).
47. Greco, C. T., Muir, V. G., Epps, T. H. III & Sullivan, M. O. Efficient tuning of siRNA dose response by combining mixed polymer nanocarriers with simple kinetic modeling. *Acta biomaterialia* **50**, 407–416 (2017).
48. Sarett, S. M. *et al*. Hydrophobic interactions between polymeric carrier and palmitic acid-conjugated siRNA improve PEGylated polyplex stability and enhance *in vivo* pharmacokinetics and tumor gene silencing. *Biomaterials* **97**, 122–132 (2016).
49. Wang, J., Masehi-Lano, J. J. & Chung, E. J. Peptide and antibody ligands for renal targeting: nanomedicine strategies for kidney disease. *Biomaterials science* **5**, 1450–1459 (2017).
50. Wang, L. *et al*. Cryoprotectant choice and analyses of freeze-drying drug suspension of nanoparticles with functional stabilisers. *Journal of microencapsulation* **35**, 241–248 (2018).
51. Muniswamy, V. J. *et al*. 'Dendrimer-Cationized-Albumin'encrusted polymeric nanoparticle improves BBB penetration and anticancer activity of doxorubicin. *International journal of pharmaceutics* **555**, 77–99 (2019).
52. Raval, N., Khunt, D. & Misra, M. Microemulsion-based delivery of triamcinolone acetonide to posterior segment of eye using chitosan and butter oil as permeation enhancer: an *in vitro* and *in vivo* investigation. *Journal of microencapsulation* **35**, 62–77 (2018).
53. Vergaro, V. *et al*. Interaction between human serum albumin and different anatase TiO2 nanoparticles: A nano-bio interface study. *Nanomaterials and Nanotechnology* **5**, 30 (2015).
54. Cun, D. *et al*. High loading efficiency and sustained release of siRNA encapsulated in PLGA nanoparticles: quality by design optimization and characterization. *European Journal of Pharmaceutics and Biopharmaceutics* **77**, 26–35 (2011).
55. Taratula, O. *et al*. Surface-engineered targeted PPI dendrimer for efficient intracellular and intratumoral siRNA delivery. *Journal of Controlled Release* **140**, 284–293 (2009).
56. Perche, F., Patel, N. R. & Torchilin, V. P. Accumulation and toxicity of antibody-targeted doxorubicin-loaded PEG–PE micelles in ovarian cancer cell spheroid model. *Journal of controlled release* **164**, 95–102 (2012).
57. Shankland, S., Pippin, J., Reiser, J. & Mundel, P. Podocytes in culture: past, present, and future. *Kidney international* **72**, 26–36 (2007).
58. Zhang, H., Kong, X., Tang, Y. & Lin, W. Hydrogen Sulfide Triggered Charge-Reversal Micelles for Cancer-Targeted Drug Delivery and Imaging. *ACS applied materials & interfaces* **8**, 16227–16239 (2016).
59. Ji, S. *et al*. RGD-conjugated albumin nanoparticles as a novel delivery vehicle in pancreatic cancer therapy. *Cancer biology & therapy* **13**, 206–215 (2012).
60. Liu, J. *et al*. Integrin-targeted pH-responsive micelles for enhanced efficiency of anticancer treatment *in vitro* and *in vivo*. *Nanoscale* **7**, 4451–4460 (2015).
61. Oe, Y. *et al*. Actively-targeted polyion complex micelles stabilized by cholesterol and disulfide cross-linking for systemic delivery of siRNA to solid tumors. *Biomaterials* **35**, 7887–7895 (2014).
62. Weber, N. *et al*. Characterization of carbosilane dendrimers as effective carriers of siRNA to HIV-infected lymphocytes. *Journal of Controlled Release* **132**, 55–64 (2008).
63. Jha, J. C. *et al*. Podocyte-specific Nox4 deletion affords renoprotection in a mouse model of diabetic nephropathy. *Diabetologia* **59**, 379–389 (2016).
64. Gai, Z. *et al*. Uninephrectomy augments the effects of high fat diet induced obesity on gene expression in mouse kidney. *Biochimica et Biophysica Acta (BBA)-Molecular Basis of Disease* **1842**, 1870–1878 (2014).
65. Grange, C. *et al*. Stem cell-derived extracellular vesicles inhibit and revert fibrosis progression in a mouse model of diabetic nephropathy. *Scientific reports* **9**, 4468 (2019).


## Acknowledgements

The research was carried out at National Institute of Pharmaceutical Education and Research-Ahmedabad with the financial support from the Department of Pharmaceuticals, Ministry of Chemicals and Fertilizers, Government of India. RKT would like to acknowledge Science and Engineering Research Board (Statutory Body Established through an Act of Parliament: SERB Act 2008), Department of Science and Technology, Government of India for a grant (Grant #ECR/2016/001964) and N-PDF funding (PDF/2016/003329) for work on targeted gene therapy in Dr. Tekade's Laboaratory. The authors would also like to acknowledge Dr. Jeffrey Kopp, National in the statute of Health (NIH), Maryland, the USA for the gift sample of the immortalized human podocyte cell line.

## Author contributions

Nidhi Raval (Conceptualization, Data curation, Formal analysis, Investigation, Methodology, Writing – original draft); Hardi Jogi (Data curation, Formal analysis, Investigation, methodology); Piyush Gondaliya (Investigation, Methodology); Kiran Kalia (Resources, Methodology); Rakesh Kumar Tekade (Conceptualization, Project administration, Supervision, Resources, Formal analysis, Writing – original draft, Reviewing of draft).

## Competing interests

**Financial Competing Interests**. The authors report a conflict of interest. The work described in this manuscript has been filed for Indian patent at Indian Patent Office (IPO), Mumbai, India; Application No.: 201921019898; Date of Application: 18/05/2019. **Non-Financial Competing Interests**. The paper reports the study on the immortalized human podocyte cell line, which was received as a free gift sample from Dr. Jeffrey Kopp, National in the statute of Health (NIH), Maryland, the USA. The research is an output of Ph.D. research work of Ms. Nidhi Raval under the mentorship of Dr. Rakesh K. Tekade carried out at NIPER-Ahmedabad by the financial support from the Department of Pharmaceuticals, Ministry of Chemicals and Fertilizers, Government of India as a senior research fellow.

## Additional information

**Supplementary information** is available for this paper at https://doi.org/10.1038/s41598-019-52390-4.

**Correspondence** and requests for materials should be addressed to R.K.T.

**Reprints and permissions information** is available at www.nature.com/reprints.

**Publisher's note** Springer Nature remains neutral with regard to jurisdictional claims in published maps and institutional affiliations.

molecular pharmaceutics

pubs.acs.org/molecularpharmaceutics

Article

# Cyclo-RGD Truncated Polymeric Nanoconstruct with Dendrimeric Templates for Targeted HDAC4 Gene Silencing in a Diabetic Nephropathy Mouse Model

Nidhi Raval, Hardi Jogi, Piyush Gondaliya, Kiran Kalia, and Rakesh K. Tekade*

Cite This: *Mol. Pharmaceutics* 2021, 18, 641−666

Read Online

ACCESS | Metrics & More | Article Recommendations | Supporting Information

**ABSTRACT:** Diabetic nephropathy (DN), a chronic progressive kidney disease, is a significant complication of diabetes mellitus. Dysregulation of the histone deacetylases (HDACs) gene has been implicated in the pathogenesis of DN. Hence, the HDAC-inhibitors have emerged as a critical class of therapeutic agents in DN; however, the currently available HDAC4-inhibitors are mostly nonselective in nature as well as inhibit multiple HDACs. RNA interference of HDAC4 (HDAC4 siRNA) has shown immense promise, but the clinical translation has been impeded due to lack of a targeted, specific, and *in vivo* applicable delivery modality. In the present investigation, we examined Cyclo(RGDfC) (cRGD) truncated polymeric nanoplex with dendrimeric templates for targeted HDAC4 Gene Silencing. The developed nanoplex exhibited enhanced encapsulation of siRNA and offered superior protection against serum RNase nucleases degradation. The nanoplex was tested on podocytes (*in vitro*), wherein it showed selective binding to the $\alpha v\beta 3$ integrin receptor, active cellular uptake, and significant *in vitro* gene silencing. The *in vivo* experiments showed remarkable suppression of the HDAC4 and inhibition in the progression of renal fibrosis in the Streptozotocin (STZ) induced DN C57BL/6 mice model. Histopathological and toxicological studies revealed nonsignificant abnormality/toxicity with the nanoplex. Conclusively, nanoplex was found as a promising tactic for targeted therapy of podocytes and could be extended for other kidney-related ailments.

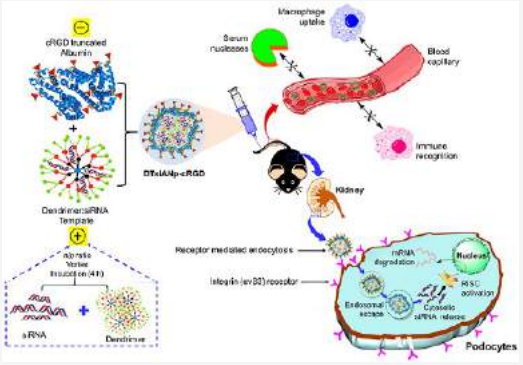


**KEYWORDS:** *gene silencing, siRNA delivery, diabetic nephropathy, polymeric nanoplex, in vitro podocytes diabetic nephropathy, diabetic nephropathy mice model*

## 1. INTRODUCTION

Diabetic nephropathy (DN), chronic progressive kidney disease is one of the severe impediments of diabetes. The main hallmark for the advancement of diabetes to DN is microalbuminuria due to the loss of the podocyte's foot process.[1] Available treatment strategies mostly involve glucocorticoids, calcineurin inhibitors, rituximab, renin-angiotensin-aldosterone system inhibitors, others mostly offer symptomatic relief and are regarded as partially active on podocytes.[2] In DN, hyperglycemia and metabolic deviations are accompanied by gene alternations in a coordinated way. In this context, histone deacetylases (HDAC4) have been implicated univocally in the pathogenesis of DN.[3] In the hyperglycemic condition of the diabetic kidney cytokines, advanced glycation end-products (AGEs) and oxidative stress are elevated. The excess of HDAC4 in renal podocytes deacetylate STAT1, which undergoes phosphorylation and enters inside the nucleus to mediate autophagy, inflammation, and apoptosis that cumulatively leads to podocytes injury. It is an essential cellular process that has been largely advocated to be checked to protect the podocytes from injury as well as apoptosis. However, the available HDAC inhibitors (like trichostatin, vorinostat, valproic acid, etc.) are mostly nonselective. They primarily suppress multiple HDAC proteins that demand a larger dose to be administered to effectively inhibit the renal HDAC. Therefore, HDAC4 represents a potent therapeutic modality that can specifically silence HDAC4.[4]

With immense potency, selectivity, and therapeutic potential of the RNA-interference (RNAi) technique, silencing HDAC4 by using small interfering RNA (siRNA) (HDAC4 siRNA) represents a viable as well as a next-generation tool to counter dysregulated HDAC4 in DN. siRNAs can selectively degrade a specific sequence of a complementary RNA molecule to mediate selective gene silencing for a target protein. The 2006 Nobel Prize of medicine has recognized the medical potential

**Special Issue:** Nanomedicines Beyond Cancer

**Received:** January 29, 2020
**Revised:** April 30, 2020
**Accepted:** May 4, 2020
**Published:** May 26, 2020







https://dx.doi.org/10.1021/acs.molpharmaceut.0c00094
*Mol. Pharmaceutics* 2021, 18, 641−666

of this approach to Craig Mello and Andrew Fire. Recently, Alnylam announced the first-ever U.S. food and drug administration (USFDA) approved RNAi therapeutic loaded lipidic nanoparticle (LNP), ONPATTRO (Patisiran; ionizable cationic lipid: distearoly phosphatidycholine (DSPC): cholesterol: PEG-lipid) for the treatment of the polyneuropathy of hereditary transthyretin-mediated amyloidosis in adults. While ONPATTRO is primarily passive and lacks precise uptake in the site of action due to the absence of targeting ligand,[5] it may be noted that despite its immense therapeutic potential, the bench-to-bedside translation of siRNA has been largely impeded or unsuccessful. The prime barriers that impede the clinical translation of siRNA therapeutics have been ascribed to the lack of a fit-to-purpose delivery system.[6] The prime challenges associated with siRNA delivery involve its rapid renal clearance, short half-life ($t_{1/2}$), degradation by circulatory serum RNase as well as deprived specificity toward the target tissue.[7] Degradation of delivered free siRNA in the endolysosomal compartment is another issue that needs attention due to the presence of an endolysosomes enzyme in an acidic environment (pH 5.5−4.5). Due to this cellular internalized and endosomal entrapped free siRNA degrades, lost its function to initiate RNAi mechanism in the cytoplasm, and thus limits its gene silencing efficiency.[8]

To resolve this issue, viral vector-based vectors were explored, but the stimulation of a host immune cascade through the generation of neutralizing antibodies was reported as a major drawback that has discouraged further developments in such projects. Liposomes represent successful delivery systems that have already made their way to the market as lipid-based siRNA delivery vectors siRNA viz. such as Lipofectamine,[9] Oligofectamine,[10] RNAifect,[11] etc. have been applied for the delivery of siRNA. However, Invivofectamine has been developed to deliver siRNA, but its application is limited to delivering siRNA to the liver.[12] However, dismal bioavailability, *in vivo* quandary, and passive biodistribution compromises the selection of gene silencing that leads to inferior therapeutic efficacy.[13,14] Cell-penetrating peptides (CPP) emerged as a potential option for the siRNA delivery tool, but its applicability is hindered due to cellular toxicity concerns.[15] The cationic polymeric constructs such as polyethylenimine,[16] ethylenediamine,[17] poly(propyleneimine),[18] poly(lysine),[19] etc. showed some promise for siRNA delivery. While its higher cationic charge limits its applicability at the cellular level.[20] In recent years, a paradigm shift has been observed in the hope of investigators toward polymeric nanoconstructs to develop a clinically viable siRNA delivery vector that is capable of efficiently loading and mediating safe *in vivo* delivery of siRNA toward target tissue.[21]

In this context, albumin, a natural biopolymer, represents a versatile platform with countless biopharmaceutical benefits such as its innate nature, nonimmunogenicity, high biocompatibility, ease of surface modification, and biodegradation aptitude to name a few. Albumin is a US-FDA approved biopolymer, and albumin-based products have already made their way to the market (e.g., Abraxane; Celgene Corporation, USA). Besides, albumin is also able to localize in the podocytes foot process in DN complications as reported by Wang et al.[22] However, for the delivery of siRNA, it has been found that the characteristic anionic architectural configuration of albumin does not afford adequate and stable loading of anionic siRNA that results in inferior loading efficiency as well as premature siRNA release.[23] Reports from our group infer albumin-based vectors to be inefficient to mediate endolysosomal escape that leads to a substantial loss to siRNA therapeutics in the harsh endolysosomal environment.[24]

This necessitates innovation in the development of albumin as a siRNA delivery vector. Hence, this investigation essentially aims to develop a fit-to-purpose delivery approach with high siRNA loading efficiency, pH-responsive endosomal escape machinery, serum RNase stability, and targeted HDAC4 silencing. We test our hypothesis in using kidney podocyte cells as well as in the DN bearing mouse model. It may be noted that HDAC4 siRNA is utilized in this study as one of the RNAi therapeutics that can be delivered by this approach. As a prototype, siRNA and it is being proposed that the reported strategy can be extended to other classes of RNAi therapeutics, namely microRNA (miRNA), small hairpin RNA (shRNA), etc.

Reports suggest that nanoparticles of size 10 nm undergo rapid renal clearance and are not able to be retained in the kidney.[25] Under normal physiological conditions, glomerular endothelium forms the first component of the glomerular filtration barrier that has the fenestrations of diameter ≈150 nm. After glomerular endothelium, the glomerular basement membrane filters the small molecules (3−10 nm) based on size and charge.[26−28] Then, besides the glomerular basement membrane, the interdigitating foot process of podocytes contains the small gap with adjacent progressions connected via glomerular filtration slits. The slit diaphragm of podocytes bears a highly specialized gap connection with size of 30−40 nm.[27,28]

In the case of diabetic kidney complications, the irregular thickening of the glomerular basement membrane generates the uneven fenestration in the glomerular basement membrane with a size pore size of 10−80 nm.[29,30] This glomerular basement membrane was connected with the podocytes anchored integrin (mainly the $\alpha_v\beta_3$ integrin).[26] This podocyte integrin played an important role in DN, making the nanoparticle for selective cellular uptake.[26] This cell-receptor binding affinity was observed via *ex vivo* studies of primary podocytes which were performed by Pollinger et al. where $\alpha_v\beta_3$ receptor selective cRGD modified quantum dots were selectively uptaken to the primary podocytes cells.[31] Therefore, in this investigation to avoid an off-target effect as well as to facilitate receptor directed cellular uptake, we selected cyclo(Arg-Gly-Asp-D-Phe-Cys) (cyclo(RGDfC)) as a sensitive integrin ($\alpha_v\beta_3$) receptor ligand.[32] The overexpression of vascular endothelial factors (VEGF), basic fibroblast growth factor (bFGF), and transforming growth factor (TNF$\alpha$) and other cytokines induces the expression of $\alpha_v\beta_3$ receptors on the surface of podocytes.[33]

Hence, albumin was modified with (cyclo(RGDfC); cRGD) using m-maleimidobenzoyl *N*-hydroxysuccinimide (MBS) cross-linker. Further to tackle the issue of low siRNA loading efficiency, the stability of siRNA, as well as offer serum RNase protection, a versatile dendrimeric template approach has been explored for the first-time to load HDAC4 inside albumin nanovector. Due to the presence of a multivalent highly branched surface with peripheral cationic amino group, the poly amidoamine dendrimer (PAMAM, 2.0G) electrostatically interacts with the phosphate backbone containing anionic siRNA therapeutics that result in the formation of a dendrimer:siRNA (*d*:siR) complex (*refer table of contents graphic*). As reported by our group, the dendrimer complex is able to stabilize siRNA from degradation, increase the shelf life


https://dx.doi.org/10.1021/acs.molpharmaceut.0c00094
Mol. Pharmaceutics 2021, 18, 641−666

of siRNA, lower cytotoxicity, enhance cellular uptake, selectively undergo protonation under acidic endosomal environment, and increase transfection efficiency.[24,34,35] Hence, the dendrimer template approach was strategically adapted to mediate endolysosomal escape following receptor-mediated endocytosis of cRGD targeted nanoplex as developed in this study (Indian patent at Indian Patent Office (IPO), Mumbai, India; Application No.: 201921019898; Date of Application: 18/05/2019).[36]

The prototype formulation method and composition for encapsulation, stabilization, and passive delivery of siRNA comprised albumin polymeric nanoplex was evaluated for the *in vitro* as well as *in vivo* DN model reported in our previous report by our group in *Scientific Reports*.[36] This is a follow-up investigation wherein the author reports the development of a fit-to-purpose targeted approach for the delivery of HDAC4 siRNA specifically to kidney podocytes via $\alpha_v\beta_3$ integrin. The prepared cRGD truncated albumin nanoplex with the dendrimeric template was designed, optimized, and evaluated for siRNA loading efficiency, serum stability, blood biocompatibility, and endonuclease RNase protection. The receptor-mediated targeting, specific cellular uptake kinetics, and targeted gene silencing ability of siRNA nanoplex was assessed and evaluated in an *in vitro* podocytes DN model and confirmed through cRGD receptor competition assay. The endosomal escape tendency of developed siRNA nanoplex was a prime claim of this project and was assessed using the lysotracker assay. Finally, the gene silencing effect, toxicological study, as well as histological evaluation of targeted nanoplex is also demonstrated in streptozotocin (STZ)-induced C57BL/6 DN mice model *in vivo*.

## 2. EXPERIMENTAL SECTION

**2.1. Materials and Reagents.** Albumin (Bovine Serum Albumin), PAMAM dendrimer (2.0G), sodium phosphate, sodium chloride, and sodium acetate were purchased from Sigma-Aldrich, Missouri, USA. MBS, m-maleimidobenzoyl *N*-hydroxysuccinimide, was purchased from Sigma-Aldrich, Missouri, USA. The bicinchoninic acid (BCA) protein assay kit and MTT reagent (3-(4,5-dimethylthiazol-2-yl)-2,5-diphenyltetrazolium bromide) were acquired from Thermo Fisher Scientific (Massachusetts, USA). RNase free water (diethyl pyrocarbonate (DEPC) treated) was procured from Invitrogen (Thermo scientific, Massachusetts, USA). Cyclo(RGDfC) was purchased from Peptide synthetics, Fareham, UK.

Agarose, polyacrylamide, and sodium chloride were obtained from Sigma-Aldrich (Mumbai, India). RPMI 1640 media, fetal bovine serum (FBS), trypsin-ethylenediamine tetra-acetic acid (EDTA), penicillin-streptomycin, 1x ITS (Insulin-Transferrin-Selenium), Opti-MEM media, and Hoechst 33342 were purchased from Invitrogen and Gibco (Invitrogen, California, USA, Gibco, Life Technologies, Grand Island, USA). Scramble (Silencer) 5′-FAM-labeled siRNA (sense: 5′-UUCUCCGAACGUGUCACGUdTdT-3′; antisense: 5′-ACGUGACACGUUCGGAGAAdTdT-3′) and HDAC4 siRNA (sense: 5′-GGUGCUUAUGGAAAGGGAUTT-3′; antisense: 5′-AUCCCUUUCCAUAAGCACCTT-3′) were procured from Thermo Fisher Scientific (Massachusetts, USA). All other reagents and solvents were of analytical grade unless otherwise specified.

**2.2. Synthesis of cRGD Conjugated Albumin (A-cRGD).** To synthesize A-cRGD, albumin (60 mg/mL) phosphate-buffered saline (PBS) was reacted with 0.15 M (5 mL) heterobifunctional cross-linker (MBS) (4.245 mg), for 0.5 h at room temperature with mild agitation (300 rpm) (Figure S1). Then, glycine (1 M; 5 $\mu$L) was added to the reaction mixture for the blocking of extra unreacted *N*-hydroxysuccinimide (NHS) groups in MBS. After incubation (0.5 h), (500 $\mu$L) PBS was added, and the reaction mixture was dialyzed using vivaspin (molecular weight cutoff, MWCO 50 kDa, GE Healthcare, Illinois, USA). The resultant MBS−albumin conjugate was allowed to react with ten molar excess of cyclo(RGDfC) (cRGD; Peptide synthetics, Hampshire, UK; 5.73 mg/mL PBS). The reaction mixture was incubated for 3 h at room temperature with mild agitation, and then the reaction was continued overnight at 4 °C. After that, cRGD−MBS−albumin conjugate was dialyzed using vivaspin to get rid-off unreacted reactants. The resultant product was lyophilized and stored at −20 ± 5 °C until further use.[37]

**2.3. Characterization of A-cRGD Conjugate.** *2.3.1. Surface Zeta Potential.* The zeta potential of the conjugate was determined using zeta sizer Nano-ZS90 (Malvern Instruments, Cambridge, UK) for confirmation of conjugation. The zeta potential of albumin and A-cRGD was measured via the dispersion of lyophilized powder in ultrapure water; then the dispersion was diluted ten times with ultrapure water. The zeta potential was calculated using Smoluchowski's equation from the electrophoretic mobility of albumin and A-cRGD at 25 ± 0.5 °C. All the samples were measured at 25 ± 0.5 °C in triplicate.[34]

*2.3.2. Sodium Dodecyl Sulfate-Polyacrylamide Gel Electrophoresis (SDS-PAGE).* SDS-PAGE was carried out using 10%v/v resolving gel and 5%v/v stacking polyacrylamide gel to gel running assembly (Mini-PROTEAN Tetra Cell, Bio-Rad Laboratories, California, USA). Albumin and A-cRGD conjugate were loaded on the gel (loading volume: 5 $\mu$L/well (15 $\mu$g/well concentration); stock solution: 3 mg/mL) and allowed to run at 80 V for 1.5 h. After electrophoresis, the gel was stained employing Coomassie blue, followed by destained with a solution containing 10%v/v methanol and 10%v/v glacial acetic acid (10:10:80::methanol:glacial acetic acid:water (v:v:v)). The gel was visualized under the Chemiluminescent Gel Doc system (Bio-Rad Laboratories, California, USA).

*2.3.3. 2,4,6-Trinitrobenzenesulfonic Acid (TNBSA) Assay.* For further confirmation of conjugation, the TNBSA assay was performed following the protocol reported by our group with slight modifications.[38] Briefly, A-cRGD conjugates were taken in concentrations ranging from 5 to 100 $\mu$g/mL in 0.1 M sodium bicarbonate pH 8.5 buffer, along with glycine (protein standard) with concentration ranging from 2 to 20 $\mu$g/mL. To this, standard solutions of 0.01%w/v TNBSA solution were added and incubated at 37 ± 0.5 °C for 2 h. Then, 10%w/v SDS and 1 N HCl were added to each sample to stop the reaction, and absorbance was measured at 335 nm in a UV−visible spectrophotometer (Shimadzu, Kyoto, Japan) to determine the number of free amine groups on the sample.

*2.3.4. Fourier-Transform Infrared Spectroscopy (FTIR).* The conjugation of albumin with cRGD peptide was examined using attenuated total reflectance (ATR) FTIR. The spectra for FTIR was obtained in 4000−1000 $cm^{-1}$ range, with 4 $cm^{-1}$ resolution at room temperature utilizing Alpha II, Bruker, Billerica, USA, and analyzed using OPUS - Spectroscopy Software, Bruker, Billerica, USA.[39]

*2.3.5. Matrix-Assisted Laser Desorption Ionization-Time of Flight Mass Spectrometry (MALDI-TOF MS).* The A-cRGD


https://dx.doi.org/10.1021/acs.molpharmaceut.0c00094
Mol. Pharmaceutics 2021, 18, 641−666

conjugate was further evaluated by MALDI-TOF MS using a 5800 MALDI-TOF MS instrument (AB SCIEX, California, USA). One microliter of the sample was mixed with an equivalent amount of the matrix used as 2,5-dihydroxybenzoic acid (DHB) in 30%v/v acetonitrile and 0.1%v/v trifluoroacetic acid. From the mixed solution, 1 $\mu$L was spotted on the target plate and then evaporated under a mild stream of warm air. All mass spectra were developed in positive reflector mode with 25 kV accelerating voltage.

**2.4. Dendrimer:siRNA (*d*:siR) Complex Ratio.** Self-assembly under a gentle vortexing method was utilized to prepare *d*:siR complex.[40] Briefly, different surface/charge ratios—nitrogen to a phosphate group (*n/p* ratio)—were selected for the preparation of the *d*:siR complex. For this, siRNA (200 pmol or 4 $\mu$g/$\mu$L in DEPC treated nuclease-free water) was mixed with 2.0G PAMAM dendrimer (Sigma-Aldrich, Missouri, USA) at increasing *n/p* ratio (0.125, 0.166, 0.25, 0.5, and 1 *n/p* ratio). After mixing, the reaction mixtures were incubated for 4 h at room temperature with a mild vortexing cycle of 30 s after every 15 min.

**2.5. Characterization of *d*:siR Complex.** After the preparation of the *d*:siR complexes at various ratios, their evaluation was done through the gel retardation assay. All *d*:siR complex ratios were homogenate loading dye (5 $\mu$L; 6X), and further sample volume was maintained through DEPC treated nuclease-free water. Then, the 15 $\mu$L volume of sample (0.3 $\mu$g siRNA) was loaded onto 2%w/v agarose gel containing ethidium bromide dye (2 $\mu$g/mL) for siRNA tracking. Agarose gel was run in Tris/Borate/EDTA (TBE) buffer (1X) at 80 V and run for 1 h (Bio-Rad Laboratories, California, USA). The siRNA retardation from *d*:siR complex ratios was observed using UV transilluminator (Bio-Rad Laboratories, California, USA).[41]

**2.6. Preparation of Albumin siRNA Nanoplex (siANp) and cRGD Targeted Albumin siRNA Nanoplex (siANp-cRGD).** The siANp/HDAC4 was prepared following the protocol reported earlier by our laboratory with appropriate modification to achieved desired sized nanoconstruct (≤70 nm).[24,42] For the preparation of siANp, a 4%w/v (606.06 M) albumin solution was prepared and incubated with siRNA (200 pmol; 4 $\mu$g/$\mu$L siRNA) for 1 h under gentle stirring at 300 rpm. To this, ethanol (4 mL) was added dropwise at an addition rate of 50 $\mu$L/min under optimized stirring condition (700 rpm; 2 h) (IKA Magnetic Stirrer, Model RT5, Staufen, Germany). The resultant nanoplex was then stabilized by adding genipin (0.1%w/v; 20 $\mu$L) to cross-link peripheral primary amino groups. The siANp was then purified by centrifugation at 14,000 g for 25 min to remove free siRNA. The resultant pellet was redispersed in DEPC treated RNase free water and characterized for hydrodynamic particle size, polydispersity index (PDI), and surface zeta potential.

For the siANp-cRGD/HDAC4, albumin:A-cRGD (90:10:: w-w) and siRNA (200 pmol; 4 $\mu$g/$\mu$L siRNA) were incubated for 1 h under 300 rpm stirring rate. Then, ethanol was added dropwise (addition rate: 50 $\mu$L/min) under stirring at 700 rpm for 2 h. Thereafter, siANp-cRGD was also stabilized using genipin cross-linker, and unentrapped siRNA was removed via centrifugation, as mentioned earlier. The resultant nanoplexes were characterized for its hydrodynamic particle size, PDI, and surface zeta potential.

**2.7. Preparation of Dendrimer-Templated Albumin siRNA Nanoplex (DTsiANp/HDAC4) and cRGD Targeted Dendrimer-Templated Albumin siRNA Nanoplex (DTsiANp-cRGD/HDAC4).** For the preparation of DTsiANp/HDAC4, an optimized *d*:siR complex (prepared at *n/p* ratio of 0.5; 200 pmol; 4 $\mu$g/$\mu$L siRNA) was incubated with albumin solution (4%w/v) under gentle stirring at 300 rpm for 1 h. Thereafter, ethanol was added dropwise at an addition rate of 50 $\mu$L/min under stirring at 700 rpm for 2 h. To it, genipin was added for stabilization (0.1%w/v; 700 rpm for 2 h). After 2 h, centrifugation was done to remove free siRNA from DTsiANp and the resultant pellet was redispersed in DEPC treated RNase free water; and then characterized for hydrodynamic particle size, PDI, and surface zeta potential.

Similarly, the DTsiANp-cRGD/HDAC4 was prepared via incubation of *d*:siR complex (*n/p* ratio: 0.5; 200 pmol; 4 $\mu$g/$\mu$L siRNA) with albumin:A-cRGD (90:10:: w-w) under mild stirring at 300 rpm for 1 h. To it, ethanol was added at an addition rate of 50 $\mu$L/min under stirring at 700 rpm for 2 h. The nanoplex was stabilized by the addition of genipin and the free siRNA was removed by centrifugation at 14,000 g for 25 min. The resultant nanoplex was lyophilized (lyophilization condition: $5 \times 10^{-2}$ mbar for 24 h) using 3%w/v trehalose.[43] For subsequent experimentations, the lyophilized nanoplex was reconstituted in nuclease-free (DEPC treated) water or PBS (1X) as per the demand of the *in vitro* and *in vivo* study. For the cellular uptake assay, endosomal escape assay, and competition binding study, fluorescent dye-labeled siRNA (FAM-siRNA) were loaded in nanoplex in place of HDAC4 siRNA.

**2.8. Characterization of siRNA Nanoplex.** The characterization was done using dynamic light scattering (DLS) (for particle size, PDI, and zeta potential) through zetasizer (Nano-ZS90, Malvern Instruments, Cambridge, UK). Briefly, the nanoplex was diluted ten times with RNase free water and was measured at using Zetasizer (Nano-ZS90, Malvern Instruments, Cambridge, UK) 633 nm and angle (173°). All the sample measurements were made at 25 ± 2 °C in triplicate, and the results were presented as mean ± SD.

Further, the morphology of prepared nanoplex was also characterized using scanning electron microscopy (SEM) in a JSM-7001FA microscope (JEOL, Tokyo, Japan). For this, the nanoplex suspension was retained on a silicon wafer that attached to a metal stub and dried under vacuum, which was enclosed with a 20 nm gold layer. The metal stubs were visualized under 5.0 kV emission and 9.5−10 mm of working distance.[38] Additional characterization of nanoplex was done through a transmission electron microscope (TEM; Philips, Tecnai 20, Holland; acceleration voltage: 200 kV) using negative staining of 1%v/v phosphotungstic acid and deposited on a carbon-coated copper grid. Then the dried samples were focused and visualized at 40,000x.[44] Atomic force microscopy (AFM; Bruker Multimode 8, Bruker, Billerica, USA) was performed under tapping at constant force 0.02−0.77 N/m and at fixed height 10−15 nm. The covered scan area was 90 $\mu$m × 90 $\mu$m and utilizing charge-coupled device monitor, the cantilever and samples were positioned. Acquired phase and images were analyzed using NanoScope 8.15 software.[45]

**2.9. Determination of siRNA Entrapment by Ribogreen Assay.** The siRNA encapsulation efficiency was determined using the ribogreen assay protocol, as reported by Liechty et al. with slight modifications.[46] Briefly, 2 mg of lyophilized nanoplexes (siANp, DTsiANp, and DTsiANp-cRGD; ∼300 ng siRNA) was dissolved in chloroform (200 $\mu$L) along with TE buffer (500 $\mu$L). siRNA was extracted from organic to aqueous phase via mixing and continuous rotation


https://dx.doi.org/10.1021/acs.molpharmaceut.0c00094
Mol. Pharmaceutics 2021, 18, 641−666

of organic and aqueous phase mixture at room temperature for 1.5 h. Following this, the centrifugation was done at 16,000*g* for 25 min at 4 °C for the separation of the aqueous and organic phases. Chloroform residues were removed by incubation of the supernatant portion at 37 ± 2 °C for 5 min. The resultant supernatant was diluted using the TE buffer, and the amount of siRNA was quantified after the addition of ribogreen reagent according to the manufacturer's instruction (Thermo Fisher Scientific, Massachusetts, USA). The absorbance was obtained via a multimode plate reader at an excitation wavelength of 485 nm and the emission wavelength of 520 nm (Varioskan LUX Multimode, Thermo Fisher Scientific, Massachusetts, USA). All analyses were done in triplicate, and the siRNA encapsulation was calculated by using eq 1.

$$siRNA\ encapsulation = \frac{loading\ of\ siRNA}{theoratical\ loading\ of\ siRNA} \quad (1)$$

**2.10. Serum Stability Assay.** For determination of serum stability assay, free siRNA, siANp, DTsiANp, and DTsiANp-cRGD (~300 ng siRNA; 2 mg) were incubated with 50 μL of complete media (RPMI 1640 comprised 10%v/v fetal bovine serum (FBS). After a predefined time interval (0, 1, 2, 4, 6, and 24 h), aliquots were taken and centrifuged at 20,000*g* for 20 min at 4 ± 2 °C. The supernatant was discarded, and the pellet was subjected to gel electrophoresis. Pellets were redispersed in 10 μL of RNase free water and mixed with DNA loading dye (5 μL (6X)) and then loaded on to 1%w/v agarose gel in 1 X TBE buffer (Tris-borate; 40 mM Tris-HCl, 1%v/v acetic acid, 1 mM EDTA) at 80 V. The electrophoretic mobility was investigated using an ultraviolet (UV) illuminator (GelDoc, Bio-Rad Laboratories, California, USA).[47] Moreover, the stability of nanoplex was also evaluated in culture media (RPMI 1640 contained 10%w/v serum). As a reference, the stability of nanoplex was also checked in the saline (0.9%w/v NaCl) solution for a better comparison. The siRNA loaded nanoplex as siANp, DTsiANp, and DTsiANp-cRGD was incubated (37 ± 0.5 °C) with serum-containing media and saline solution for the different periods (0, 1, 2, 4, 6, and 24 h). Then, particle size, PDI, and zeta potential were measured via Zetasizer Nano ZS90 (Malvern Instruments, UK). The experiment was performed in triplicate at 37 ± 0.5 °C.[38]

**2.11. *In Vitro* DN Model in Human Podocyte Cells (*In Vitro* Podocytes DN Model) Generation.** Human podocyte cells were obtained from Dr. Jeffrey Kopp Lab, National Institute of Health (NIH), Maryland, USA, and the cell culture was performed following the protocol, as explained earlier.[48] Briefly, podocytes cells were grown in RPMI 1640 (containing 11.11 mM D-glucose) containing 10%v/v FBS, 1XITS (Insulin-Transferrin-Selenium) and 100 IU/mL penicillin and 100 μg/mL streptomycin sulfate as antibiotics. Initially, cells were cultured on Type-1 collagen-coated culture tissue culture flask (Dimension: 25 $cm^3$; BD Falcon, Bedford, USA) at 33 ± 0.5 °C with 5% $CO_2$ underneath permissive growth situation. After reaching 60−70% confluency, the cells were moved to 37 ± 0.5 °C with 5% $CO_2$ for the next 10−14 days for differentiation. Following, an *in vitro* podocytes DN model was produced on differentiated podocytes (6 well plates; 2 × $10^5$ cells/well) using 20−40 mM glucose in FBS (1%v/v) compromised RPMI 1640 media for 48 h.[49] Among these ranges, the majority of the reports suggests the utilization of 30 mM high glucose (HG) concentration (the median value) as a high glucose model for diabetic nephropathy of podocytes. Hence, our research work generated an HG model of podocytes using 30 mM, as stated in Imasawa et al.[50] The developed *in vitro* DN podocytes model was further applied for several experiments, which are discussed in the following section.

**2.12. Biocompatibility Assay.** The cellular biocompatibility of developed nanoplexes toward human podocyte cells was assessed by employing an MTT assay.[51] Briefly, differentiated podocyte cells were cultured in 96 well plates ($10^4$ cells/well) in RPMI 1640 complete medium for 24 h, and an *in vitro* DN model was generated as discussed. Thereafter, free HDAC4 siRNA, DTANp, siANp/HDAC4, DTsiANp/HDAC4, DTsiANp-cRGD/HDAC4, and DTANp-cRGD were treated in siRNA equivalent amounts (10 pmol equivalent siRNA/well). After treatment, the cells were incubated for 24 h and then were treated with MTT reagent (20 μL/well; 5 mg/mL; Sigma-Aldrich, Missouri, USA) and incubated for 4 h. Then, DMSO (100 μL/well) was added to solubilize the formazan crystals. Finally, absorbance was measured at 575 nm using a UV microplate reader (Multiscan GO, Thermo Fisher Scientific, Massachusetts, USA) at 37 ± 0.5 °C. The cell viability was calculated by using eq 2.

$$Cell\ viability\ (\%) = \frac{Absorbance\ (sample)}{Absorbance\ (control)} \times 100 \quad (2)$$

**2.13. Cellular Uptake Assay of siRNA Nanoplex.** The cellular uptake study was performed to evaluate the internalization efficiency of FAM-siRNA when delivered using developed nanoplexes in HG-treated DN podocytes model. Briefly, differentiated podocytes cells were seeded into a 6-well plate (2 × $10^5$ cells/well) bearing a glass coverslip for 24 h, and the *in vitro* DN model was generated. After that, media was replaced with an Opti-MEM containing free FAM-siRNA, and FAM-siRNA loaded siANp, DTsiANp, and DTsiANp-cRGD (30 pmol equivalent siRNA/well; 10 μM). At 8 h post-treatment, the confocal fluorescent microscopic images were taken after staining the nucleus with Hoechst 33342. Then, the cells were fixed in 4%v/v paraformaldehyde and again washed with PBS; the coverslip was mounted on a glass slide (Borosil, Mumbai, India) for visualization via confocal microscopy (Excitation max: 494 nm; Emission max: 520 nm, Leica TCS SP5 AOBS Confocal microscopy system (Leica, Germany)).[52]

**2.14. Endosome/Lysosome Escape Assay.** To evaluate the endolysosomal escape tendency of developed nanoplexes, differentiated podocytes were seeded on glass coverslips in 6 well culture plates (1 × $10^6$ cells/well) and incubated for 24 h and *in vitro* DN model was produced. The cells were then treated with FAM-labeled siRNA (30 pmol; 3−4 μg/μL) loaded DTsiANp-cRGD and siANp. After 6 and 8 h of incubation, podocytes were washed thrice with PBS (1×) and then treated with lysotracker dye (Thermo Fisher Scientific, Massachusetts, USA) for 30 min. Afterward, the podocytes cells were again washed with PBS (1×) and fixed by Fluoroshield histology mounting medium (Sigma-Aldrich, Missouri, USA) on a glass-slide (Borosil, Mumbai, India) and visualized using a Leica TCS SP5 AOBS Confocal microscopy system (Leica, Wetzlar, Germany).[47]

**2.15. Competitive Receptor Binding Assay to Confirm Integrin Receptor-Mediated Internalization.** To confirm the receptor directed cellular uptake of DTsiANp-cRGD, the competitive cellular uptake study was investigated using FAM-labeled siRNA loaded nanoplexes by flow cytometry (Bio-Rad


https://dx.doi.org/10.1021/acs.molpharmaceut.0c00094
Mol. Pharmaceutics 2021, 18, 641−666

Laboratories, California, USA). Briefly, differentiated podocytes cells were seeded in 6-well plates at a density of $2 \times 10^5$ cells/well and allowed to grow overnight under 5% $CO_2$ at 37 ± 0.5 °C and *in vitro* DN model was produced. Then, the media from each well was replaced with FBS compromised media having free cRGD (100 nM; 1 mg/mL) and incubated for 1 h. After 1 h, free cRGD pretreated cells were incubated with nanoplexes as DTsiANp-cRGD and siANp (30 pmol equivalents FAM-siRNA/well). After 6 h of incubation, cells were harvested using trypsin-EDTA and centrifuged at 2000*g* for 7 min. Then, the pellet was redispersed in 1× PBS (500 μL) and again centrifuged to remove debris from the cells. After centrifugation pellet was dispersed in 300 μL PBS (1×). The prepared cell suspension was evaluated for cellular uptake using a Beckman Coulter flow cytometer (S3e Cell Sorter, Bio-Rad Laboratories, California, USA). In all the cases, at least 10,000 gated events were acquired from each sample.[53]

**2.16. Gene Silencing Efficiency: Quantitative RT-PCR (qRT-PCR).** Quantitative Real-time PCR was performed to assess the HDAC4 silencing efficiency through HDAC4-siRNA loaded nanoplex. Briefly, differentiated podocytes cells were seeded in 6 well plates ($2 \times 10^5$ cells/well) for 24 h, and the *in vitro* DN model was generated.[54] Later, media was replaced with an Opti-MEM containing Free HDAC4 siRNA, DTsiANp/HDAC4, DTsiANp-cRGD/HDAC4, and DTsiANp-cRGD/scramble (30 pmol siRNA/well equivalent) and incubated for 24 h. Here, DTsiANp-cRGD/Scramble selected as a negative control. After 48 h, total RNA was extracted using the RNeasy mini kit (Qiagen, Hilden, Germany) as stated by the manufacturer's protocol and quantified using Nanodrop 2000 spectrophotometer (Thermo Fisher Scientific, Massachusetts, USA). The cDNA was prepared by the iScript cDNA synthesis kit (Bio-Rad Laboratories, California, USA). Then, HDAC4 gene expression was quantified with a 1:10 dilution of cDNA using the iScript SYBR green supermix (Bio-Rad Laboratories, California, USA) through Step One Real-time PCR (Applied Biosystems, California, USA). PCR KiCqStart primers (Sigma-Aldrich, Missouri, USA) were utilized to amplify 18s (forward: 5′-GTAACCCGTTGAACCCCATT-3′ and reverse: 5′-CCATCCAATCGGTAGTAGCG-3′) and HDAC4 gene (forward: 5′-AGTGTCGACCTCCTATAACCA-3′ and reverse: 5′-GCTTTAGCCTGGACCGTAAT-3′). The HDAC4 expression level was analyzed via Ct values (cycle threshold). The experiments were performed in triplicate.

**2.17. Western Blot Analysis: *In Vitro* and *In Vivo*.** The expression of HDAC4 was evaluated in podocyte protein levels through Western blot analysis. Differentiated cells were grown in 6 well plates ($3 \times 10^5$ cells/well) and treated with HG (30 mM) in serum compromised media for 48 h. These cells were treated with free HDAC4 siRNA, DTsiANp/HDAC4, DTsiANp/Scramble, DTsiANp-cRGD/HDAC4 at an equivalent treatment concentration of 30 pmol/well siRNA for 48 h. The cell lysate was suspended in radioimmunoprecipitation assay buffer (RIPA) lysis buffer containing protease inhibitor cocktail (1 μL). Protein concentration was assessed using bicinchoninic acid assay (BCA) reagent. Briefly, protein (25 μg/well) was resolved through 10%v/v acrylamide gel, then transferred over polyvinylidene difluoride (PVDF) membrane utilizing RTA Trans Turbo kit (Bio-Rad Laboratories, California, USA). Specific protein was detected via primary antibody incubation against (HDAC4 (1:1000 dilution in 1% w/v casein blocker; Abcam, Cambridge, UK) and (β-actin (1:5000 dilution in 1%w/v casein blocker), Santacruz, Texas, USA) at 4 ± 2 °C overnight. After overnight incubation with the primary antibody, 0.1%w/v TBST was used for membrane washing and subsequently incubated with secondary antibody (HRP-conjugated) (Goat antimouse IgG-HRP 1:20000 dilution in 1%w/v Casein, Santacruz, Texas, USA and Goat antirabbit IgG-HRP 1:20000, dilution in 1%w/v Casein, Abcam, Cambridge, UK) at room temperature for 2 h. The protein bands were detected using chemiluminescence substrate (Bio-Rad Laboratories, California, USA) and quantified using ImageJ software (NIH, Bethesda, Maryland).[55]

For determination of *in vivo* gene silencing efficacy, Western blot analysis was performed on kidneys excised from treatment groups including (i) normal healthy mice, (ii) STZ induced DN mice, and (iii) nanoplex treated DN mice. The dose of siRNA administered to the DN mice group was 1 mg/kg given twice in a week (0, 3,7,10, 13, 17, 20, 23, 27 days). After 4 weeks of treatment, the mice were sacrificed, and kidneys were excised. The glomerular portion of excised kidneys was homogenized using tissue lyser (TissueLyser LT, Qiagen, Hilden, Germany) and centrifuged at 12,000*g* for 5 min to remove tissue remaining. The supernatant was collected for protein extraction, and protein content was measured using the BCA method. The samples (30 μg/well) were loaded on an acrylamide gel, and the remaining process for Western blots analysis for HDAC4 (Abcam, Cambridge, UK), and fibrotic markers such as fibronectin (Abcam, Cambridge, UK), collagen IV (Abcam, Cambridge, UK), N-cadherin (Santacruz, Texas, USA), and E-cadherin (Abcam, Cambridge, UK) has remained the same as mentioned above for *in vitro*.[56]

**2.18. Determination of Podocytes Apoptosis: *In Vitro*.** In DN, HG-induced expression of HDAC4 in podocytes that resulted in podocytes apoptosis, inflammation, and podocytes injury. Therefore, the effect of podocyte apoptosis after treatment with nanoplex was measured using flow cytometry. Briefly, differentiated podocytes cells were plated in a 6-well plate at a cell density of $2 \times 10^6$ cells/well for 24 h (30 pmol/well equivalent siRNA). Then cells were exposed to HG for *in vitro* DN model induction for 48 h. After that, the cells were treated with free HDAC4 siRNA, DTsiANp/HDAC4, DTsiANp-cRGD/HDAC4, and incubated for 24 h. After incubation, the cells were trypsinized and washed (2×) with cold phosphate-buffered saline (PBS 1×) and suspended in 200 μL of binding buffer (1×) containing annexin V (5 μL) and propidium iodide (2 μL) for 15 min in dark condition at room temperature. Annexin V-FITC apoptosis kit (Thermo Fisher Scientific, Massachusetts, USA) was utilized to evaluate the population of apoptotic cells by flow cytometry in the Beckman Coulter flow cytometer (Bio-Rad Laboratories, California, USA) by following the manufacturer's protocol (Bio-Rad Laboratories, California, USA). A minimum of 10,000 gated events was obtained from each sample. Results are expressed as the total percentage of apoptotic cells (PI and Annexin V positive) in the gated cell population.[57]

**2.19. *In Vivo* Diabetic Nephropathy Model in C57BL/6 Male Mice.** All animal studies were performed following the National Institute of Pharmaceutical Education and Research (NIPER-A) guidelines for the care and use of laboratory animals. All animal experiments were performed according to the protocols approved by the institutional animal ethics committee (IAEC) at NIPER-Ahmedabad, Gujarat, India (Approval ID: NIPER-A/IAEC/2017/034; Date: 17/07/


https://dx.doi.org/10.1021/acs.molpharmaceut.0c00094
Mol. Pharmaceutics 2021, 18, 641−666

2017). For the investigation, 50 mg/kg dose of STZ (in 0.1 M citrate buffer) was given to C57BL/6 male mice (18−24 g) (Zydus Research Centre, Ahmedabad, India) via intraperitoneal injection for five consecutive days to avoid acute toxicity of STZ. Control animals were treated with plain vehicles as 0.1 M citrate buffer.[58] The development of diabetes in mice was confirmed through blood glucose levels Accu Chek-Active glucometer via ready to use strips; Accucheck active, Roche, Indiana, USA). After attaining blood glucose level (fasting glucose >12 mmol), mice were randomized into five experimental groups having six mice per groups, namely (i) DN mice, (ii) free HDAC4 siRNA, (iii) DTsiANp-cRGD/Scramble, (iv) DTsiANp/HDAC4, and (v) DTsiANp-cRGD/HDAC4. After model generation at 6−7 weeks, the treatment was given until 4 weeks at 1 mg/kg dose of equivalent siRNA twice a week intravenously.[59] Then mice were kept in a metabolic cage for evaluation of metabolic parameters including creatinine clearance, blood urea nitrogen level (BUN), and blood glucose, serum creatinine through creatinine test kit (identify, Jeev diagnostic Pvt. Ltd., Tamil Nadu, India). Urine albumin was determined as urinary albumin excretion rate (UAER), through Albumin mouse ELISA kit (Abcam, Cambridge, UK) as per manufacturer's protocol.[60]

N-Acetyl glucosamine activity (NAG; Abcam, Cambridge, UK) was also determined as per manufacturers protocol. Creatinine clearance was obtained as urinary creatinine (mmol/L) × urine volume (mL/min)/serum creatinine (mmol/L) and was expressed as mL/min/kg.[61] The mice were sacrificed through ketamine/xylazine anesthesia, and kidneys were immediately harvested. The excised kidneys were homogenized in lysis buffer for Western blotting, and another part was fixed under 4% paraformaldehyde for paraffin-embedded sections preparation and stained hematoxylin-eosin staining as well as modified Masson's trichrome stain (Abcam, Cambridge, UK) for collagen accumulation and evaluation of percentage fibrosis analysis. The glomerular expansion area was calculated from hematoxylin-eosin staining.[62] Here, the treatment of siRNA loaded nanoplex was given to DN mice for 4 weeks to evaluate the subacute toxicity by studying change in hematological, biochemical, and histopathological parameters.[63]

**2.20. Renal Histological Evaluation.** The isolated kidneys were embedded in paraffin using 4%w/v paraformaldehyde,[64] and three-micrometer thick sections were cut using Microtome (Leica RM2235, Germany). The sliced sections of kidneys were processed for hematoxylin and eosin (H&E) staining as well as by modified Masson's trichrome staining (Abcam, Cambridge, UK) according to the manufacturer's protocol. The fibrotic area was measured through Masson's trichrome-stained sections using ImageJ software.[65] The histological changes in the kidney as glomerular area, the number of glomeruli, and glomerular basement membrane thickening for glomerular injury were determined by H&E staining using at least 15 random cortex-region images per mouse under a low magnification field of vision (×400). The number of glomeruli was counted on light microscopy under low magnification (×100). The number of per section for each kidney section for each slide was calculated via the point-counting technique, and their mean was reported.[66] The glomerular basement membrane thickening was done through ImageJ software from at least 15 glomeruli per group section and six animals per treatment group.[67]

**2.21. Immunohistochemistry.** Paraffin-embedded kidney sections (3 $\mu$m) were deparaffinized in xylene and rehydrated in ethanol (gradation of concentration). The retrieval of the heat epitope section was placed in a 10 mM citrate buffer (pH 6). Then blocking of endogenous peroxidase activity was done via 0.3% hydrogen peroxide solution incubation for 10 min. After that section was incubated for 20 min with serum blocking solution (Vectastain Elite ABC Kits, Vector Laboratories Ltd., Peterborough, UK), and then sections were incubated with primary antibody against HDAC4 (1:200 dilution, Abcam, Cambridge, UK) and then incubated for 30 min with the secondary biotinylated antibody. The development of the section was done via 3,3′-diaminobenzidine chromogen (Sigma-Aldrich, Missouri, USA) after incubation with the respective horseradish-peroxidase (HRP) substrate, and then it was counterstained employing hematoxylin. The quantification of the section was done via taking 10 to 12 nonoverlapping areas of the renal cortex at 400× magnification with a Leica microscope (DFC 480, Leica, Wetzlar, Germany). The quantification for the percentage of stained area relative to the entire area in each field was evaluated via image J software (National Institutes of Health, Maryland, USA).[60]

**2.22. Toxicity Determination by Hematological, Biochemical, and Histological Analysis.** Blood was collected (volume: 300 $\mu$L) from the retro-orbital bulb of mice into a potassium EDTA (10%w/v) coated tube for hematological investigations on day 14 and day 28 following the standard protocols.[68] At a 4-week time point (28 days p.i.), the mice were sacrificed by isoflurane and exsanguinated with phosphate-buffered saline using an angio-catheter. The blood samples were tested to determine the levels of platelets, hematocrit, hemoglobin, red blood cells, white blood cells (WBC), mean corpuscular volume (MCV), mean corpuscular hemoglobin (MCH), and mean corpuscular hemoglobin concentration (MCHC), eosinophil, neutrophil, leukocytes, and basophil using hematology analyzer (KX-21, Kobe, Japan). The biochemical parameters such as alanine transaminase and aspartate transaminase were also measured using a semi-automatic analyzer (TP Analyzer Plus, Thermoplate-China) to evaluate the liver toxicity emerging from the treatment (if any) using the commercially available kits (Diagnostic LabtestSA, Minas Gerais, Brazil). After the treatment of nanoplex, the whole mice were perfused and fixed using 10%w/v buffered formalin for the fixing of the organ. The liver, spleen, and lungs were then collected, and histology was performed for evaluation of the presence of any toxicity.

**2.23. *In Vitro* Hemo-Compatibility Assay.** For determination of the *in vitro* biocompatibility of nanoplex hemocompatibility assay was performed.[24,38] In brief, mouse blood was collected in heparinized vials (5000 IU/mL, Himedia, Mumbai, India) and centrifuged for 10 min at 1000*g* for collection of RBCs pellet. The obtained RBC pellet was resuspended and washed with the 0.9%w/v normal saline (1X). Then, the RBC solution was diluted for determination. After that, a solution of RBC was mixed with ANp, DTANp, siANp, DTsiANp, ANp-cRGD, DTANp-cRGD, siANp-cRGD, and DTsiANp-cRGD at 1, 2.5, and 5 $\mu$g/mL concentrations of the dendrimer, 0.9%w/v saline as a negative control, and Triton X-100 (0.1%v/v) as a positive control and incubated for 2 h at 37 ± 0.5 °C for interaction. After 2 h, the nanoplex containing RBC suspension was centrifuged for 10 min at 1000*g*, and then, the obtained supernatant was analyzed via UV microplate reader (Varioskan LUX Multimode, Thermo Fisher


https://dx.doi.org/10.1021/acs.molpharmaceut.0c00094
Mol. Pharmaceutics 2021, 18, 641−666

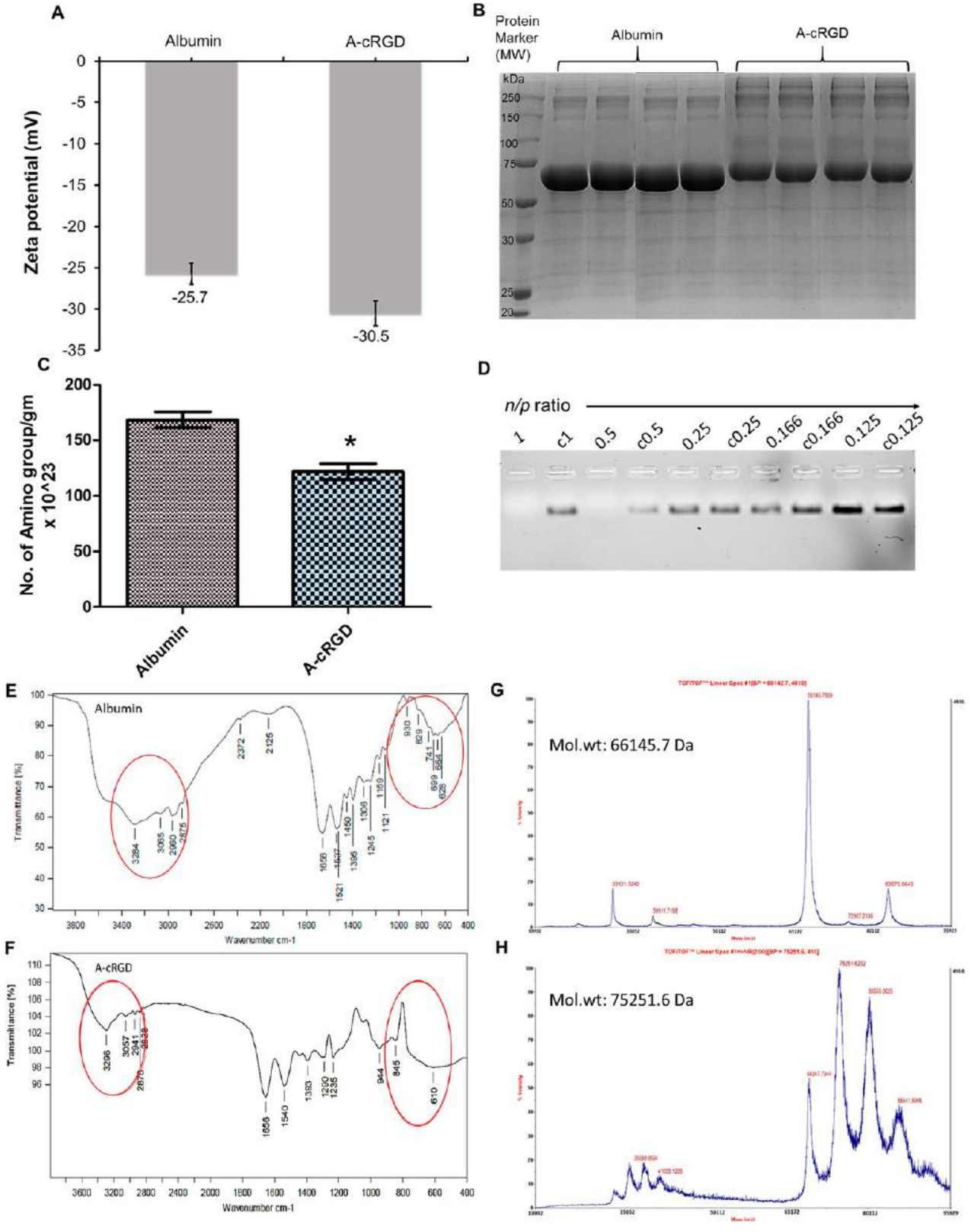


**Figure 1.** (A) Surface zeta potential of albumin before and after conjugation with cRGD. (B) SDS-PAGE representation albumin and A-cRGD. (C) Number of the amino groups per gram of albumin obtained using TNBSA assay, *$p < 0.05$. (D) gel retardation assay for selection of *d*:siR complex ratio. Here, lane 1: 1 *n/p*; lane 2: c1; as control free siRNA of siRNA without dendrimer; lane 3: 0.5 *n/p*; lane 4: c0.5; lane 5: control free siRNA of 0.5 *n/p*; lane 6: 0.25 *n/p*; lane 7: c0.25; control free siRNA of 0.25 *n/p*; lane 8: 0.166 *n/p*; lane 9: c0.166; control free siRNA of 0.166 *n/p*; lane 10: 0.125 *n/p*; lane 11: control free siRNA of 0.125 *n/p*. Results are represented as mean ± SD ($n = 3$). (E) Representative FTIR spectra of albumin. (F) A-cRGD conjugate using attenuated total reflectance Fourier-transform infrared spectroscopy (ATR-FTIR, Alpha II, Bruker, Billerica, USA). (G) MALDI-TOF spectra of albumin presenting molecular weight of 66159.3 Da. (H) MALDI-TOF spectra of A-cRGD conjugate representing molecular weight at 75245.7 Da.


https://dx.doi.org/10.1021/acs.molpharmaceut.0c00094
*Mol. Pharmaceutics* 2021, 18, 641−666

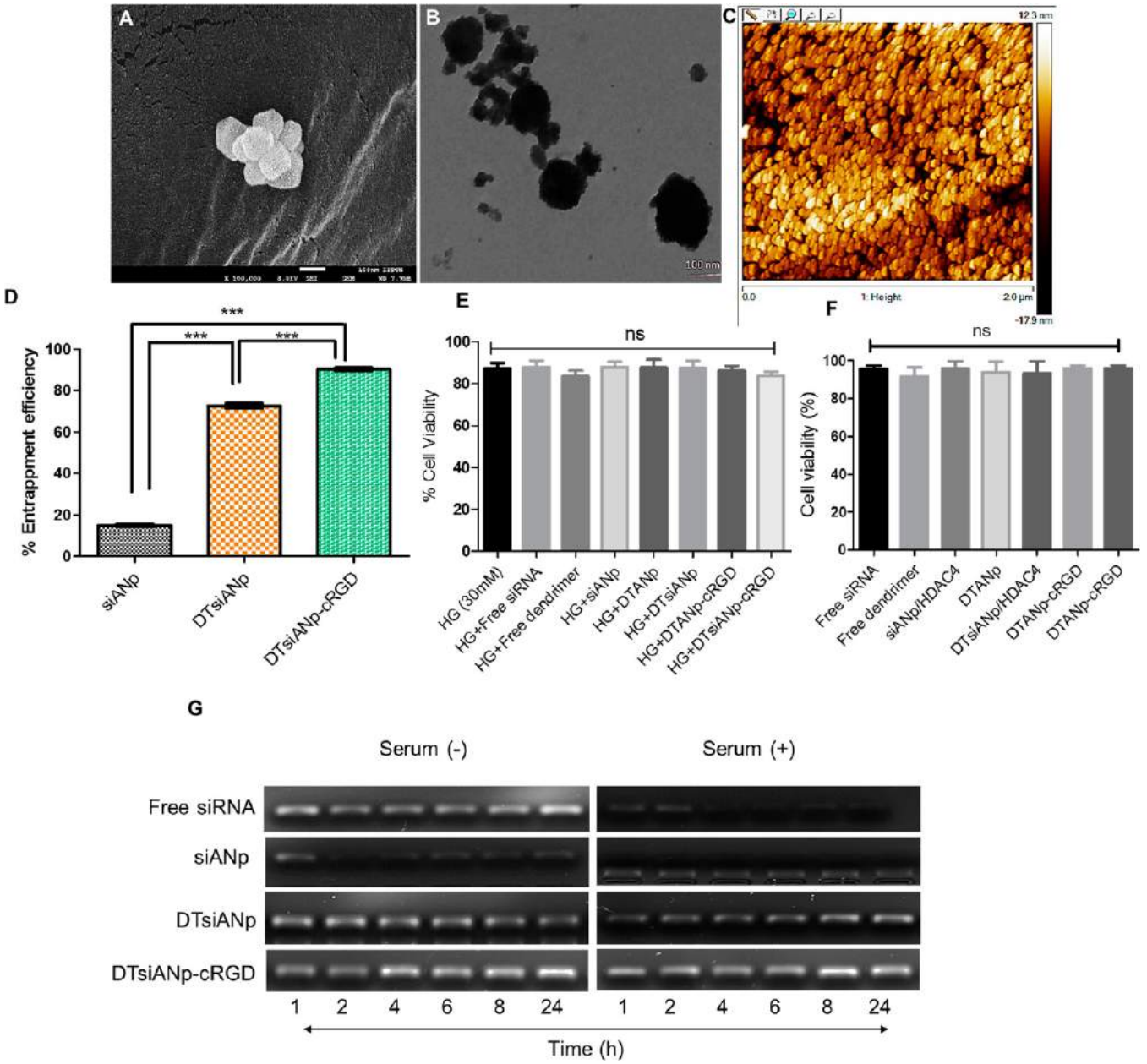


**Figure 2.** Representation of physical characterization of DTsiANp-cRGD nanoplex through (A) SEM (5.0 kV emission and 9.5−10 mm of working distance; scale: 100 nm), (B) TEM (acceleration voltage: 200 kV; scale: 100 nm), and (C) AFM (constant force 0.02−0.77 N/m; scale: 2 $\mu$m). (D) Entrapment efficiency of siRNA in siANp, DTsiANp, DTsiANp-cRGD using ribogreen assay; ***$p < 0.001$. (E) Percentage cell viability of different nanoplexes in HG exposed *in vitro* DN model of podocytes. ($p > 0.05$, nonsignificant). (F) Percentage cell viability of different nanoplex podocytes ($p > 0.05$, nonsignificant). (G) Serum stability assay in the presence and in the absence of serum for free siRNA, siANp, DTsiANp, and DTsiANp-cRGD. Results are represented as mean ± SD ($n = 3$).

Scientific, Massachusetts, USA) at 540 nm for the hemoglobin content. The following equation was used for the determination of the percentage of hemolysis.

$$\%Hemolysis = 100 \times \frac{(Abs.\ Sample - Abs.\ Negative\ Control)}{(Abs.\ Positive\ Control - Abs.\ Negative\ Ccontrol)} \quad (3)$$

where Abs. Sample indicates sample absorbance, Abs. Negative Control indicates the negative control absorbance (0.9%w/v saline), and Abs. Positive Control indicates the positive control absorbance (Triton-X).

**2.24. Statistical Analysis.** Statistical differences among the groups were assessed utilizing one-way analysis of variance (ANOVA) with following to that Bonferroni's post-test using GraphPad Prism 6.01 software (GraphPad Software Inc., San Diego, California). A level of probability as $p < 0.05$, $p < 0.01$, and $p < 0.001$ was considered to be significant and highly significant as well as if $p > 0.05$ greater than that would be considered as nonsignificant. Results are represented as mean ± SD or mean ± SEM.

## 3. RESULTS

**3.1. Characterization of Conjugation A-cRGD.** To attain kidney selective targeted delivery of siRNA in the


https://dx.doi.org/10.1021/acs.molpharmaceut.0c00094
Mol. Pharmaceutics 2021, 18, 641−666

podocytes of DN kidney by employing $\alpha_v\beta_3$ receptors, albumin was modified using cRGD peptide to prepare integrin selective A-cRGD conjugate. The A-cRGD conjugate was synthesized by following nucleophilic addition reaction, as shown in Figure S1. First, the albumin was conjugated with MBS linker by an amide linkage. Then, the maleimide group of MBS was reacted with the freely available sulfhydryl group of the cysteine residue of cRGD to form the A-cRGD conjugate.[37] The confirmation of A-cRGD synthesis was done by several techniques, including surface zeta potential, SDS-PAGE, TNBSA assay, ATR-FTIR, and MALDI-TOF MS.

As shown in Figure 1A, the surface zeta potential of plain albumin was found to be −26 ± 2 mV, which shifted to −31 ± 4 mV in the case of A-cRGD. This corresponds to a decrement in surface zeta potential A-cRGD conjugation formation. The A-cRGD conjugate was also characterized by SDS-PAGE by evaluating the change in the mass/charge ratio of the protein.[69] As shown in Figure 1B, the plain albumin showed the prominent band at 66 kDa as against A-cRGD conjugate that showed the emergence of a newer band near 75 kDa.

Further, the confirmation of conjugation was also done through TNBSA assay for the determination of primary amines in samples. The TNBSA reagent reacts rapidly with the primary amino groups at pH 8.0.[70] The outcome of this investigation infers that after conjugation, the primary amino groups of albumins were decreased from 168 ± 10 × $10^{23}$ to 122 ± 10 × $10^{23}$ ($p < 0.05$) per gram of albumin (Figure 1C).

Further, the conjugation was also characterized through ATR-FTIR spectroscopy to observe the functional groups before and after conjugation (Figure 1E and F). For this study, the prepared A-cRGD conjugate was dried through the lyophilization method (yield: ∼ 95%; 5 × $10^{-2}$ mbar for 24 h; ilShinbiobase, Netherlands, Europe). The representative ATR-FTIR peaks of albumin at 3284 $cm^{-1}$, 1658 $cm^{-1}$, and 1537 $cm^{-1}$ indicate a stretching vibration of −OH, amide-I (−NH stretching vibration), amide-II (mainly C═O stretching vibrations), and amide III (the coupling of bending vibrate of N−H and C−N stretching vibration), respectively (Figure 1E).[71] In the case of A-cRGD conjugate, the −OH vibrational stretching was reduced, and amide stretching vibration was observed with reduced intensity at 3296 $cm^{-1}$, whereas absorption peaks in albumin at 1658 and 1537 $cm^{-1}$ due to the amide-I and II and were retained in the case of A-cRGD (at 1656 and 1540 $cm^{-1}$). This infers that the retained amide peaks were suggesting a successful formation of amide linkage in A-cRGD. Notably, the characteristic C−S stretching peak thatis typically observed between 800 and 600 $cm^{-1}$ in albumin became intense in A-cRGD due to the C−S conjugation of a maleimide group of MBS with the freely available sulfhydryl group of the Cys residue of cRGD (Figure 1F).[72] The A-cRGD conjugate was also identified through MALDI-TOF MS, which exhibited the enhancement in the molecular weight of A-cRGD as compared to the plain albumin. The MALDI-TOF MS analysis showed a 13.76% increment in the molecular weight of A-cRGD (Mw 75251.6 Da; Figure 1G) compared to plain albumin (Mw 66145.7 Da; Figure 1H). Therefore, from the results, we can say that approximately 15 molecules of cRGD conjugated with each albumin.

**3.2. Dendrimer:siRNA (*d*:siR) Complex Ratio.** The preparation of the *d*:siR complex was accomplished at different *n/p* (surface to charge) ratio and investigated via agarose gel electrophoresis.[73] As shown in Figure 1D, the *d*:siR complex formed, and at 1 and 0.5 *n/p* ratio, the corresponding bands of siRNA were not visible in agarose gel, whereas as the *d*:siR ratio decreased, the bands corresponding to free siRNA were shown. On the other hand, the *d*:siR complex formed at a *n/p ration of* <0.5 showed the bands in the gel electrophoresis corresponding to free or leaked siRNA inferring incomplete or unstable complexation. Hence, in this investigation, we have selected the *d*:siR complex formed at a 0.5 *n/p* ratio by anticipating a stable *d*:siR complex.

**3.3. Characterization of siRNA Nanoplex.** The hydrodynamic particle size and zeta potential of prepared DTsiANp-cRGD/HDAC4 nanoplex were found to be 65.31 ± 1.83 nm (0.187 ± 0.064 PDI) and −17.4 ± 1.08 mV, as shown in Figure S2. The DTsiANp/HDAC4 was also found in the nanometric size of the similar range (64.51 ± 0.83 nm, $\zeta$, −16.6 ± 1.12 mV; PDI: 0.197 ± 0.09). The particle size of plain (unloaded) nanoplexes as ANp, DTANp, and DTANp-cRGD, was found to be 66.13 ± 0.58 nm (PDI: 0.148 ± 0.054; $\zeta$: −25.6 ± 1.78 mV), 67.20 ± 0.81 nm (PDI: 0.144 ± 0.025; $\zeta$: −16.1 ± 1.06 mV), 69.40 ± 1.06 nm (PDI: 0.151 ± 0.028; $\zeta$: −19.8 ± 3.57 mV), respectively. There does exist a difference in particle size of plain and ligand conjugated nanoplex by 0.8 nm. However, the difference in particle size of plain and ligand conjugated nanoplex was found to be insignificant statistically ($p > 0.05$; n = 5).

The surface characterization of DTsiANp-cRGD/HDAC4 was confirmed through SEM, TEM, and AFM (Figure 2A−C). The SEM and TEM imaging of DTsiANp-cRGD/HDAC4 shows the representative image from the whole batch with an average particle size of ∼70 nm, which is in agreement with the average particle size of nanoplex as determined by DLS. In agreement with TEM results, representative AFM images also showed the morphology of DTsiANp-cRGD/HDAC4 to be spherical. Conclusively, representative SEM, TEM, and AFM report revealed developed DTsiANp-cRGD/HDAC4 to be a nanosized particle with intact spherical morphology.

**3.4. Entrapment of siRNA: Ribogreen Assay.** Typically, Ribogreen assay is utilized for the quantification of siRNA encapsulated in the nanoplexes or nanoparticles. As expected, an extremely low encapsulation of siRNA about 15 ± 2% was seen in conventional albumin nanoplex siANp. It was observed that in cases of dendrimer templated siRNA loading (DTsiANp and DTsiANp-cRGD) the siRNA loading was significantly very high. In the case of DTsiANp and DTsiANp-cRGD nanoplex showed a significantly high siRNA encapsulation of 73 ± 3% and 90 ± 2%, respectively (Figure 2D; $p < 0.001$). The enhancement in siRNA encapsulation efficiency was found to be 4 ± 0.3-fold compared to DTsiANp and 5 ± 0.4-fold in DTsiANp-cRGD, respectively, compared to siANp. Further, encapsulated siRNA was evaluated for its stability in the presence of serum, and serum stability assay was performed.

**3.5. Serum Stability Assay.** The serum stability was measured by agarose gel electrophoresis following the treatment of prepared siRNA formulation with serum (10% v/v FBS) for 24 h. Results indicated that free siRNA gets immediately degraded in the serum environment within 1 h due to a lack of protection. After 2 h, siRNA bands were not observed in siANp. In contrast, siRNA encapsulated in DTsiANp and DTsiANp-cRGD were found to be more resistant toward nuclease attack in the serum. The encapsulated siRNA remained intact even after 24 h of incubation in the serum (Figure 2G). Furthermore, the stability of siRNA loaded nanoplex was determined in saline (0.9%w/v NaCl)


https://dx.doi.org/10.1021/acs.molpharmaceut.0c00094
Mol. Pharmaceutics 2021, 18, 641−666

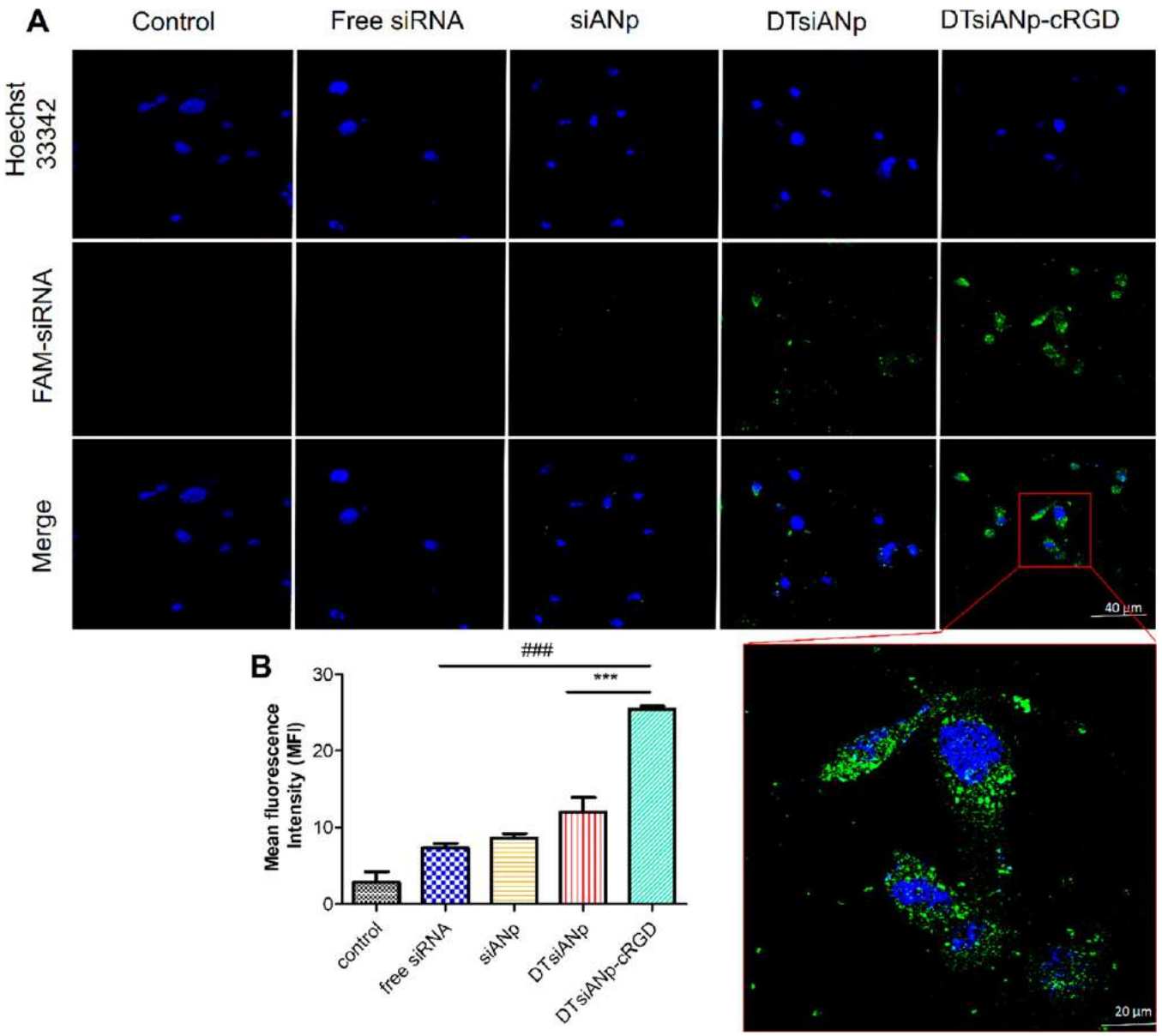


**Figure 3.** (A) Cellular uptake image of FAM-siRNA in HG exposed podocytes treated with free FAM-siRNA, siANp, DTsiANp, and DTsiANp-cRGD after 8 h treatment. Nucleus was stained with Hoechst 33342 (Blue). (B) Mean fluorescent intensity of cells after treatment with nanoplex. $^{***}p < 0.001$ vs DTsiANp and $^{\#\#\#}p < 0.001$ vs Free FAM-siRNA. *Cellular uptake image of FAM-siRNA in HG exposed podocytes after treatment has been visualized via a confocal microscope (Leica TCS SP5 AOBS, Leica, Wetzlar, Germany).*

and cultured media. After incubation of the nanoplex for the predefined time points, particle size, PDI, and zeta potential were measured. The results (Figure S4; $p > 0.05$) suggested that there was no significant difference in particle size, PDI, and zeta potential observed even after the 24 h incubation. It was also reported that high glucose (HG) condition stimulates the expression of HDAC4 in kidney podocytes which is the major cause for the loss of podocytes and death events in the podocytes of the kidney.[3] Hence, the viability of podocytes following the treatment of siRNA nanoplex was evaluated in the HG Podocytes DN model.

**3.6. Biocompatibility Assay.** The *in vitro* DN model was developed in differentiated podocyte cells by following the protocol, as mentioned earlier. Briefly, differentiated podocyte cells were exposed to HG (30 mM; 6 well plates; $2 \times 10^5$ cells/well; complete RPMI 1640 media for 48 h).[50] Here, the low glucose model is normal podocytes cells because normal podocytes required RPMI 1640 media comprised 11.11 mM glucose for the growth and differentiation of podocytes. The normal podocytes (glucose concentration 11.11 mM) and HG exposed podocytes were then treated with free HDAC4 siRNA, free dendrimer, siANp/HDAC4, DTANp, DTsiANp/HDAC4, DTANp-cRGD, and DTsiANp-cRGD/HDAC4 for 24 h. The result of the cell viability assay suggested no notable cytotoxicity events or toxicity concerns in the case of all the treatment groups (Figure 2E and F; $p > 0.05$, ns). This study concluded that all the nanoplexes prepared under investigation were biocompatible and safe for the treatment in the HG exposed *in vitro* DN model of podocytes.

**3.7. Cellular Uptake Assay of siRNA Nanoplex.** The cellular uptake and cytoplasmic release of encapsulated siRNA are the essential steps that must take place for an effective gene silencing. Results from cellular uptake assay suggested that free siRNA was not able to diffuse inside the cell membrane due to


https://dx.doi.org/10.1021/acs.molpharmaceut.0c00094
*Mol. Pharmaceutics* 2021, 18, 641−666

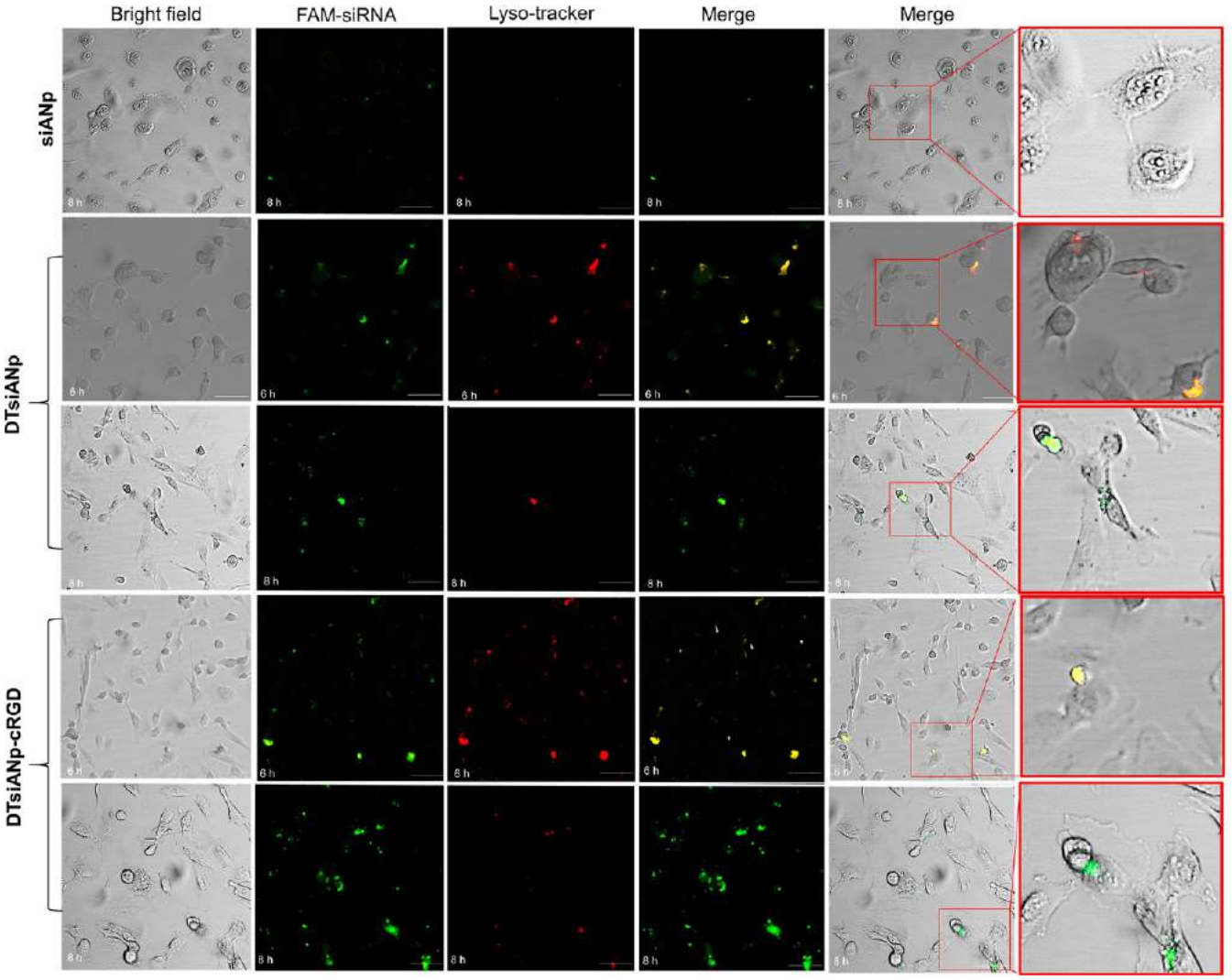


**Figure 4.** Intracellular distribution of siANp, DTsiANp, and DTsiANp-cRGD; the confocal image of podocytes treated with siANp, DTsiANp, and DTsiANp-cRGD for different time points showed endosome or lysosome escape of DTsiANp and DTsiANp-cRGD. Green fluorescence of FAM-siRNA and red fluorescence from endosome or lysosome due to lyso-tracker red, as well as merged images, are also presented. Arrow represented the colocalization of the FAM-siRNA endosome or lysosome as yellow fluorescence. Scale bar indicates 40 $\mu$m, and the inset image scale bar represents 20 $\mu$m.

its anionic nature, larger molecular weight, and hydrophobic nature.[74] In the case of DTsiANp-cRGD, the FAM-siRNA associated green fluorescence appeared in the intracellular compartment of podocytes suggesting successful cellular uptake and siRNA delivery inside the cells (Figure 3A). The cellular uptake was further calculated using mean fluorescent intensity, which was found 3 ± 0.6-fold enhanced after incubation of podocytes with DTsiANp-cRGD compared to free FAM-siRNA (Figure 3B; $p < 0.001$). Results confirm that the integrin directed DTsiANp-cRGD nanoplex was able to internalize significantly higher as compared to the nontargeted counterpart, DTsiANp.

**3.8. Endosome/Lysosome Escape Assay.** As shown in the results (Figure 4), siANp was not showing any fluorescence as well as endosomal escape. At the initial time point of 3 h, no significant green fluorescence and red fluorescence of endolysosome specific lysotracker were observed in podocytes in the case of DTsiANp and DTsiANp-cRGD (Figure S5), whereas, in the case of DTsiANp, significant green fluorescent of FAM-siRNA and red fluorescent of endosome selective lyso-tracker dye associated was observed after 6 h indicating the endosomal uptake of DTsiANp which was confirmed via yellow colocalization. The observation of DTsiANp (6 h) infers that the FMA-siRNA loaded nanoplex gets entrapped in the endolysosomal compartment of the cell. After 8 h, the observed red fluorescent was diffused in the cytoplasmic area signifying the capability to escape from the endosome of DTsiANp. As represented in Figure 4, in the case of DTsiANp-cRGD, the existence of green fluorescence of FAM-siRNA and red fluorescence of endolysosome labeled Lyso-Tracker dye infer the successful colocalization via yellow fluorescence of DTsiANp-cRGD in endosome/lysozyme following 6 h of treatment, at an earlier stage than DTsiANp. Interestingly, as the incubation time of nanoplex was increased with cell (8 and 10 h), a marked reduction in endosome selective red fluorescence, as well as yellow fluorescence of colocalization and a parallel enhancement in the FAM-siRNA associated green fluorescence in the cytoplasm, was noted (Figure S5). This infers that the encapsulated FAM-siRNA gets released from the endolysosomal compartment into the cytoplasm of


https://dx.doi.org/10.1021/acs.molpharmaceut.0c00094
Mol. Pharmaceutics 2021, 18, 641−666

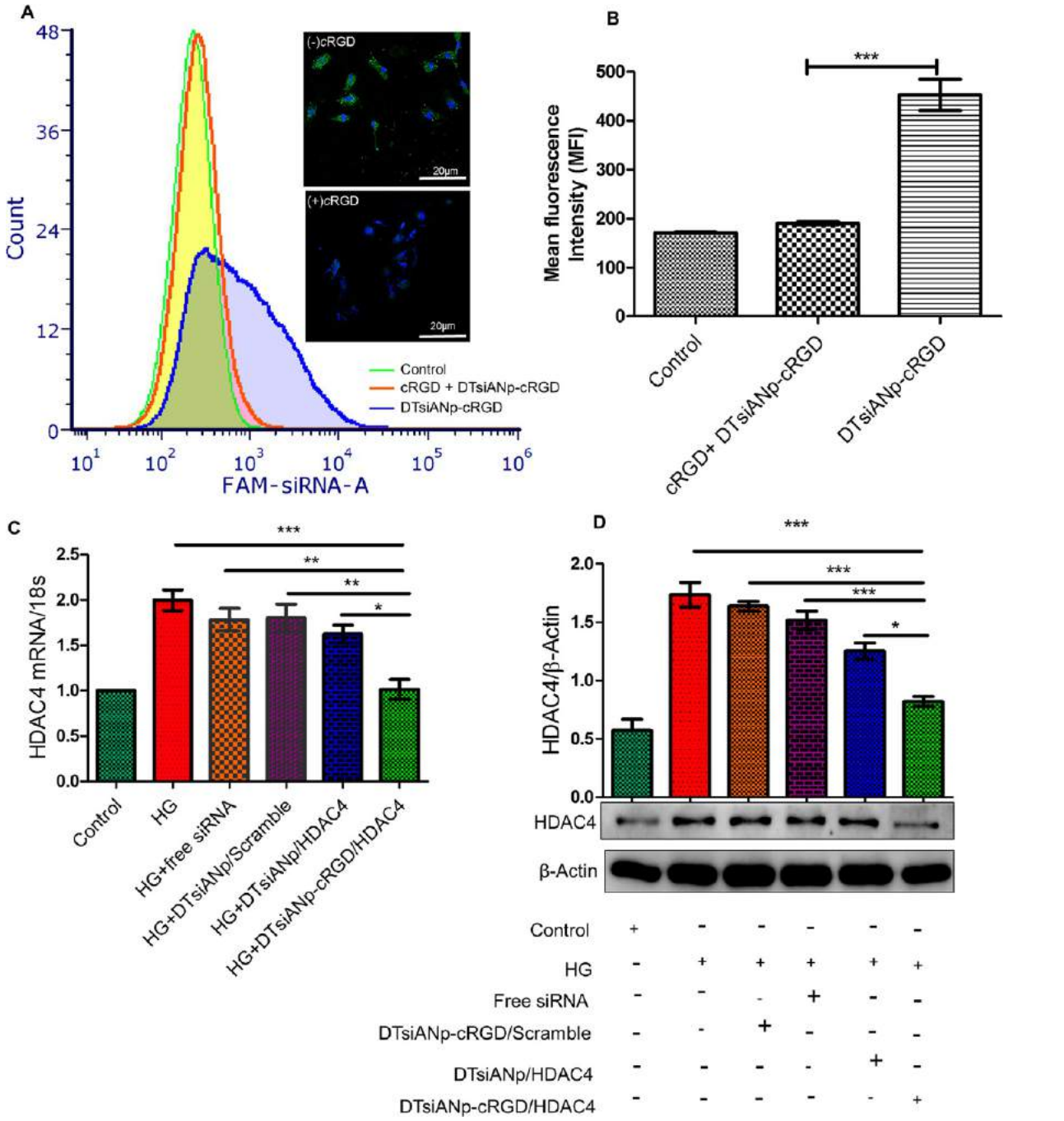


**Figure 5.** (A) Flow cytometry analysis of HG exposed podocytes after incubation free cRGD with DTsiANp-cRGD (+) and with DTsiANp-cRGD (−). Green fluorescence represents FAM-siRNA and blue fluorescence for Hoechst 33342. Scale bar: 20 $\mu$m. (B) Quantitative uptake of DTsiANp-cRGD with free cRGD blocking and without cRGD blocking in HG exposed podocytes. $p < 0.001$ vs cRGD + DTsiANp-cRGD. (C) HDAC4 silencing ability through qRT-PCR in HG-treated podocytes. HG exposed podocyte cells were treated with free HDAC4 siRNA, DTsiANp-cRGD/Scramble, DTsiANp/HDAC4, and DTsiANp-cRGD/HDAC4 in serum-free media. HDAC4 mRNA expression was measured concerning 18s mRNA. Here, *$p < 0.05$ vs DTsiANp/HDAC4; **$p < 0.01$ vs Free HDAC4 siRNA; ***$p < 0.001$ vs DTsiANp-cRGD/Scramble. (D) Western blot analysis for *in vitro* HDAC4 (140 kDa) protein expression with reference to $\beta$-actin (42 kDa) in HG exposed cell were treated with nanoplex. Western blot analysis was done using ImageJ (NIH, Bethesda, MD). Here, *$p < 0.05$ vs DTsiANp/HDAC4; ***$p < 0.001$ vs Free siRNA and DTsiANp-cRGD/Scramble. Results are represented as mean ± SD ($n = 3$).

the cell after internalization in a time-dependent manner. The event of endosomal escape is also revealed by the reduction of red fluorescence in the endosomal compartment, followed by a gradual increment in the green fluorescence of FAM-siRNA in the cytoplasm. Hence, because of this reason, some panel of Figure 4 is not showing the red signal prominently.

Further, the receptor-mediated internalization potential of DTsiANp-cRGD nanoplex was characterized using a competition assay.

**3.9. Competitive Receptor Binding Assay to Confirm $\alpha_v\beta_3$ Integrin Receptor-Mediated Internalization of DTsiANp-cRGD.** It was well reported that cRGD has a selective binding affinity toward $\alpha_v\beta_3$ receptors of podocytes. It


https://dx.doi.org/10.1021/acs.molpharmaceut.0c00094
Mol. Pharmaceutics 2021, 18, 641−666

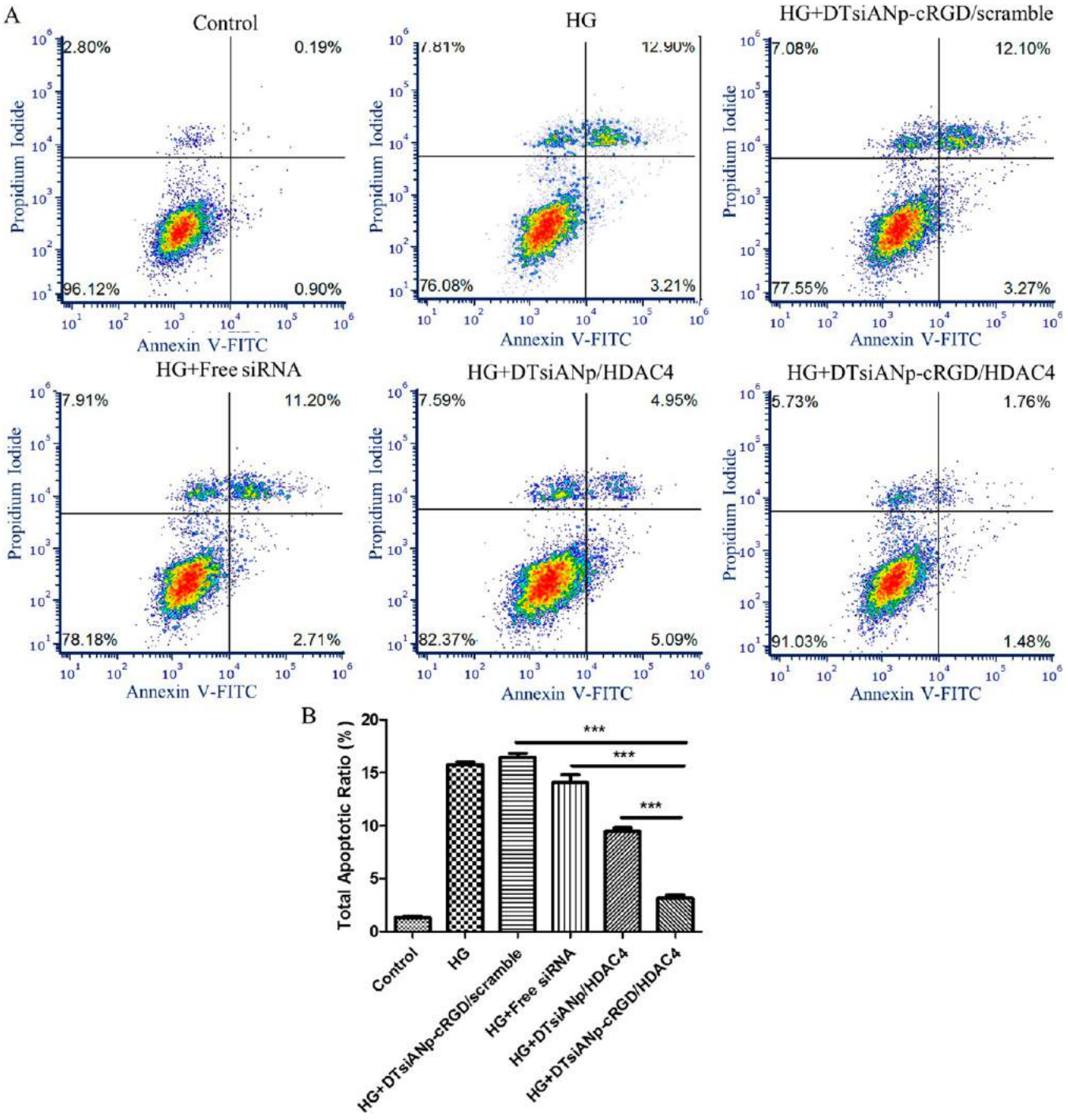


**Figure 6.** (A) Data representing apoptosis assay determined using flow cytometry after the treatment of free HDAC4 siRNA, DTsiANp/HDAC4, and DTsiANp-cRGD/HDAC4 in HG exposed *in vitro* DN model of podocytes. (B) Total apoptotic cell ratio. ***$p < 0.001$ vs free siRNA and DTsiANp/HDAC4. Results are represented as mean ± SD ($n = 3$).

was also reported that cRGD conjugated nanoparticles also retain the binding efficiency toward $\alpha v\beta 3$ receptors.[31] The cellular uptake profile (flow cytometry) of DTsiANp-cRGD was studied in the presence of excess free cRGD (that is after blocking the $\alpha v\beta 3$ receptors) to affirm the $\alpha_v\beta_3$ receptor binding efficiency and $\alpha v\beta 3$ receptors selective cellular uptake of DTsiANp-cRGD. After treating the cells with free cRGD, the DTsiANp-cRGD started behaving like DTsiANp. The mean fluorescence intensity (MFI) of DTsiANp-cRGD was found to be 191 ± 7 owing to cellular uptake after the blockade of $\alpha_v\beta_3$ receptors on podocytes following the treatment of free cRGD, whereas, without free cRGD, treated cells showed MFI was 483 ± 26 ($p < 0.001$). Therefore, it can be said that after treatment with free cRGD, 61 ± 0.7% reduction in MFI of DTsiANp-cRGD ensued (Figure 5A–B; $p < 0.001$).

**3.10. HDAC4 Gene Silencing Efficiency of siRNA Nanoplex *In Vitro* DN Podocyte Model: mRNA Level.** The HDAC4 gene silencing efficiency of HDAC4 siRNA delivered through various nanoplex developed in this study was evaluated by qRT-PCR. When HG exposed podocytes cells


https://dx.doi.org/10.1021/acs.molpharmaceut.0c00094
Mol. Pharmaceutics 2021, 18, 641−666

Table 1. Metabolic Parameters in DN Induced Mice after Treatment of siRNA Nanoplex[a]

| Metabolic Parameters | Healthy Control | DN mice | DTsiANp-cRGD/ Scramble | Free HDAC4 siRNA | DTsiANp/ HDAC4 | DTsiANp-cRGD/ HDAC4 |
|---|---|---|---|---|---|---|
| Blood glucose (mmol) | 9 ± 1 | 25 ± 3 | 22 ± 2.8 | 20 ± 2 | 19 ± 1.6 | 17 ± 1 |
| Creatinine clearance (mL/min) | 1.2 ± 0.4 | 0.4 ± 0.3 | 0.4 ± 0.2 | 0.4 ± 0.1 | 0.5 ± 0.1* | 0.6 ± 0.2** |
| Serum BUN | 25 ± 1 | 33 ± 2 | 32 ± 2 | 30 ± 3 | 30 ± 1 | 28 ± 2* |
| Serum creatinine(μmol/L) | 53 ± 16 | 97 ± 11 | 103 ± 12 | 93 ± 5 | 94 ± 12 | 83 ± 14** |
| NAG Activity (U/L) | 0.009 ± 0.0002 | 0.020 ± 0.001 | 0.0198 ± 0.001 | 0.016 ± 0.001 | 0.016 ± 0.002# | 0.013 ± 0.0004*, ### |
| UAER | 0.11 ± 0.02 | 1.8 ± 0.6 | 2 ± 0.5 | 1 ± 0.3 | 1.1 ± 0.3 # | 0.8 ± 0.43**, ### |

[a]Metabolic parameters were determined in control as well as in DN mice following the treatment of free HDAC4 siRNA, DTsiANp-cRGD/ scramble, DTsiANp/HDAC4, and DTsiANp-cRGD/HDAC4 at a dose of 1 mg/kg equivalent siRNA. After treatment, the blood glucose level was determined using an Accu Chek-Active glucometer (ready to use strips, Accucheck active, Roche, Indiana, USA). The serum creatinine and urine creatinine levels were measured using a creatinine test kit (identifi, Jeev diagnostic Pvt. Ltd., Tamil Nadu, India). Serum and urine urea measurement were done through the urea kinetic test kit (identifi, Jeev diagnostic Pvt. Ltd., Tamil Nadu, India). UAER was measured through the Albumin mouse ELISA kit (Abcam, Cambridge, UK) as per manufacturer's protocol, and NAG activity was measured using the NAG activity kit as per manufacturer's protocol (NAG; Abcam, Cambridge, UK). Results are represented as mean ± SD. Six mice in each group ($n = 6$). Here, *$p <$ 0.05, **$p < 0.01$ vs DN mice, #$p < 0.05$, and ###$p < 0.01$ vs DTsiANp-cRGD/scramble. BUN: blood urea nitrogen, NAG: N-acetyl glucosamine activity, UAER: urinary albumin excretion rate.

were treated with DTsiANp-cRGD/HDAC4, 49 ± 0.2% ($p <$ 0.001), 44 ± 0.2% ($p < 0.01$), and 37 ± 0.2% ($p < 0.05$) (Figure 5C), suppression in the expression of HDAC4 gene was observed as compared to DTsiANp-cRGD/scramble, free HDAC4 siRNA, and DTsiANp/HDAC4, respectively. The DTsiANp/HDAC4 could down-regulate the HDAC4 gene only up to 10 ± 0.2% compared to free HDAC4 siRNA. Therefore, from the results, it can be said that selective targeting of DTsiANp-cRGD/HDAC4 able to suppress the overexpression of the HDAC4 gene in podocytes *in vitro* DN model. In addition to qRT-PCR, the HDAC4 gene silencing efficiency of siRNA nanoplex was further confirmed using Western blot analysis at the protein level.

**3.11. HDAC4 Gene Silencing Efficiency of siRNA Nanoplex *In Vitro* DN Podocyte Model: Protein Level.** In line with qRT-PCR data, HDAC4 protein was found to be significantly downregulated up to 46 ± 0.1% ($p < 0.001$) in the case of DTsiANp-cRGD/HDAC4 treated cells as compared to free HDAC4 siRNA. Further, the down-regulation of HDAC4 protein (140 kDa) by DTsiANp-cRGD/HDAC4 was 34 ± 0.1% ($p < 0.05$) in comparison to DTsiANp/HDAC4 (Figure 5D). DTsiANp-cRGD/HDAC4 showed 50 ± 2% ($p < 0.001$) down-regulation of HDAC4 protein with reference to DTsiANp-cRGD/Scramble. It is suggested that the suppression of HDAC4 was due to a specific HDAC4 siRNA sequence only.

**3.12. Apoptosis Assay *In Vitro* DN Podocyte Model.** When HG exposed podocytes were treated with free HDAC4 siRNA, there was no significant suppression of cellular apoptosis observed, and besides, it enhanced the apoptotic population up to 16 ± 0.4%. But after treatment with DTsiANp/HDAC4 and DTsiANp-cRGD/HDAC4, apoptosis was reduced compared to free HDAC4 siRNA. The DTsiANp/HDAC4 and DTsiANp-cRGD/HDAC4 showed 9 ± 0.6% and 3 ± 0.6% of apoptosis ($p < 0.001$; Figure 6A–B), respectively. Here, from the results, it can be said that the DTsiANp-cRGD/HDAC4 was able to suppress apoptosis by 80 ± 1% ($p < 0.001$) in HG exposed podocytes compared to free HDAC4 siRNA and 67 ± 1% ($p < 0.001$) in comparison with DTsiANp/HDAC4. However, DTsiANp-cRGD/scramble (4%; $p > 0.0$) was unable to suppress the HG exposure caused by enhanced apoptosis compared to DTsiANp-cRGD/HDAC4. The observed 12% apoptosis in the free siRNA group was due to HG exposure of podocytes, not because of free siRNA, while free siRNA degrades in the presence of serum.

**3.13. Effect of siRNA Nanoplex on Various Metabolic Parameters in the DN Mice Model.** The *in vivo* experiments were performed to evaluate the therapeutic efficiency of siRNA nanoplex in STZ induced DN mice. As shown in Table 1, the STZ treated DN mice showed a significantly elevated glucose level (25 ± 3 mmol/L; $p < 0.001$) as compared to the healthy control mice (9 ± 1 mmol/L). Additionally, as compared to the control group, there was a significant decrement in creatinine clearance in DN mice (from 1.2 ± 0.4 mL/min to 0.4 ± 0.2 mL/min; $p < 0.05$) along with an enhancement in the levels of serum BUN (from 25 ± 1 to 33 ± 2; $p < 0.001$), serum creatinine (from 53 ± 16 μmol/L to 97 ± 11 μmol/L; $p <$ 0.001), and NAG activity (from 0.009 ± 0.0002 U/L to 0.020 ± 0.001 U/L; $p < 0.001$). Further, the urinary albumin excretion rate (UAER) was found to be enhanced from 0.1 ± 0.02 to 2 ± 0.5 as compared to healthy control ($p < 0.001$). Our results were analogous to the literature that reports for the generation of the DN model in mice,[55] which confirms the successful development of DN conditions in an experimental mouse model.

A 4 weeks treatment of DTsiANp-cRGD/HDAC4 nanoplex in DN mice significantly improved the kidney function as evidenced by reversal of abnormally altered pathological levels of metabolic parameters in DN mouse model as compared to other treatment groups (Table 1). Specifically, the creatinine clearance level was found to be 0.4 ± 0.2 mL/min, 0.4 ± 0.1 mL/min, 0.5 ± 0.1 mL/min, and 0.6 ± 0.2 mL/min for DTsiANp-cRGD/scramble, free HDAC4 siRNA, DTsiANp/HDAC4, and DTsiANp-cRGD/HDAC4. After 4 weeks of treatment of free HDAC4 siRNA to DN mice group lead to a slight restoration in the creatinine clearance level up to 5 ± 0.2%, only. On the other hand, DTsiANp/HDAC4 and DTsiANp-cRGD/HDAC4 lead to a 38 ± 0.2% ($p < 0.01$) and 19 ± 0.2% ($p < 0.05$) restoration, respectively, as compared to the DN control. Further, the serum BUN level after the treatment of DTsiANp-cRGD/scramble, free HDAC4 siRNA, DTsiANp/HDAC4, and DTsiANp-cRGD/HDAC4 was found to be 32 ± 2, 30 ± 3, 30 ± 3, and 28 ± 2, respectively, as against to DN mice (33 ± 2). The restoration of serum BUN level toward the normal level was nonsignificant in cases of


https://dx.doi.org/10.1021/acs.molpharmaceut.0c00094
Mol. Pharmaceutics 2021, 18, 641–666

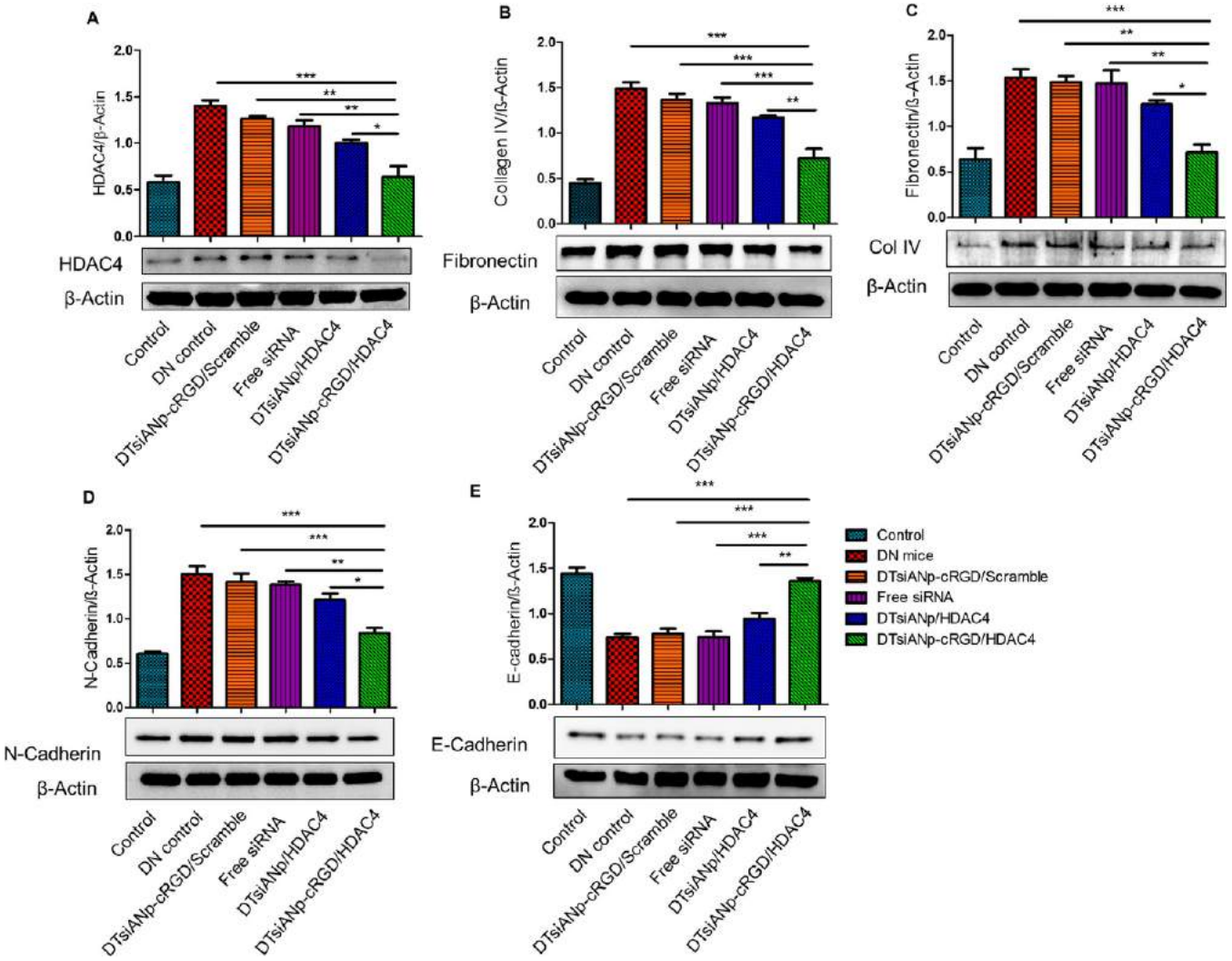


**Figure 7.** (A) Representative Western blot analysis showing expression of HDAC4 in C57BL/6 mice following the treatment of free HDAC4 siRNA, DTsiANp-cRGD/Scramble, DTsiANp/HDAC4, and DTsiANp-cRGD/HDAC4. (B) Relative expression of fibronectin (285 kDa) with reference to $\beta$-actin after treatment. (C) Relative expression of collagen IV (COL IV) with reference to $\beta$-actin after treatment. (D) Relative expression of N-cadherin (132 kDa) with reference to $\beta$-actin after treatment. (E) Relative expression of E-cadherin (120 kDa) with reference to $\beta$-actin after treatment. The analysis was performed using ImageJ (NIH, Bethesda, MD). ***$p < 0.001$,**$p < 0.01$. and *$p < 0.05$. Results are represented as mean ± SEM ($n = 3$).

DTsiANp-cRGD/scramble, HDAC4 siRNA, and HDAC4 siRNA treated DN mice with a 2 ± 2% ($p > 0.05$), 8 ± 2% ($p > 0.05$), and 7 ± 2% ($p > 0.05$) restoration, respectively. On the other hand, significant restoration of serum BUN level was observed in the case of DN mice treated with DTsiANp-cRGD/HDAC4, which showed a restoration of 11 ± 2% ($p < 0.05$).

Besides, the NAG activity after the treatment of nanoplex was found to be 0.0198 ± 0.001 U/L, 0.016 ± 0.001 U/L, 0.016 ± 0.002 U/L, and 0.013 ± 0.0004 U/L, respectively, for DTsiANp-cRGD/scramble, free HDAC4 siRNA, DTsiANp/HDAC4, and DTsiANp-cRGD/HDAC4. The obtained NAG activity was reduced markedly by 33 ± 4% ($p < 0.05$) following the treatment of DTsiANp-cRGD/HDAC4 over DTsiANp-cRGD/scramble (20.0 ± 0.006%; $p > 0.05$), free HDAC4 siRNA (20 ± 1%; $p > 0.05$), and DTsiANp/HDAC4 (10 ± 1%; $p > 0.05$).

The level of serum creatinine gets elevated markedly in the DN condition that mediates the reduction in glomerular filtration rate (GFR).[75] The treatment of free HDAC4 siRNA (93 ± 5 $\mu$mol/L), DTsiANp-cRGD/scramble (103 ± 12 $\mu$mol/L), and DTsiANp/HDAC4 (94 ± 12 $\mu$mol/L) treated mice group did not reduce the serum creatinine concerning DN control group. Besides, the DTsiANp-cRGD/HDAC4 treated DN mice group showed a successful reduction in the serum creatinine level by 83 ± 14 $\mu$mol/L (15 ± 1% reduction; $p < 0.01$).

The enhancement in the urinary protein level is a key marker for the albuminuria that exists in DN. It was observed that following the treatment of DTsiANp/HDAC4 and DTsiANp-cRGD/HDAC4, and the UAER level was reduced to 0.8 ± 0.4 (52 ± 1%; $p < 0.01$) and 1.15 ± 0.34 (36 ± 1%; $p < 0.05$), respectively. Whereas, in the case of DTsiANp-cRGD/scramble and free HDAC4 siRNA, the UAER level was not significantly changed and were found to be 1.3 ± 0.3 and 1.8 ± 0.5, respectively (Table 1). From these results; it can be said that DTsiANp-cRGD/HDAC4 significantly improves the metabolic parameters in DN mice. Further, the effect of siRNA nanoplex was evaluated utilizing gene silencing using Western


https://dx.doi.org/10.1021/acs.molpharmaceut.0c00094
Mol. Pharmaceutics 2021, 18, 641−666

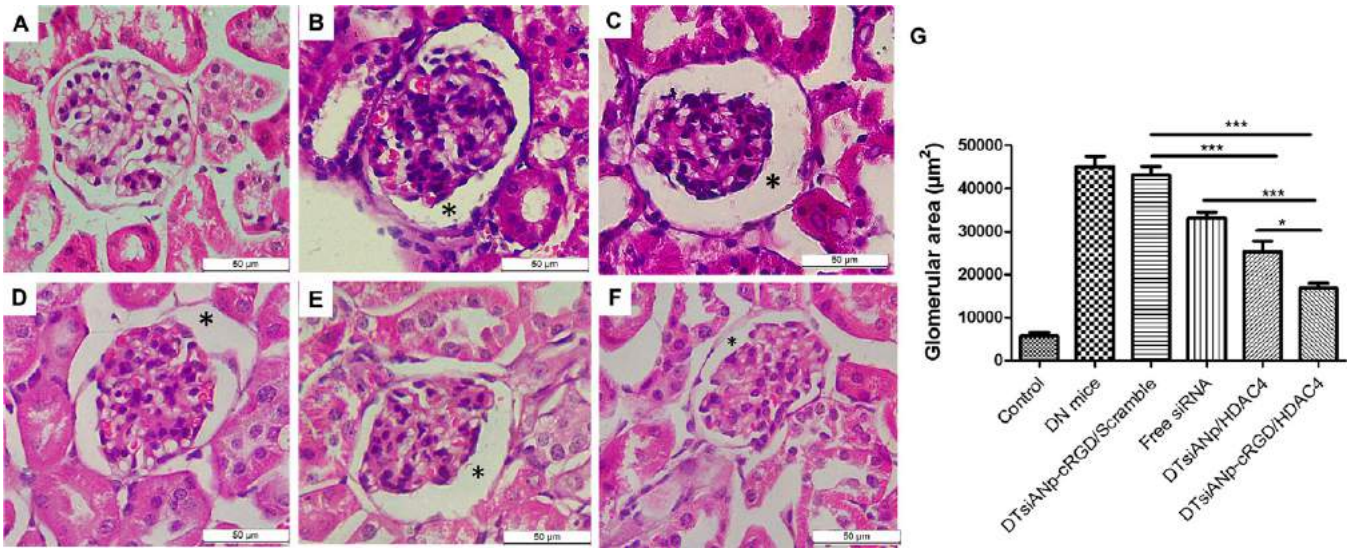


**Figure 8.** Histopathological analysis of kidney sample through hematoxylineosin staining: (A) control healthy group, (B) DN mice, (C) DTsiANp-cRGD/Scramble, (D) free HDAC4 siRNA, (E) DTsiANp/HDAC4, (F) DTsiANp-cRGD/HDAC4 (asterisk representing glomerular area), (G) glomerular area ($\mu m^2$) of ten random glomeruli; *$p < 0.05$ vs DTsiANp/HDAC4; ***$p < 0.001$ vs Free HDAC4 siRNA and DTsiANp-cRGD/scramble; ***$p < 0.001$ for DTsiANp-cRGD/scramble vs DTsiANp/HDAC4. Results are represented as mean ± SD (10 random cortex region images per mice).

blot and mice kidney tissue histology analysis, as presented below.

**3.14. *In Vivo* Gene Silencing Efficiency on C57BL/6 DN Mice Model.** The level of HDAC4 protein gets selectively overexpressed in the DN kidney. Notably, this rise in the expression of HDAC4 is primarily responsible for mediating podocytes injury and resulting in a pathologic situation called albuminuria.[3] To assess the curative and reversal effect of proposed siRNA therapeutics, the levels of HDAC4 protein expression were assessed following a 4-week treatment of various siRNA nanoplex including free HDAC4 siRNA, scramble, DTsiANp/HDAC4, and DTsiANp-cRGD/HDAC4.

As shown in Figure 7A, free HDAC4 siRNA treated DN mice group does not significantly repress the expression of HDAC4 (0.2 ± 0.1-fold; $p > 0.05$) in DN mice treated with saline. In the DTsiANp-cRGD/Scramble treated group, the relative expression of HDAC4 (1.3 ± 0.04) was found to be similar to the DN group (1.4 ± 0.1; $p > 0.05$), whereas DTsiANp/HDAC4 downregulates the relative expression of HDAC4 up to 0.3 ± 0.1-fold ($p < 0.05$) concerning DN mice and DTsiANp-cRGD/Scramble. The expression of HDAC4 gets relatively suppressed following the treatment of DTsiANp-cRGD/HDAC4 (0.6 ± 0.1-fold and 0.5 ± 0.1; $p < 0.001$) compared to the DN group and DTsiANp-cRGD/Scramble. Therefore, the results suggested that DTsiANp-cRGD/HDAC4 effectively lessened the HDAC4 expression *in vivo* after effective and targeted delivery of DTsiANp-cRGD/HDAC4 which might be selectively retained at podocytes and improve the kidney situation in DN condition.

The knock-down of HDAC4 was also examined in mice kidney via immunohistochemistry (IHC). While HDAC4 was localized in podocytes containing glomerulus region of DN mice (Figure 9). The increased level of HDAC4 in DN mice had been suppressed via DTsiANp-cRGD/HDAC4 compared to the DN mice (Figure 9J and L; $p < 0.01$). The obtained results were consistent with the Western blot analysis, and the results suggested that DTsiANp-cRGD/HDAC4 was able to knock-down elevated HDAC4 expression in podocytes of DN mice.

**3.15. Effect of Nanoplex on DN Induced Extracellular Matrix (ECM) and Epithelial-Mesenchymal Transition (EMT).** In hyperglycaemic kidney condition as an ECM marker, collagen is increased and responsible for kidney fibrosis. Similar to collagen, with fibronectin also appearing in the early phase of renal fibrosis.[60] So, the renal fibrotic marker was evaluated after treatment with the HDAC4 nanoplex to DN mice. Treatment with DTsiANp-cRGD/HDAC4 results in significant suppression in fibronectin 38 ± 4% ($p < 0.01$), 46 ± 3% ($p < 0.001$), 47 ± 4% ($p < 0.001$), and 52 ± 3% ($p < 0.001$) compared to DTsiANp/HDAC4, free siRNA, DTsiANp-cRGD/scramble, and DN mice, and no significant difference from control (Figure 7B). Collagen IV (COL IV) is an inherent component of the kidney tissue and was found upregulated in the DN mice kidney up to 59 ± 3% ($p < 0.001$). After the treatment with the DTsiANp-cRGD/HDAC4 the elevated COL IV expression (Figure 7C) was down-regulated by 42 ± 5% ($p < 0.05$), 50 ± 4% ($p < 0.01$), 52 ± 2% ($p < 0.01$), and 53 ± 2% ($p < 0.001$) in comparison to DTsiANp/HDAC4, free siRNA, DTsiANp-cRGD/scramble, and DN mice. Therefore, the reduction in expression of the fibrotic marker was observed after the treatment with the HDAC4 nanoplex.

However, to evaluate the effect of nanoplex on hyperglycemia elevated podocytes EMT, we examined mainly N-cadherin and E-cadherin. The results suggested that the DN condition of kidney increases podocytes EMT which were reduced upon treatment of DTsiANp-cRGD/HDAC4 significantly (Figure 7D). The DTsiANp-cRGD/HDAC4 treated DN mice exhibited 31 ± 2% ($p < 0.05$), 39 ± 4% ($p < 0.01$), 40 ± 3% ($p < 0.001$), and 44 ± 3% ($p < 0.001$) suppression of N-cadherin compared to DTsiANp/HDAC4, free siRNA, DTsiANp-cRGD/scramble, and DN mice, whereas another EMT marker such as E-cadherin (Figure 7E) was found to be elevated after treatment with the DTsiANp-cRGD/HDAC4 by 21 ± 2% ($p < 0.01$), 34 ± 3% ($p < 0.001$), 38 ± 4% ($p <$


https://dx.doi.org/10.1021/acs.molpharmaceut.0c00094
*Mol. Pharmaceutics* 2021, 18, 641−666

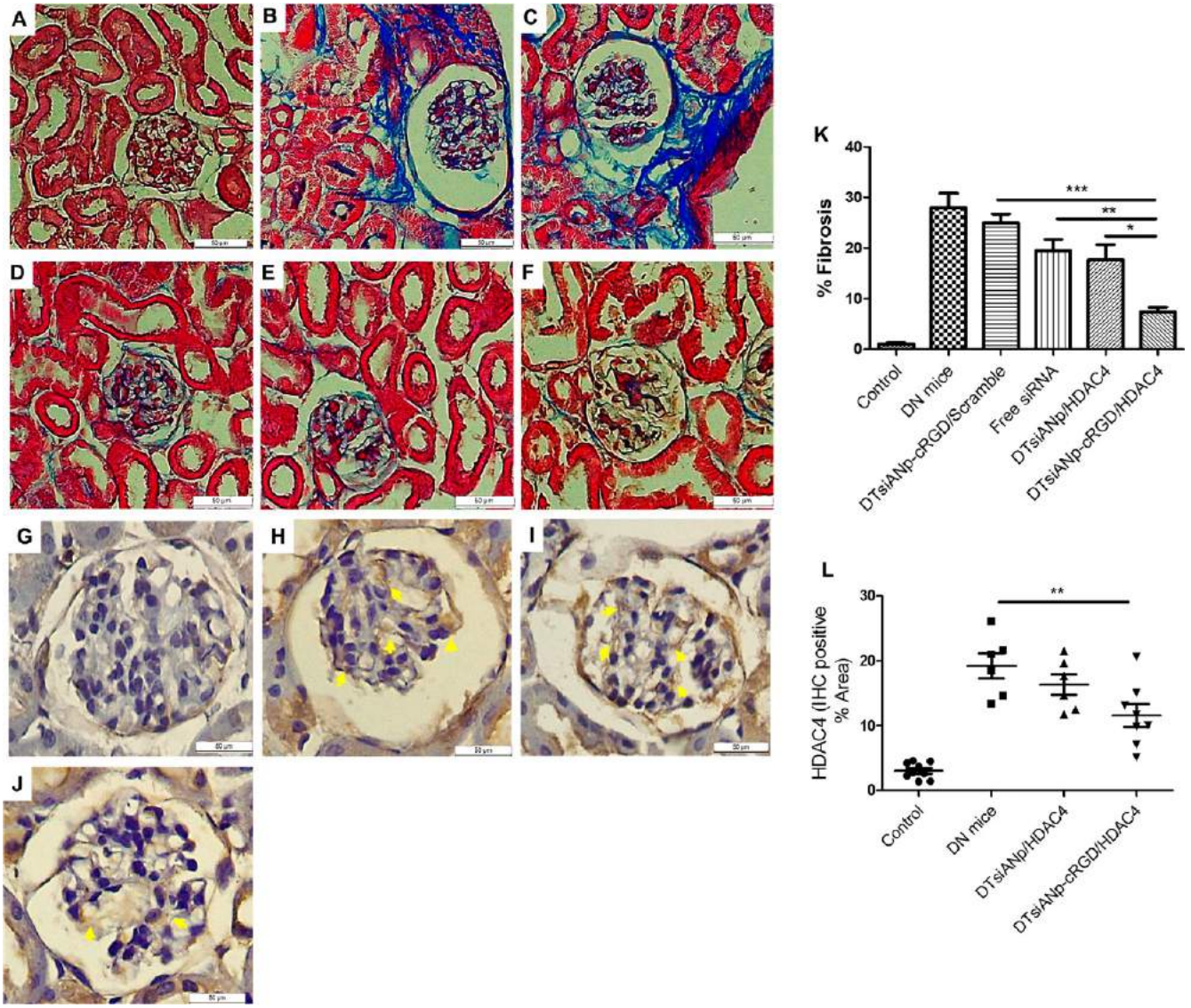


**Figure 9.** Modified Masson's trichrome staining for valuation of glomerular fibrosis: (A) control healthy group, (B) DN mice (C) DTsiANp-cRGD/Scramble, (D) free HDAC4 siRNA, (E) DTsiANp/HDAC4, (F) DTsiANp-cRGD/HDAC4. (G) IHC staining ($n$ = 6−8) of control, (H) DN mice, (I) DTsiANp/HDAC4, (J) DTsiANp-cRGD/HDAC4 (yellow arrowhead representing HDAC4 positive area as brown region), (K) percentage fibrosis of ten random glomeruli ($n$ = 10), (L) quantification of the IHC staining mean ± SD; *$p$ < 0.05, **$p$ < 0.01, ***$p$ < 0.001 (Scale: ×400). Results are represented as mean ± SD (15 random cortex region images per mouse).

0.001), and 39 ± 2% ($p$ < 0.001), compared to DTsiANp/HDAC4, free siRNA, DTsiANp-cRGD/scramble, and DN mice.

**3.16. Renal Histological Evaluation.** The pathological variations in kidney glomerular are observed using hematoxylin-eosin staining and modified Masson's trichrome staining.[60] In DN kidney, a common feature, viz. glomerular area expansion, was observed by 0.9 ± 0.1-fold ($p$ < 0.001; Figure 8B) as compared to healthy control mice, whereas in the case of free siRNA treated group, the glomerular area was enhanced by 0.8 ± 0.04-fold in comparison to healthy control mice (Figure 8D). In the case of DTsiANp/HDAC4 treated DN mice group, the glomerular area expansion was slightly reduced (0.4 ± 0.1-fold and 0.4 ± 0.11-fold; $p$ < 0.001) in comparison to DN mice and DTsiANp-cRGD/scramble. The DN mice group treated with DTsiANp-cRGD/HDAC4 showed the improvement in the expanded glomerular area by 0.6 ± 0.1-fold ($p$ < 0.001) and as compared to DN group, 0.6 ± 0.03-fold ($p$ < 0.001) as compared to DTsiANp-cRGD/scramble, 0.5 ± 0.1-fold ($p$ < 0.01) compared to free HDAC4 siRNA, and 0.3 ± 0.1 ($p$ < 0.05)-fold reference to DTsiANp/HDAC4 (Figure 8F and G). These pathological abnormalities in DN mice get alleviated following the treatment of DTsiANp-cRGD/HDAC4 as compared to DTsiANp-cRGD/Scramble, DTsiANp/HDAC4, and DTsiANp-cRGD/HDAC4 nanoplexes. Further, the DTsiANp-cRGD/HDAC4 markedly reduced the expanded glomerular area of the bowman's space.

In DN, due to glomerular hypertrophy, the glomerular number was decreased compared to control mice.[76,77] However, at the early stage of the DN also triggers fibrosis of glomerular and tubular region.[60] After that, fibrosis was further confirmed using trichrome staining.

In a healthy kidney, collagen is expressed at a minimal level, while an increased level was associated with events of renal fibrosis.[78] The modified Masson's trichrome staining exhibited significant enhancement in the accumulation of extracellular


https://dx.doi.org/10.1021/acs.molpharmaceut.0c00094
Mol. Pharmaceutics 2021, 18, 641−666

matrix-associated collagen or fibrosis in the glomerular interstitial area of DN mice (Figure 9B). After treatment with free HDAC4 siRNA, the fibrosis got reduced by 0.3 ± 0.2-fold ($p > 0.05$) as compared to the DN mice group (Figure 9D), whereas DTsiANp/HDAC4 treated mice group significantly reduced the accumulated fibrosis by 0.4 ± 0.1-fold ($p < 0.05$) and 0.3 ± 0.1-fold ($p > 0.05$) over the DN mice group and DTsiANp-cRGD/scramble (Figure 9E). The DTsiANp-cRGD/scramble treated group did not show any significant effect on extracellular matrix accumulation (Figure 9C). However, the treatment of DTsiANp-cRGD/HDAC4 to the DN mice group significantly reduced the collagen by 0.7 ± 0.1-fold ($p < 0.001$; Figure 9F).

The reduction in fibrosis by DTsiANp-cRGD/HDAC4 was found to be 0.7 ± 0.1-fold ($p < 0.01$) and 0.6 ± 0.1-fold ($p < 0.05$) (Figure 9K), respectively, in comparison with free HDAC4 siRNA and DTsiANp/HDAC4. The fibrosis was also reduced by 0.7 ± 0.1-fold ($p < 0.01$) though DTsiANp-cRGD/HDAC4 after the treatment of DTsiANp-cRGD/scramble. The finding suggested that *in vivo* HDAC4 delivered via DTsiANp-cRGD/HDAC4 was able to reduce the renal injury and inhibit fibrosis through a reduction in collagen accumulation and expansion of the glomerular area.

**3.17. Toxicity Determination by Hematological, Biochemical, and Histological Analysis.** The subacute toxicity of DTsiANp-cRGD/HDAC4 was evaluated on days 0, 14, and 28 days following a similar treatment regimen as employed in the pharmacodynamics study.[79] Further, the hematology and biochemistry parameters [such as platelets (PLT), hemoglobin, red blood cells, white blood cells (WBC), mean corpuscular volume (MCV), mean corpuscular hemoglobin (MCH), mean corpuscular hemoglobin concentration (MCHC), and red cell distribution width (RDW)] were also studied to infer the toxicity status of a developed nanoplex.[80] A comprehensive toxicity evaluation report following the administration of DTsiANp-cRGD/HDAC4 nanoplex is presented in Table S1.

The PLT is known for the initiation and propagation of the coagulation process that maintains the homeostasis. The count of PLT is acting as a key indicator of bleeding risk. Here, the PLT count was found to be 5 ± 1 × $10^5/\mu$L for the day "0" control mice, and it remained unchanged after the treatment of DTsiANp-cRGD/HDAC4 at 14 days (4 ± 1 × $10^5/\mu$L) as well as 28 days (4 ± 1 × $10^5/\mu$L) (Table S1). The normal level of PLT manifests maintaining the normal homeostatic condition for the coagulation. This infers an insignificant alternation in the PLT value even after the 28 days of DTsiANp-cRGD/HDAC4 treatment, concluding its biocompatibility.[81] Further, the interaction of nanoplex with hemoglobin was also demonstrated. Interaction of nanoplex with hemoglobin might change the surface property and count of hemoglobin. The hemoglobin level in DTsiANp-cRGD/HDAC4 treated group at 14 days (17 ± 1 × $10^5/\mu$L) and 28 days (19 ± 1 × $10^5/\mu$L) was found to be similar as compared today "0" control (13 ± 1 × $10^5/\mu$L). The outcomes suggested that DTsiANp-cRGD/HDAC4 was not interacting with the hemoglobin and maintaining normal hemoglobin levels.[80]

Here, MCV is considered as the average volume of red blood cells, and if the MCV changed, it indicates the MCV associated anemia. Here, the MCV was 46 ± 1 fL in the day "0" control group, while in DTsiANp-cRGD/HDAC4 treated mice it was shown as 45 ± 1 fL (14 days) and 57 ± 4 fL (28 days) (Table S1). Here, the mean corpuscular volume was enhanced significantly at the 28-day treatment of DTsiANp-cRGD/HDAC4 but was found in the standard range of mean corpuscular volume for mice (40−55 fL). It suggests the absence of any indication of anemia.[82] MCH represents the average amount of hemoglobin from the red blood cells. The altered level of MCH has indicated the hypochromic anemia. In the present investigation, MCH obtained for the day "0" control, DTsiANp-cRGD/HDAC4 for 14 days and 28 days as 14 ± 0.2 pg, 15 ± 0.2 pg, and 15 ± 1 pg, respectively, remained unaltered after the treatment. Here, after the treatment of DTsiANp-cRGD/HDAC4MCH the value remained similar to the day "0" control signifying the absence of any hypochromic anemic indication.[83]

Similarly, MCHC is the average concentration of hemoglobin in red blood cells. The changed level of MCHC might cause macrocytic or microcytic anemia. Therefore, values in the case of the siRNA nanoplex treated group were found to be similar to that of the day "0" control group (31 ± 0.1 g/dL), wherein the MCHC level following the administration of DTsiANp-cRGD/HDAC4 was found to be 33 ± 0.5 and 33 ± 1 g/dL at 14 and 28 days, respectively (Table S1). From the unaltered level of MCHC after DTsiANp-cRGD/HDAC4 treatment, it can be said that there was no indication for macrocytic or microcytic anemia.[83] However, RDW is indicating an erythrocyte volume index. The varied level of RDW alerted the life span of erythrocytes and might be responsible for anemia. Here, the RDW was found to be 14 ± 0.3% in the case of day "0" control, which roused insignificantly to 15 ± 1 and 15 ± 1.2% following the treatment of DTsiANp-cRGD/HDAC4 at 14 days as well as 28 days. This result infers that insignificant change in the RDW level inferred the biological compatibility of the nanoplex.

The WBC's are well reported to elicit inflammatory and antigenic response following the parenteral administration of toxic products.[82] An insignificant change in the WBC level was observed following the parenteral administration of DTsiANp-cRGD/HDAC4 for 28 days as compared to the day "0" control group. The control WBC count was found to be 8 ± 0.4 × $10^3/\mu$L that remained statistically intact at 7 ± 2 × $10^3/\mu$L and 7 ± 1 × $10^3/\mu$L, respectively, at 14 and 28 days (Table S1) suggesting the absence of any inflammatory response. Our results were found analogous with the Rugo et al. where hematological parameter was evaluated for biocompatibility of albumin-bound paclitaxel and paclitaxel.[84]

Furthermore, the differentiated WBC counts, such as neutrophil, eosinophils, lymphocytes, and basophils, are important components of the immune system. The levels of these components get altered in the case of infections. After administration of DTsiANp-cRGD/HDAC4, the neutrophil level was found to be 4 ± 1%, 4 ± 0.4%, and 3 ± 1.8 at 0-day, 14 days, and 28 days, respectively, inferring an insignificant change ($p > 0.05$). Similarly, the level of lymphocytes remained unchanged with statistically similar values at day "0" control (88 ± 1%), day 14 (87 ± 1; $p > 0.05$), and day 28 (85 ± 2; $p > 0.05$). This outcome suggests the absence of any antigenic response with DTsiANp-cRGD/HDAC4. The minor cell types such as eosinophil were also studied that showed the same level at day "0" (2 ± 0.3%), day 14 (2 ± 1%; $p > 0.05$), and at day 28 (2 ± 1%; $p > 0.05$). And monocytes (0.1 ± 0.1, 0.1 ± 0.2, and 0.2 ± 0.9, respectively, for control, at 14 days and 28 days treatment) also remained unchanged (Table S1; $p > 0.05$). The outcomes were suggesting the absence of any type of chronic infection or inflammatory or allergic responses.[83]


https://dx.doi.org/10.1021/acs.molpharmaceut.0c00094
Mol. Pharmaceutics 2021, 18, 641−666

Concomitantly, we also investigated the biochemical effect of DTsiANp-cRGD/HDAC4 on DN mice, as shown in Table S2. The ALT and AST are mostly distributed in liver cell cytoplasm and mitochondria. It is well reported that the levels of ALT and AST get changed corresponding to the level of liver damage and are also employed as a common pathological indicator of liver damage.[80] The level of AST was found to be 24 ± 2 IU/L, 22 ± 2 IU/L, and 23 ± 2 IU/L ($p > 0.05$), respectively, for the day "0" control group, after 14 days and 28 days of the treatment of DTsiANp-cRGD/HDAC4. Similarly, the ALT was also measured at day "0" to be 19 ± 1 IU/L, which remained unaltered at 14 days and 28 days following the treatment of DTsiANp-cRGD/HDAC4 as 21 ± 2 IU/L ($p > 0.05$) and 22 ± 2 IU/L ($p > 0.05$), respectively. Therefore, results indicated that siRNA nanoplex were found safe and devoid of any liver toxicity.

The liver, spleen, and lungs are the critical organs that get most affected by parenterally administered formulations following macrophage uptake.[80] As Figure S5 showed histological observation of these critical body organs, wherein no gross and microscopic alteration was found of these organs compared to the day "0" control. Additionally, the small microscopic change was observed in the histology of lungs, liver, and spleen that can be ascribed to an elevated blood glucose level in STZ induced DN mice. In the case of liver histology, the observed pathological changes included the sinus dilation around the central vein and monocyte infiltration. The lung showed infiltration of the inflammatory cells and indicated inflammation to some extent. Besides, in the case of spleen histology, marginal zone degeneration was observed due to high blood glucose.[85,86] Therefore, the observed pathological changes were not significant with the DTsiANp-cRGD/HDAC4 treated DN mice group. Hence, STZ induced acute diabetes showed some extent of pathological changes in the lungs, liver, and spleen and remained even after the treatment with the nanoplex.

**3.18. *In Vitro* Hemocompatibility Assay.** The results of the hemocompatibility assay are as mentioned in Figure S3. The results suggested that the ANp, siANp, ANp-cRGD, DTANp-cRGD, siANp-cRGD, and DTsiANp-cRGD showed not more than 0.7% hemolysis ($p > 0.05$) when experimented on different dendrimer concentrations. From the results it is inferred that prepared nanoplexes were found safe as well as biologically compatible due to the presence of endogenous albumin.[36]

## 4. DISCUSSION

Accumulation of extracellular matrix proteins, viz. collagen, leading to fibrosis and mesangial matrix expansion results in hypertrophy as well as glomerular damage in the tubular regions of the kidney that primarily contributes to renal failure in DN condition. The HG level also adversely impacts the kidney by mediating the effacement of podocytes' foot process, loss in podocytes counts and its progressive suppression of autophagy. The $\alpha_v\beta_3$ integrin that is overexpressed on renal podocytes plays a pivotal role in the development and functionalization of the kidney (example: in adhesion of crescentic cells, etc.). Reports suggest that the expression of $\alpha_v\beta_3$ integrin enhanced on the surface of podocytes in DN due to the enhancement of the expression of VEGF, bFGF, TNF$\alpha$, and other cytokines.[33] Reports also suggest that in proteinuric kidney diseases including DN, the soluble urokinase receptor activates the $\alpha_v\beta_3$ receptor, which led to podocytes effacement. While the specifically arg-gly asp motif of cRGD [cyclo-(Arg-Gly-Asp-D-Phe-Cys)] bears the highest affinity toward the $\alpha_v\beta_3$ integrin to modulate the podocytes adhesion process.[32] In context, Pollinger et al. proved specific $\alpha_v\beta_3$ receptor binding with cRGD modified quantum dots in podocytes cells.[31]

In this investigation, the nanoplex technology developed and reported in this work comprises albumin as a natural biodegradable FDA approved biopolymeric carrier. The investigation examines the cRGD-truncated polymeric nanoplex with dendrimeric templates (DTsiANp-cRGD) for targeted HDAC4 gene silencing. To acquire $\alpha_v\beta_3$ integrin receptor-mediated specific targeting, albumin biopolymer was modified with cRGD peptide, which was then utilized to complex siRNA employing an in-house developed dendrimeric templated approach. The developed nanoplex encapsulates as well as stabilizes HDAC4 siRNA inside the developed polymeric nanoconstruct using the dendrimer templated approach. The prepared cRGD truncated nanoplex was tested on a human podocytes DN model for receptor-selective binding of nanoplex using a competition binding assay. The gene silencing effect of HDAC4 siRNA was evaluated on the *in vitro* DN model and *in vivo* C57BL/6 DN mice model as well. The kidney functionality in C57BL/6 DN mice was evaluated using renal histological analysis after the treatment with cRGD truncated nanoplex. A systematic mention of the results and the associated discussion are presented in the below section of the manuscript.

The albumin was effectively conjugated with cRGDfC using MBS cross-linker and characterized for surface zeta potential. A 19 ± 3% (Figure 1A) decrement in surface zeta potential was found after modification of albumin to A-cRGD conjugation, which can be ascribed that free amino group of albumins were utilized in conjugation with maleimide benzoyl via amide linkage and then conjugated with cRGD. That might lead to a reduction in the free amino group of albumin and remaining −COOH group showed a more negative charge, owing to the availability of more oxygen molecules.[87] The primary evaluation of the increment in the molecular weight of albumin was done by SDS-PAGE and found enhanced molecular weight based on the location of the protein band (Figure 1B). The enhancement in the molecular weight of albumin suggests conjugation of cRGD on albumin.

Similarly, conjugation was further confirmed by TNBS assay for utilization of free primary amino group and found 28 ± 2% ($p < 0.05$) decrement in the free primary amino group. From the results, it can be said that almost 47 ± 9 × $10^{23}$ (Figure 1C) amino groups have taken part in the conjugation of MBS or cRGD. The functional group of the conjugation was analyzed through FT-IR and found additional C−S conjugation because of free Cys residue of the peptide (Figure 1E). This outcome confirms the conjugation of cRGD with albumin via MBS cross-linker. Our results are analogous to that of Yu et al. where cRGD was conjugated with human serum albumin and similar observations were made.[87] The final confirmation was done through MALDI-TOF MS and suggesting successful conjugation of 15 molecules of cRGD with one molecule of albumin in the A-cRGD conjugate (Figure 1G).

The siRNA was efficiently forming a complex with the dendrimer due to electrostatic interaction. At a higher *n/p* ratio, no siRNA bands were visible in the gel. This infers that in the case of *d*:siR complex formed at *n/p* ratio of 1 and 0.5, the siRNA gets completely involved in the complexation with


https://dx.doi.org/10.1021/acs.molpharmaceut.0c00094
Mol. Pharmaceutics 2021, 18, 641−666

dendrimer branch structure crevices thus making it technically unavailable for reaction with ethidium bromide dye (Figure 1D). It may be noted that positively charged ethidium bromide dye bears a sensitive potency to detect the negatively charged siRNA. The absence of ethidium bromide dye-binding as evinced by the absence of siRNA specific bands in the case of *d*:siR complex forms at *n/p ration of* ≥0.5 infers unavailability of free or leaked siRNA. The reason behind the complex formation of siRNA with dendrimer was electrostatic interaction of negatively charged phosphate groups of siRNA with positively charged $NH_2$ terminal ends of the dendrimer.[73] Similarly, Ma et al. also reported that at a higher *n/p* ratio, the complete blocking of siRNA was observed in PAMAM dendrimeric nanoplex due to sufficient cationic charge of dendrimer being able to effectively bind with siRNA.[88]

The resultant DTsiANp-cRGD/HDAC4 exhibited slight decrement in zeta potential as compared to DTsiANp/HDAC4 and can be ascribed to the utilization of a more negatively charged A-cRGD conjugate that has been used for the preparation of DTsiANp. The formulated nanoplexes were found spherical and in the nanometric range. The DTsiANp-cRGD/HDAC4 representing enhanced siRNA encapsulation efficiency and found less entrapment in siANp (Figure 2D). Our results are in agreement with the existing literature that also briefs low encapsulation efficiency to be one of the major issues associated with conventional albumin-based particles.[24] Hence, one of the major prepositions of this research was to overcome this issue and enhance siRNA encapsulation efficiency. In this context, a versatile dendrimer templated approach was adopted in this work. It may be noted that albumin and A-cRGD are negatively charged biopolymers and hence show poor interaction with the negatively charged siRNA (anionic phosphate side chain), which creates a repulsive environment for the encapsulation of anionic siRNA molecules. The poor biopolymer albumin−siRNA interaction can be ascribed to be the prime reason for poor siRNA encapsulation efficiency in the case of conventional albumin nanoplex, siANp.[89,90] The higher siRNA encapsulation in cases of DTsiANp and DTsiANp-cRGD can be ascribed to the adaption of a systematic dendrimer templated approach for siRNA encapsulation. It may be noted that the net anionic albumin/A-cRGD undergoes an effective interaction with the systematically designed cationic *d*:siR complex as compared to the anionic siRNA alone. The developed nanoplex containing a simple mix and deliver dendrimeric template strategy has been developed to encapsulate HDAC4 siRNA in the albumin compartment with high loading efficiency.

The stability of encapsulated siRNA is yet another major challenge in systemic siRNA delivery owing to its degradation by circulatory endonuclease in the bloodstream.[91] Therefore, there is a need to evaluate the stability of siRNA in the presence and absence of serum endonuclease enzyme for siANp, DTsiANp, and DTsiANp-cRGD concerning free siRNA. The serum stability results suggest that the siRNA encapsulated inside DTsiANp-cRGD was found to primarily retain in the loading well due to the higher density of the DTsiANp-cRGD formulation but was stable throughout the experimentation (Figure 2G). The enhanced stability of siRNA in the presence of serum endonuclease was due to polycationic and siRNA interaction complex (*d*:siR complex) via charge-based interaction that might not allow unwanted interchange of siRNA with other polyions exterior to the cells which result in less delivery of siRNA.[92] The stability study profile was further evaluated in serum-containing media as well as in saline (0.9%w/v NaCl). From the results, it can be said that there was no interaction observed even after 24 h incubation of siANp, DTsiANp, and DTsiANp-cRGD in terms of particle size, PDI, and zeta potential. This deduces the stability of nanoplex in serum-containing media as well as in saline solution, which can be attributed to the natural albumin biopolymeric skeleton.[25] The strategically developed dendrimer templated loading enhances the encapsulation of siRNA as well as being capable of protecting the loaded siRNA from the serum degradation.

The formulated nanoplexes were found to be nontoxic and compatible with the HG model of podocytes and found safe for the delivery. The anionic charge of siRNA impedes the cellular uptake of free siRNA, whereas the targeted cationic dendrimeric template bearing nanoplex was found to enhance the cellular uptake compared to free siRNA and nontargeted formulations probably because of the active targeting through $\alpha_v\beta_3$ receptors on HG treated podocytes (Figure 3). It is well-known that the expression levels of $\alpha_v\beta_3$ receptors get increased in the presence of HG condition as exists in DN.[93] The DTsiANp-cRGD nanoplex containing cRGDfC motif as Arg-Gly-Asp having the highest affinity with the $\alpha$- and $\beta$-subunits of the $\alpha_v\beta_3$ receptor and providing higher cellular uptake via integrin-dependent endocytosis pathway[33,94] and targeting ability toward $\alpha_v\beta_3$ receptors of cRGDfC was confirmed through the competition binding assay.

After cellular uptake, the release of encapsulated siRNA is yet another key event that must take place to mediate successful siRNA delivery of siRNA and mark the RNA interference process. The main impediment with siRNA and related formulations is endolysosomal degradation after uptaking through cells because of the endolysosomes enzyme (Figure 4). Therefore, one of the predominant goals of the formulated nanoplex was an endolysosomal escape. Our previous research was suggesting that dendrimer is having the ability to undergo pH-responsive changes (*proton-sponge-effect*) due to the architecture of the dendrimer.[42] Hence, the endosome/lysosome escape assay was performed to assess the endosomal escape tendency of nanoplex and infer cytosolic siRNA delivery. The results of endolysosomal escape assay ascribed the presence of a dendrimeric template in DTsiANp and DTsiANp-cRGD and provide better endosomal escape capability due to proton sponge effect of the dendrimeric template at the lower pH of endo/lysozyme.[35,95] The probable reason behind pH-responsive changes of dendrimer was the protonation of the free primary amino group in the presence of acidic pH conditions of the endolysosomal compartment (pH 5.5−4.5). This protonation enhances the net surface positive charges as well as induces the net repulsive microenvironment within an endosomal acidic environment that leads to increment in ionic concentration osmotically and enhancement in the hydrodynamic size of a dendrimer with appearance swelling. This swelling creates pressure on the endosomal membrane that leads to rupture of the endosomal membrane and releases siRNA in the cytosolic region.[35,96] Therefore, it can be said that the architecture has the in-built capability to deliver the loaded siRNA in the cytosolic compartment by evading endosomal degradation by the endosomal escape process. Further, the presence of the cRGDfC peptide motif in the base polymeric chain of albumin assists in attaining integrin


https://dx.doi.org/10.1021/acs.molpharmaceut.0c00094
Mol. Pharmaceutics 2021, 18, 641−666

receptor-mediated selective uptake in the DN podocytes, thus avoiding the off-target effect.

The ultimate goal of developing this innovative class of nanoplex was to obtain a higher fold of therapeutic benefit following improved and efficient gene silencing. In a healthy state, HDAC4 plays a vital role in the maintenance of the podocyte's foot process. But under HG state as exists in DN condition, the expression of HDAC4 gets up-regulated which is responsible for initiating podocytes injury via deacetylation of STAT1.[4] In this regard, it was observed that DTsiANp-cRGD/HDAC4 treatment is able to alleviate damaged podocytes through repression of HDAC4 expression in HG treated podocyte cells at mRNA level as well as protein level (Figure 5). The elevated level of HDAC4 leads to podocytes apoptosis. And the DTsiANp-cRGD/HDAC4 successfully down-regulates the enhanced apoptosis in HG treated podocytes. The reason for the decrement in the apoptotic population after treatment with DTsiANp/HDAC4 and DTsiANp-cRGD/HDAC4 has enhanced cellular uptake and gene silencing efficiency of HDAC4 *in vitro* DN model of podocytes (Figure 6).

The DTsiANp-cRGD/HDAC4 nanoplex effectively reduced the elevated albumin excretion rate inferring a greater therapeutic potential of nanoplex. It was also found to suppress the overexpressed HADC4 protein in C57BL/6 DN mice after the treatment of the DTsiANp-cRGD/HDAC4, and similar results were found via IHC studies (Figure 9J). The EMT of podocytes is the main factor in glomerular complications of DN which involve proteinuria as well as fibrosis.[97] From the results, it can be said that HDAC4 nanoplex treatment able to suppress the fibronectin, COL IV, and N-cadherin while subsequently elevating the expression of E-cadherin in contrast to DN mice. After the treatment of DTsiANp-cRGD/HDAC4, the elevated glomerular area was reduced by 0.6-fold and also able to reduce fibrosis or accumulation of the collagen by 0.7-fold compared to DTsiANp-cRGD/scramble (Figure 5B−D). Our results are analogous to that of Grange et al. where stem cell-derived extracellular vesicles regress the progression of fibrosis and expansion of the glomerular area in the DN mice model.[78] As reported in the literature the nanoparticles of size 70−80 nm are not recognized by the macrophages as well as specifically getting localized in the kidney podocytes.[98−100] Therefore, the systemically administered nanoplex reached to the diabetic kidney from the blood circulation via large glomerular endothelial fenestration (approximately 150 nm) and reached to the glomerular basement membrane. Due to the pathophysiology of the STZ treated DN mice kidney alters, the morphology of the glomerular basement membrane resulted in the enlargement of the glomerular basement pores (10−80 nm) due to irregular glomerular basement membrane thickening. That enables the nanoplex to reach toward podocytes via glomerular basement membrane-anchored podocytes $\alpha_v\beta_3$ integrin via cRGD and offers receptor-mediated selectivity toward the renal podocytes exhibiting selective delivery of nanoplex to renal podocytes in DN. This could be a probable mechanism for the distribution and delivery of the cRGD gated nanoplex toward the renal podocytes. In summary, the results suggest that there was no significant difference found among the hematological parameters following the administration of DTsiANp-cRGD/HDAC4, suggesting it to be highly biocompatible. A similar observation was made by Zhang et al. to evaluate the toxicity of the polyethylene glycol-coated nanoparticle.[80] Hence, we inferred that the observed pathological changes were due to the use of STZ during the DN model generation and not because of the nanoplex treatment. Therefore, the nanoplex showed high safety and biocompatibility due to the utilization of albumin (a natural biodegradable FDA approved biopolymer) as a base material in the architectural composition of the nanoplex.

## 5. CONCLUSION

This investigation examines the cRGD-truncated polymeric nanoplex with dendrimeric templates (DTsiANp-cRGD) for targeted HDAC4 gene silencing in the treatment of DN. As reported earlier by our group, the dendrimer complex selectively undergoes protonation under acidic endosomal environment. Hence, the dendrimer templated approach was strategically adapted to mediate endolysosomal escape following receptor-mediated endocytosis of cRGD targeted nanoplex as developed in this study (Indian patent Application No.: 201921019898; Date of Application: 18/05/2019). The developed nanoplex exhibited enhanced encapsulation of siRNA using the dendrimer templated approach as well as offering superior protection against serum RNase nucleases degradation. The nanoplex showed selective binding toward the $\alpha v\beta 3$ integrin receptor, higher cellular uptake, and significant *in vitro* gene silencing, when tested on HG treated podocytes. It also significantly enhanced the selective receptor-mediated cellular uptake and bears endosomal/lysosome escape tendency that is mandatory for the cytosolic delivery as well as the initiation of gene silencing activity. DTsiANp-cRGD/HDAC4 nanoplex down-regulated the expression of HDAC4 more efficiently as compared to the other counterparts, including nontargeted DTsiANp/HDAC4 and free HDAC4 siRNA.

The outcomes of *in vivo* experiments showed remarkable suppression of the HDAC4 and inhibition in the progression of renal fibrosis in the STZ induced DN C57BL/6 mice model. The DTsiANp-cRGD/HDAC4 nanoplex treated group showed a reduced level of albuminuria and was found safe with no toxicity as well as alleviated the abnormal kidney function. Histopathological and toxicological studies revealed nonsignificant abnormality/toxicity with the nanoplex. Conclusively, the developed nanoplex was found as a promising tactic for targeted therapy of podocytes and could be extended for other kidney-related ailments. The current work reposts a viable solution to the ongoing problems associated with the clinical translation of siRNA therapeutics for therapeutic interventions taking DN as a case in hand. It is believed that shortly the knowledge and understanding reported in this manuscript would pave a remarkable step toward the development of clinically translatable approaches for the treatment of DN and podocyte-associated diseases.

## ■ ASSOCIATED CONTENT

### Supporting Information

The Supporting Information is available free of charge at https://pubs.acs.org/doi/10.1021/acs.molpharmaceut.0c00094.

Schematic representation of albumin-cRGD conjugation, physical characterization of DTsiANp-cRGD nanoplex via dynamic light scattering and zeta potential graph obtained from Malvern zeta sizer, in vitro hemolysis assay of nanoplexes with mouse red blood cells, time-



https://dx.doi.org/10.1021/acs.molpharmaceut.0c00094
Mol. Pharmaceutics 2021, 18, 641−666

dependent stability study of siANp, DTsiANp, and DTsiANp-cRGD, intracellular distribution of siANp, DTsiANp, and DTsiANp-cRGD, histopathology of liver, lung, and spleen in healthy control and at 14 and 28-day treatment of DTsiANp-cRGD/HDAC4, hematological parameters for toxicity assessment in mice treated with DTsiANp-cRGD/HDAC4, biochemical parameters for toxicity assessment in mice treated with DTsiANp-cRGD/HDAC4 (PDF)

## AUTHOR INFORMATION


### Corresponding Author

**Rakesh K. Tekade** − *National Institute of Pharmaceutical Education and Research (NIPER) − Ahmedabad, Palaj (An Institute of National Importance), Gandhinagar 382355, Gujarat, India;* orcid.org/0000-0002-3024-3148; Phone: 079-6674550; Email: rakeshtekade@gmail.com, rakeshtekade@niperahm.ac.in; Fax: 07966745560

### Authors

**Nidhi Raval** − *National Institute of Pharmaceutical Education and Research (NIPER) − Ahmedabad, Palaj (An Institute of National Importance), Gandhinagar 382355, Gujarat, India*

**Hardi Jogi** − *National Institute of Pharmaceutical Education and Research (NIPER) − Ahmedabad, Palaj (An Institute of National Importance), Gandhinagar 382355, Gujarat, India*

**Piyush Gondaliya** − *National Institute of Pharmaceutical Education and Research (NIPER) − Ahmedabad, Palaj (An Institute of National Importance), Gandhinagar 382355, Gujarat, India*

**Kiran Kalia** − *National Institute of Pharmaceutical Education and Research (NIPER) − Ahmedabad, Palaj (An Institute of National Importance), Gandhinagar 382355, Gujarat, India*

Complete contact information is available at: https://pubs.acs.org/10.1021/acs.molpharmaceut.0c00094


### Notes

The authors declare the following competing financial interest(s): A part of the work described in this manuscript has been filed for Indian patent at Indian Patent Office (IPO), Mumbai, India; Application No.: 201921019898; Date of Application: 18/05/2019.

## ACKNOWLEDGMENTS

The research was carried out at the National Institute of Pharmaceutical Education and Research-Ahmedabad with the financial support from the Department of Pharmaceuticals, Ministry of Chemicals and Fertilizers, Government of India. RKT would like to acknowledge the Science and Engineering Research Board (Statutory Body Established through an Act of Parliament: SERB Act 2008), Department of Science and Technology, Government of India for a grant (Grant #ECR/2016/001964) and N-PDF funding (PDF/2016/003329) for work in Dr. Tekade's Laboratory. The authors would also like to acknowledge Jeffrey Kopp, National in the statute of Health (NIH), Maryland, USA, for the gift sample of the immortalized human podocyte cell line.

## REFERENCES


(1) Tagawa, A.; Yasuda, M.; Kume, S.; Yamahara, K.; Nakazawa, J.; Chin-Kanasaki, M.; Araki, H.; Araki, S.-i.; Koya, D.; Asanuma, K. Impaired podocyte autophagy exacerbates proteinuria in diabetic nephropathy. *Diabetes* **2016**, *65* (3), 755−767.

(2) Lal, M. A.; Young, K. W.; Andag, U. Targeting the podocyte to treat glomerular kidney disease. *Drug Discovery Today* **2015**, *20* (10), 1228−1234.

(3) Wei, Q.; Dong, Z. HDAC4 blocks autophagy to trigger podocyte injury: non-epigenetic action in diabetic nephropathy. *Kidney Int.* **2014**, *86* (4), 666−668.

(4) Wang, X.; Liu, J.; Zhen, J.; Zhang, C.; Wan, Q.; Liu, G.; Wei, X.; Zhang, Y.; Wang, Z.; Han, H. Histone deacetylase 4 selectively contributes to podocyte injury in diabetic nephropathy. *Kidney Int.* **2014**, *86* (4), 712−725.

(5) Kulkarni, J. A.; Darjuan, M. M.; Mercer, J. E.; Chen, S.; van der Meel, R.; Thewalt, J. L.; Tam, Y. Y. C.; Cullis, P. R. On the Formation and Morphology of Lipid Nanoparticles Containing Ionizable Cationic Lipids and siRNA. *ACS Nano* **2018**, *12* (5), 4787−4795.

(6) Wittrup, A.; Lieberman, J. Knocking down disease: a progress report on siRNA therapeutics. *Nat. Rev. Genet.* **2015**, *16* (9), 543.

(7) Zhao, X.; Li, F.; Li, Y.; Wang, H.; Ren, H.; Chen, J.; Nie, G.; Hao, J. Co-delivery of HIF1$\alpha$ siRNA and gemcitabine via biocompatible lipid-polymer hybrid nanoparticles for effective treatment of pancreatic cancer. *Biomaterials* **2015**, *46*, 13−25.

(8) Djemaa, S. B.; Munnier, E.; Chourpa, I.; Allard-Vannier, E.; David, S. Versatile electrostatically assembled polymeric siRNA nanovectors: Can they overcome the limits of siRNA tumor delivery? *Int. J. Pharm.* **2019**, *567*, 118432.

(9) Hoang, M.-D.; Vandamme, M.; Kratassiouk, G.; Pinna, G.; Gravel, E.; Doris, E. Tuning the cationic interface of simple polydiacetylene micelles to improve siRNA delivery at the cellular level. *Nanoscale Adv.* **2019**, *1*, 4331.

(10) Bruniaux, J.; Allard-Vannier, E.; Aubrey, N.; Lakhrif, Z.; Djemaa, S. B.; Eljack, S.; Marchais, H.; Hervé-Aubert, K.; Chourpa, I.; David, S. Magnetic nanocarriers for the specific delivery of siRNA: Contribution of breast cancer cells active targeting for down-regulation efficiency. *Int. J. Pharm.* **2019**, *569*, 118572.

(11) Manda, V.; Josyula, V. R.; Hariharapura, R. C. siRNA intervention inhibiting viral replication and delivery strategies for treating herpes simplex viral infection. *VirusDisease* **2019**, *30* (2), 180−185.

(12) Kasuya, T.; Hori, S.-i.; Watanabe, A.; Nakajima, M.; Gahara, Y.; Rokushima, M.; Yanagimoto, T.; Kugimiya, A. Ribonuclease H1-dependent hepatotoxicity caused by locked nucleic acid-modified gapmer antisense oligonucleotides. *Sci. Rep.* **2016**, *6*, 30377.

(13) Yu, X.; Liang, X.; Xie, H.; Kumar, S.; Ravinder, N.; Potter, J.; du Jeu, X. d. M.; Chesnut, J. D. Improved delivery of Cas9 protein/gRNA complexes using lipofectamine CRISPRMAX. *Biotechnol. Lett.* **2016**, *38* (6), 919−929.

(14) Andre, E.; Pensado, A.; Resnier, P.; Braz, L.; da Costa, A. R.; Passirani, C.; Sánchez, A.; Montero-Menei, C. Characterization and comparison of two novel nanosystems associated with siRNA for cellular therapy. *Int. J. Pharm.* **2016**, *497* (1−2), 255−267.

(15) Copolovici, D. M.; Langel, K.; Eriste, E.; Langel, U. Cell-penetrating peptides: design, synthesis, and applications. *ACS Nano* **2014**, *8* (3), 1972−1994.

(16) Mendes, L. P.; Sarisozen, C.; Luther, E.; Pan, J.; Torchilin, V. P. Surface-engineered polyethyleneimine-modified liposomes as novel carrier of siRNA and chemotherapeutics for combination treatment of drug-resistant cancers. *Drug Delivery* **2019**, *26* (1), 443−458.

(17) Takemoto, H.; Wang, C. L.; Nomoto, T.; Matsui, M.; Tomoda, K.; Nishiyama, N. Pyruvate responsiveness based on $\alpha$-oxohydrazone formation for intracellular siRNA release from polyion complex (PIC)-based carriers. *Biomacromolecules* **2019**, *20*, 2305.

(18) Shukla, R.; Singh, A.; Pardhi, V.; Kashyap, K.; Dubey, S. K.; Dandela, R.; Kesharwani, P. Dendrimer-Based Nanoparticulate Delivery System for Cancer Therapy. *Polymeric Nanoparticles as a Promising Tool for Anti-cancer Therapeutics*; Elsevier, 2019; pp 233−255.

(19) Hong, C. A.; Son, H. Y.; Nam, Y. S. Layer-by-layer siRNA/poly (L-lysine) multilayers on polydopamine-coated surface for efficient cell adhesion and gene silencing. *Sci. Rep.* **2018**, *8* (1), 7738.

(20) Ho, W.; Zhang, X. Q.; Xu, X. Biomaterials in siRNA delivery: a comprehensive review. *Adv. Healthcare Mater.* **2016**, *5* (21), 2715−2731.
(21) Choi, C. K. K.; Zhang, L.; Choi, C. H. J. Efficient siRNA delivery with non-cationic carriers. *Nature Biomedical Engineering* **2018**, *2* (5), 275.
(22) Wang, J.; Masehi-Lano, J. J.; Chung, E. J. Peptide and antibody ligands for renal targeting: nanomedicine strategies for kidney disease. *Biomater. Sci.* **2017**, *5* (8), 1450−1459.
(23) Zhang, Q.; Zhang, L.; Li, Z.; Xie, X.; Gao, X.; Xu, X. Inducing controlled release and increased tumor-targeted delivery of chlorambucil via albumin/liposome hybrid nanoparticles. *AAPS PharmSciTech* **2017**, *18* (8), 2977−2986.
(24) Tekade, R. K.; Tekade, M.; Kumar, M.; Chauhan, A. S. Dendrimer-stabilized smart-nanoparticle (DSSN) platform for targeted delivery of hydrophobic antitumor therapeutics. *Pharm. Res.* **2015**, *32* (3), 910−928.
(25) Tan, Y. L.; Ho, H. K. Navigating albumin-based nanoparticles through various drug delivery routes. *Drug Discovery Today* **2018**, *23* (5), 1108−1114.
(26) Jefferson, J.; Shankland, S.; Pichler, R. Proteinuria in diabetic kidney disease: a mechanistic viewpoint. *Kidney Int.* **2008**, *74* (1), 22−36.
(27) Zuckerman, J. E.; Choi, C. H. J.; Han, H.; Davis, M. E. Polycation-siRNA nanoparticles can disassemble at the kidney glomerular basement membrane. *Proc. Natl. Acad. Sci. U. S. A.* **2012**, *109* (8), 3137−3142.
(28) Choi, C. H. J.; Zuckerman, J. E.; Webster, P.; Davis, M. E. Targeting kidney mesangium by nanoparticles of defined size. *Proc. Natl. Acad. Sci. U. S. A.* **2011**, *108* (16), 6656−6661.
(29) Ota, K.; Ota, Z.; Shikata, K.; Makino, H. The ultrastructural disruption of the glomerular basement membrane in diabetic nephropathy revealed by "tissue negative staining method. *Journal of Diabetes and its Complications* **1995**, *9* (4), 285−287.
(30) Du, B.; Yu, M.; Zheng, J. Transport and interactions of nanoparticles in the kidneys. *Nature Reviews Materials* **2018**, *3* (10), 358−374.
(31) Pollinger, K.; Hennig, R.; Breunig, M.; Tessmar, J.; Ohlmann, A.; Tamm, E. R.; Witzgall, R.; Goepferich, A. Kidney Podocytes as Specific Targets for cyclo (RGDfC)-Modified Nanoparticles. *Small* **2012**, *8* (21), 3368−3375.
(32) Koh, K. H.; Cao, Y.; Mangos, S.; Tardi, N. J.; Dande, R. R.; Lee, H. W.; Samelko, B.; Altintas, M. M.; Schmitz, V. P.; Lee, H. Non-immune cell-derived ICOS ligand functions as a renoprotective $\alpha v\beta 3$ integrin-selective antagonist. *J. Clin. Invest.* **2019**, *129*, 1713.
(33) Hafdi, Z.; Lesavre, P.; Nejjari, M.; Halbwachs-Mecarelli, L.; Droz, D.; Noëul, L. Distribution of $\alpha v\beta$T3, $\alpha v\beta$TB5 integrins and the Integrin Associated Protein—IAP (CD47) in human glomerular diseases. *Cell adhesion and communication* **2000**, *7* (6), 441−451.
(34) Youngren, S. R.; Tekade, R. K.; Gustilo, B.; Hoffmann, P. R.; Chougule, M. B. STAT6 siRNA matrix-loaded gelatin nanocarriers: formulation, characterization, and ex vivo proof of concept using adenocarcinoma cells. *BioMed Res. Int.* **2013**, *2013*, 1.
(35) Tekade, R. K.; Dutta, T.; Tyagi, A.; Bharti, A. C.; Das, B. C.; Jain, N. K. Surface-engineered dendrimers for dual drug delivery: a receptor up-regulation and enhanced cancer targeting strategy. *J. Drug Targeting* **2008**, *16* (10), 758−772.
(36) Raval, N.; Jogi, H.; Gondaliya, P.; Kalia, K.; Tekade, R. K. Method and its Composition for encapsulation, stabilization, and delivery of siRNA in Anionic polymeric nanoplex: An In vitro- In vivo Assessment. *Sci. Rep.* **2019**, *9* (1), 16047.
(37) Tomita, M.; Sugi, H.; Ozawa, K.; Tsong, T. Y.; Yoshimura, T. Targeting antigen-specific receptors on B lymphocytes to generate high yields of specific monoclonal antibodies directed against biologically active lower antigenic peptides within presenilin 1. *J. Immunol. Methods* **2001**, *251* (1−2), 31−43.
(38) Muniswamy, V. J.; Raval, N.; Gondaliya, P.; Tambe, V.; Kalia, K.; Tekade, R. K. 'Dendrimer-Cationized-Albumin'encrusted polymeric nanoparticle improves BBB penetration and anticancer activity of doxorubicin. *Int. J. Pharm.* **2019**, *555*, 77−99.
(39) León, A.; Reuquen, P.; Garín, C.; Segura, R.; Vargas, P.; Zapata, P.; Orihuela, P. FTIR and Raman characterization of TiO2 nanoparticles coated with polyethylene glycol as carrier for 2-methoxyestradiol. *Appl. Sci.* **2017**, *7* (1), 49.
(40) Greco, C. T.; Muir, V. G.; Epps, T. H., III; Sullivan, M. O. Efficient tuning of siRNA dose response by combining mixed polymer nanocarriers with simple kinetic modeling. *Acta Biomater.* **2017**, *50*, 407−416.
(41) Sarett, S. M.; Werfel, T. A.; Chandra, I.; Jackson, M. A.; Kavanaugh, T. E.; Hattaway, M. E.; Giorgio, T. D.; Duvall, C. L. Hydrophobic interactions between polymeric carrier and palmitic acid-conjugated siRNA improve PEGylated polyplex stability and enhance in vivo pharmacokinetics and tumor gene silencing. *Biomaterials* **2016**, *97*, 122−132.
(42) Tekade, R. K.; Chougule, M. B. Formulation development and evaluation of hybrid nanocarrier for cancer therapy: Taguchi orthogonal array based design. *BioMed Res. Int.* **2013**, *2013*, 1.
(43) Wang, L.; Ma, Y.; Gu, Y.; Liu, Y.; Zhao, J.; Yan, B.; Wang, Y. Cryoprotectant choice and analyses of freeze-drying drug suspension of nanoparticles with functional stabilisers. *J. Microencapsulation* **2018**, *35* (3), 241−248.
(44) Raval, N.; Khunt, D.; Misra, M. Microemulsion-based delivery of triamcinolone acetonide to posterior segment of eye using chitosan and butter oil as permeation enhancer: an in vitro and in vivo investigation. *J. Microencapsulation* **2018**, *35* (1), 62−77.
(45) Lu, P.-J.; Huang, S.-C.; Chen, Y.-P.; Chiueh, L.-C.; Shih, D. Y.-C. Analysis of titanium dioxide and zinc oxide nanoparticles in cosmetics. *Journal of food and drug analysis* **2015**, *23* (3), 587−594.
(46) Liechty, W. B.; Scheuerle, R. L.; Ramirez, J. E. V.; Peppas, N. A. Cytoplasmic Delivery of Functional siRNA Using pH-Responsive Nanoscale Hydrogels. *Int. J. Pharm.* **2019**, *562*, 249.
(47) Han, J.; Wang, Q.; Zhang, Z.; Gong, T.; Sun, X. Cationic bovine serum albumin based self-assembled nanoparticles as siRNA delivery vector for treating lung metastatic cancer. *Small* **2014**, *10* (3), 524−535.
(48) Kopp, J. B.; Heymann, J. c-Src is in the effector pathway linking uPAR and podocyte injury. *J. Clin. Invest.* **2019**, *129* (5), 1827.
(49) Herman-Edelstein, M.; Thomas, M. C.; Thallas-Bonke, V.; Saleem, M.; Cooper, M. E.; Kantharidis, P. Dedifferentiation of immortalized human podocytes in response to transforming growth factor-$\beta$: a model for diabetic podocytopathy. *Diabetes* **2011**, *60* (6), 1779−1788.
(50) Imasawa, T.; Obre, E.; Bellance, N.; Lavie, J.; Imasawa, T.; Rigothier, C.; Delmas, Y.; Combe, C.; Lacombe, D.; Benard, G. High glucose repatterns human podocyte energy metabolism during differentiation and diabetic nephropathy. *FASEB J.* **2017**, *31* (1), 294−307.
(51) Pandey, P. K.; Maheshwari, R.; Raval, N.; Gondaliya, P.; Kalia, K.; Tekade, R. K. Nanogold-core multifunctional dendrimer for pulsatile chemo-, photothermal-and photodynamic-therapy of rheumatoid arthritis. *J. Colloid Interface Sci.* **2019**, *544*, 61−77.
(52) Liu, J.; Deng, H.; Liu, Q.; Chu, L.; Zhang, Y.; Yang, C.; Zhao, X.; Huang, P.; Deng, L.; Dong, A. Integrin-targeted pH-responsive micelles for enhanced efficiency of anticancer treatment in vitro and in vivo. *Nanoscale* **2015**, *7* (10), 4451−4460.
(53) Kong, L.; Wu, Y.; Alves, C. S.; Shi, X. Efficient delivery of therapeutic siRNA into glioblastoma cells using multifunctional dendrimer-entrapped gold nanoparticles. *Nanomedicine* **2016**, *12* (23), 3103−3115.
(54) Oe, Y.; Christie, R. J.; Naito, M.; Low, S. A.; Fukushima, S.; Toh, K.; Miura, Y.; Matsumoto, Y.; Nishiyama, N.; Miyata, K. Actively-targeted polyion complex micelles stabilized by cholesterol and disulfide cross-linking for systemic delivery of siRNA to solid tumors. *Biomaterials* **2014**, *35* (27), 7887−7895.
(55) Zhou, Z.; Wan, J.; Hou, X.; Geng, J.; Li, X.; Bai, X. MicroRNA-27a promotes podocyte injury via PPAR$\gamma$-mediated $\beta$-catenin activation in diabetic nephropathy. *Cell Death Dis.* **2017**, *8* (3), e2658.


https://dx.doi.org/10.1021/acs.molpharmaceut.0c00094
*Mol. Pharmaceutics* 2021, 18, 641−666

(56) Zeng, W.; Qi, W.; Mu, J.; Wei, Y.; Yang, L.-L.; Zhang, Q.; Wu, Q.; Tang, J.-Y.; Feng, B. MG132 protects against renal dysfunction by regulating Akt-mediated inflammation in diabetic nephropathy. *Sci. Rep.* **2019**, *9* (1), 2049.
(57) Reddy, T. L.; Garikapati, K. R.; Reddy, S. G.; Reddy, B. S.; Yadav, J.; Bhadra, U.; Bhadra, M. P. Simultaneous delivery of Paclitaxel and Bcl-2 siRNA via pH-Sensitive liposomal nanocarrier for the synergistic treatment of melanoma. *Sci. Rep.* **2016**, *6*, 35223.
(58) Breyer, M. D.; Böttinger, E.; Brosius, F. C.; Coffman, T. M.; Harris, R. C.; Heilig, C. W.; Sharma, K. Mouse models of diabetic nephropathy. *J. Am. Soc. Nephrol.* **2005**, *16* (1), 27−45.
(59) Hauser, P. V.; Pippin, J. W.; Kaiser, C.; Krofft, R. D.; Brinkkoetter, P. T.; Hudkins, K. L.; Kerjaschki, D.; Reiser, J.; Alpers, C. E.; Shankland, S. J. Novel siRNA delivery system to target podocytes in vivo. *PLoS One* **2010**, *5* (3), e9463.
(60) Stangenberg, S.; Saad, S.; Schilter, H. C.; Zaky, A.; Gill, A.; Pollock, C. A.; Wong, M. G. Lysyl oxidase-like 2 inhibition ameliorates glomerulosclerosis and albuminuria in diabetic nephropathy. *Sci. Rep.* **2018**, *8* (1), 9423.
(61) Jha, J. C.; Thallas-Bonke, V.; Banal, C.; Gray, S. P.; Chow, B. S.; Ramm, G.; Quaggin, S. E.; Cooper, M. E.; Schmidt, H. H.; Jandeleit-Dahm, K. A. Podocyte-specific Nox4 deletion affords renoprotection in a mouse model of diabetic nephropathy. *Diabetologia* **2016**, *59* (2), 379−389.
(62) Gai, Z.; Hiller, C.; Chin, S. H.; Hofstetter, L.; Stieger, B.; Konrad, D.; Kullak-Ublick, G. A. Uninephrectomy augments the effects of high fat diet induced obesity on gene expression in mouse kidney. *Biochim. Biophys. Acta, Mol. Basis Dis.* **2014**, *1842* (9), 1870−1878.
(63) Ramesh, N.; Mandal, A. K. A. Encapsulation of epigallocatechin-3-gallate into albumin nanoparticles improves pharmacokinetic and bioavailability in rat model. *3 Biotech* **2019**, *9* (6), 238.
(64) Sawaguchi, A.; Kamimura, T.; Yamashita, A.; Takahashi, N.; Ichikawa, K.; Aoyama, F.; Asada, Y. Informative three-dimensional survey of cell/tissue architectures in thick paraffin sections by simple low-vacuum scanning electron microscopy. *Sci. Rep.* **2018**, *8* (1), 7479.
(65) Shi, M.; McMillan, K. L.; Wu, J.; Gillings, N.; Flores, B.; Moe, O. W.; Hu, M. C. *Cisplatin nephrotoxicity as a model of chronic kidney disease*; 1530-0307; Nature Publishing Group, 2018.
(66) Arsenault, M. G.; Miao, Y.; Jones, K.; Sims, D.; Spears, J.; Wright, G. M.; Hartwig, S. Estimation of total glomerular number using an integrated disector method in embryonic and postnatal kidneys. *Canadian Journal of Kidney Health and Disease* **2014**, *1* (1), 12.
(67) Stojanović, V. R.; Jovanović, I. D.; Ugrenović, S. Z.; Vasović, L. P.; Živković, V. S.; Jocić, M. V.; Kundalić, B. K.; Pavlović, M. N. Morphometric analysis of nonsclerosed Glomeruli size and connective tissue content during the aging process. *Sci. World J.* **2012**, *2012*, 1.
(68) Tsai, P.-P.; Schlichtig, A.; Ziegler, E.; Ernst, H.; Haberstroh, J.; Stelzer, H. D.; Hackbarth, H. Effects of different blood collection methods on indicators of welfare in mice. *Lab animal* **2015**, *44* (8), 301.
(69) Hyun, H.; Park, J.; Willis, K.; Park, J. E.; Lyle, L. T.; Lee, W.; Yeo, Y. Surface modification of polymer nanoparticles with native albumin for enhancing drug delivery to solid tumors. *Biomaterials* **2018**, *180*, 206−224.
(70) Babaei, M.; Eshghi, H.; Abnous, K.; Rahimizadeh, M.; Ramezani, M. Promising gene delivery system based on polyethylenimine-modified silica nanoparticles. *Cancer Gene Ther.* **2017**, *24* (4), 156.
(71) Huang, P.; Li, Z.; Hu, H.; Cui, D. Synthesis and characterization of bovine serum albumin-conjugated copper sulfide nanocomposites. *J. Nanomater.* **2010**, *2010*, 33.
(72) Gularte, M. S.; Anghinoni, J. M.; Abenante, L.; Voss, G. T.; de Oliveira, R. L.; Vaucher, R. A.; Luchese, C.; Wilhelm, E. A.; Lenardão, E. J.; Fajardo, A. R. Synthesis of chitosan derivatives with organoselenium and organosulfur compounds: Characterization, antimicrobial properties and application as biomaterials. *Carbohydr. Polym.* **2019**, *219*, 240.
(73) Li, X.; Sun, A.-n.; Liu, Y.-j.; Zhang, W.-j.; Pang, N.; Cheng, S.-x.; Qi, X.-r. Amphiphilic dendrimer engineered nanocarrier systems for co-delivery of siRNA and paclitaxel to matrix metalloproteinase-rich tumors for synergistic therapy. *NPG Asia Mater.* **2018**, *10* (4), 238.
(74) Şalva, E.; Ekentok, C.; Turan, S. Ö.; Akbuğa, J. l. Non-viral siRNA and shRNA Delivery Systems in Cancer Therapy. *RNA Interference*; IntechOpen, 2016.
(75) Mian, A. N.; Schwartz, G. J. Measurement and estimation of glomerular filtration rate in children. *Advances in chronic kidney disease* **2017**, *24* (6), 348−356.
(76) Bellin, A. R.; Zhang, Y.; Thai, K.; Rosenblum, N. D.; Cullen-McEwen, L. A.; Bertram, J. F.; Gilbert, R. E. Impaired SIRT 1 activity leads to diminution in glomerular endowment without accelerating age-associated GFR decline. *Physiol. Rep.* **2019**, *7* (9), e14044.
(77) Takiyama, Y.; Sera, T.; Nakamura, M.; Ishizeki, K.; Saijo, Y.; Yanagimachi, T.; Maeda, M.; Bessho, R.; Takiyama, T.; Kitsunai, H. Impacts of Diabetes and an SGLT2 Inhibitor on the Glomerular Number and Volume in db/db Mice, as Estimated by Synchrotron Radiation Micro-CT at SPring-8. *EBioMedicine* **2018**, *36*, 329−346.
(78) Grange, C.; Tritta, S.; Tapparo, M.; Cedrino, M.; Tetta, C.; Camussi, G.; Brizzi, M. F. Stem cell-derived extracellular vesicles inhibit and revert fibrosis progression in a mouse model of diabetic nephropathy. *Sci. Rep.* **2019**, *9* (1), 4468.
(79) Bugata, L. S. P.; Pitta Venkata, P.; Gundu, A. R.; Mohammed Fazlur, R.; Reddy, U. A.; Kumar, J. M.; Mekala, V. R.; Bojja, S.; Mahboob, M. Acute and subacute oral toxicity of copper oxide nanoparticles in female albino Wistar rats. *J. Appl. Toxicol.* **2019**, *39* (5), 702−716.
(80) Zhang, X.-D.; Wu, D.; Shen, X.; Liu, P.-X.; Yang, N.; Zhao, B.; Zhang, H.; Sun, Y.-M.; Zhang, L.-A.; Fan, F.-Y. Size-dependent in vivo toxicity of PEG-coated gold nanoparticles. *Int. J. Nanomed.* **2011**, *6*, 2071.
(81) Wei, X.; Gao, J.; Fang, R. H.; Luk, B. T.; Kroll, A. V.; Dehaini, D.; Zhou, J.; Kim, H. W.; Gao, W.; Lu, W. Nanoparticles camouflaged in platelet membrane coating as an antibody decoy for the treatment of immune thrombocytopenia. *Biomaterials* **2016**, *111*, 116−123.
(82) Lundberg, P.; Skoda, R. Hematology Testing in Mice. *Current protocols in mouse biology* **2011**, *1* (3), 323−46.
(83) Bhunia, A.; Kamilya, T.; Saha, S. Silver nanoparticle-human hemoglobin interface: time evolution of the corona formation and interaction phenomenon. *Nano Convergence* **2017**, *4* (1), 28.
(84) Rugo, H. S.; Barry, W. T.; Moreno-Aspitia, A.; Lyss, A. P.; Cirrincione, C.; Leung, E.; Mayer, E. L.; Naughton, M.; Toppmeyer, D.; Carey, L. A. Randomized phase III trial of paclitaxel once per week compared with nanoparticle albumin-bound nab-paclitaxel once per week or ixabepilone with bevacizumab as first-line chemotherapy for locally recurrent or metastatic breast cancer: CALGB 40502/NCCTG N063H (Alliance). *J. Clin. Oncol.* **2015**, *33* (21), 2361.
(85) Kume, E.; Fujimura, H.; Matsuki, N.; Ito, M.; Aruga, C.; Toriumi, W.; Kitamura, K.; Doi, K. Hepatic changes in the acute phase of streptozotocin (SZ)-induced diabetes in mice. *Exp. Toxicol. Pathol.* **2004**, *55* (6), 467−480.
(86) Al-Mahmood, S.; Razak, T. A.; Abdullah, S. T.; Fatnoon NA, N. N.; Mohamed, A. H.; Al-Ani, I. M. A comprehensive study of chronic diabetes complications in streptozotocin-induced diabetic rat. *Makara Journal of Health Research* **2016**, *20*, 48−56.
(87) Yu, X.; Song, Y.; Di, Y.; He, H.; Fu, D.; Jin, C. Enhanced tumor targeting of cRGD peptide-conjugated albumin nanoparticles in the BxPC-3 cell line. *Sci. Rep.* **2016**, *6*, 31539.
(88) Ma, Y.; Sha, M.; Cheng, S.; Yao, W.; Li, Z.; Qi, X.-R. Construction of Hyaluronic Tetrasaccharide Clusters Modified Polyamidoamine siRNA Delivery System. *Nanomaterials* **2018**, *8* (6), 433.
(89) Kratz, F. Albumin as a drug carrier: design of prodrugs, drug conjugates and nanoparticles. *J. Controlled Release* **2008**, *132* (3), 171−183.

(90) Wen, H.; Yin, Y.; Huang, C.; Pan, W.; Liang, D. Encapsulation of RNA by negatively charged human serum albumin via physical interactions. *Sci. China: Chem.* **2017**, *60* (1), 130−135.
(91) Kumawat, A.; Dapse, P.; Kumar, N.; Mishra, D. K.; Maheshwari, R.; Bhattacharya, P.; Tekade, R. K. Budding Alliance of Nanotechnology in RNA Interference Therapeutics. *Curr. Pharm. Des.* **2018**, *24* (23), 2632−2643.
(92) Jang, M.; Kim, J. H.; Nam, H. Y.; Kwon, I. C.; Ahn, H. J. Design of a platform technology for systemic delivery of siRNA to tumours using rolling circle transcription. *Nat. Commun.* **2015**, *6*, 7930.
(93) Dal Monte, M.; Cammalleri, M.; Pecci, V.; Carmosino, M.; Procino, G.; Pini, A.; De Rosa, M.; Pavone, V.; Svelto, M.; Bagnoli, P. Inhibiting the urokinase-type plasminogen activator receptor system recovers STZ-induced diabetic nephropathy. *Journal of cellular and molecular medicine* **2019**, *23* (2), 1034−1049.
(94) Danhier, F.; Le Breton, A.; Préat, V. r. RGD-based strategies to target alpha (v) beta (3) integrin in cancer therapy and diagnosis. *Mol. Pharmaceutics* **2012**, *9* (11), 2961−2973.
(95) Tekade, R. K.; Dutta, T.; Gajbhiye, V.; Jain, N. K. Exploring dendrimer towards dual drug delivery: pH responsive simultaneous drug-release kinetics. *J. Microencapsulation* **2009**, *26* (4), 287−296.
(96) Tekade, R. K.; Kumar, P. V.; Jain, N. K. Dendrimers in oncology: an expanding horizon. *Chem. Rev.* **2009**, *109* (1), 49−87.
(97) Wang, X.; Gao, Y.; Tian, N.; Wang, T.; Shi, Y.; Xu, J.; Wu, B. Astragaloside IV inhibits glucose-induced epithelial-mesenchymal transition of podocytes through autophagy enhancement via the SIRT−NF-κB p65 axis. *Sci. Rep.* **2019**, *9* (1), 323.
(98) Dubreil, C.; Sainte Catherine, O.; Lalatonne, Y.; Journé, C.; Ou, P.; van Endert, P.; Motte, L. Tolerogenic iron oxide nanoparticles in type 1 diabetes: biodistribution and pharmacokinetics studies in nonobese diabetic mice. *Small* **2018**, *14* (40), 1802053.
(99) Leeuwis, J. W.; Nguyen, T. Q.; Dendooven, A.; Kok, R. J.; Goldschmeding, R. Targeting podocyte-associated diseases. *Adv. Drug Delivery Rev.* **2010**, *62* (14), 1325−1336.
(100) Xu, J.; Li, Z.; Xu, P.; Xiao, L.; Yang, Z. Nanosized copper oxide induces apoptosis through oxidative stress in podocytes. *Arch. Toxicol.* **2013**, *87* (6), 1067−1073.


https://dx.doi.org/10.1021/acs.molpharmaceut.0c00094
*Mol. Pharmaceutics* 2021, 18, 641−666